Investigation into power distribution / grid interfacing for subsea tidal generation - Rectification to a common DC-bus.

Shoan Mbabazi

The University Of Sheffield.

Thesis submitted in accordance with the requirements for the degree of Doctor of Philosophy

to the

Department of Electrical and Electronics Engineering

Machines and Drives Group

September 2015

Declaration

I hereby confirm that the work submitted is my own, and that it contains no material previously submitted for the award of any other degree. Appropriate credit has been given where reference has been made to the work of others.

By direction from the project sponsors that includes Rolls-Royce and Tidal Generation Limited, publication of this work was not permitted.

This copy has been supplied on the understanding that it is copyright material and that no quotation from the thesis may be published without proper authorisation and acknowledgement.

Shoan Mbabazi

Acknowledgements

This research project would not have been possible without the support of many people.

I would like to express my deepest gratitude to my supervisors, Prof David Stone and Prof Jiabin Wang, for their excellent guidance, caring, patience, and providing me with an excellent atmosphere for doing research in addition to patiently correcting my writing.

Special thanks also goes to all my graduate friends, especially my research colleagues in room E129 for sharing the literature and invaluable assistance.

Abstract

The research objective was to investigate the generation and collection of power generated in a distributed tidal generation site, and realise the most economic grid connection methodology for a practical installation. Current tidal steam prototype designs utilise variable speed gear boxes, power frequency converters and variable pitch blades in the nacelle, thus requiring complicated, heavy and expensive equipment in the nacelle. Moreover the variable blade pitch mechanism has a large power demand, and has to operate day after day submerged in water at depths between 30m – 80m. The approach taken in this research is to replace major cost components with much cheaper ones, as well as locating as many components as possible onshore where costs are less.

This thesis investigates a novel tidal stream power generation system referred to as "passive rectification to a common DC-bus" where an array of 3-phase synchronous generators operating at diverse speeds are connected to a common DC bus via passive diode rectifiers. The proposed tidal stream topology shows that variable pitched blades, variable speed gearboxes and frequency converters in the nacelle can be replaced by a much simpler system that uses fixed pitch blades, a fixed ratio gearbox, generator excitation control system, and a diode bridge rectifier. These components are generally cheaper, lighter, have a lower power demand and are more reliable than the components they replace. Also some of the voltage and frequency conversion is carried out ashore where costs are less, in addition to the overall reduction in the number of components required as some of the components are shared by multiple devices. As a result system efficiency is maximised, in addition to facilitating a reduction in capital, installation and operational costs.

Power conversion from the tidal generation power system to shore is achieved via passive rectification to a common DC-bus, thus system power regulation is achieved by individual generator field current control, to attain optimum system operation including, maximum power extraction, power limitation and stall control, in turn improving system reliability and controllability. Furthermore passive stall control via generator field current regulation eliminates the need for mechanical brakes which reduces cost and improves reliability.

The feasibility of the proposed power generation system was carried out via computer simulations and later validated via small scale laboratory hardware simulations.

Preface

This thesis investigates the generation and collection of power generated in a distributed tidal stream generation site, examining the most economic grid connection methodology for a large scale practical installation and its content is organised as follows:

Chapter 1 presents background information and literature review on tidal stream energy extraction, describing its advantages and disadvantages as well current state of the art tidal stream generators.

In **Chapter 2** a novel tidal stream power harnessing methodology referred to as "passive rectification to a common DC-bus" is presented. This scheme aims to optimise current tidal turbine prototype designs by minimising capital installation and maintenance time/costs, moreover maximising reliability, efficiency, controllability and grid-connection compliance. Furthermore, this facilitates the use of multiple generators running at diverse speeds, voltage and power, connected onto a common DC-link circuit (DC-bus).

Chapter 3 describes the development of the dynamic model of the proposed tidal turbine topology including all of its main components, as well as its averaged model with reference to system's power transfer.

Chapter 4 describes the control and performance of the proposed tidal system topology as well as some aspects of its components selection. Only the steady state operation of the system has been analysed. The feasibility of the proposed tidal stream power generation topology is carried out for a 0.91MW tidal device via computer simulations

Chapter 5 focuses on the hardware based tidal turbine simulation rig design and development, along with its preparation and practical analysis. Testing was done in a laboratory environment therefore a scaled down tidal power generation system was considered to validate the computer simulation results presented in **Chapter 4**.

Finally **Chapter 6** presents a summary and conclusions of all presented chapters as well as detailing future works.

Table of Contents

Contents

List of Tables

List of Figures

Contents

CHAPTER 1

1 INTRODUCTION

It is well known that electricity and heat are modern human life essentials. Currently electrical and heat energy is primarily generated from coal, oil and gas. However, the combustion of these fossil fuels creates an excess of carbon dioxide (CO_2) in the atmosphere which leads to a number of environmental issues such as the greenhouse effect, and may accelerate climate change. For that reason, the UK is planning to reduce its CO_2 emissions by not less than 60% in comparison to those reported in 1990 [1-2]. However, due to the amount of energy used today, replacing all fossil fuels with an alternative power source would mean that this alternative would have to be mechanically and environmentally acceptable, in addition to being economically profitable, if it is to attract investors and developers. Therefore, it is currently thought that a sustainable energy future will have to be based on more efficient fossil fuel combustion technologies, together with the use of renewable energy sources, resulting in a mix of energy power generation.

In December 2007 the UK ratified a legally binding renewable energy target of the EU under the Bali Protocol, which suggested that at least 40% of electrical power generation in the UK will have to come from renewable sources by 2020 [2-3]. This target was set in an effort to moderate the excessive exploitation of fossil fuels and the diminution of their reserves within the last 20 years, in addition to the emergent concern over the increase of greenhouse gases in the atmosphere [4-6].

There are a variety of alternatives by which clean renewable energy could be generated, these include: solar photovoltaic, wind, wave, geothermal and tidal power. However in the UK, wind and tidal power are considered to be the most available and practically viable renewable energy resources, due to country's geographical location. The emerging wind energy industry has been relatively successful to date, and already provides commercial electrical power to homes in some parts of the UK [7]. Nonetheless wind as a source of energy is unpredictable, thus the turbines generate

power only when the wind is blowing, making it difficult to plan for when and how this power can be utilised. On the other hand tidal currents can be accurately predicted in magnitude for decades ahead; moreover tidal currents have better velocity distribution compared to wind [8], giving tidal power a distinctive advantage over wind energy in terms of predictability.

The potential benefits of tidal energy development are already known to the UK government and potential investors, i.e. the marine energy industry could potentially generate an income of approximately £6.1 billion to the country's economy by 2035 in addition to generating around 20,000 jobs [9]. Furthermore, the Department of Business, innovation and Skills has reported that almost 10% of the UK's electrical power needs could be generated from tidal power alone [10]. However, tidal stream power harnessing devices need to be distributed over large areas if they are to economically compete with conventional power generation technologies that utilise relatively cheap oil or coal which is presently available.

The technology used for tidal stream power capture is similar to that of wind power; which means that tidal power developers can now be confident of its viability by falling back on the wind power industry for experience and practicality. Nonetheless, there are some major differences between these two sources of energy. For example, tidal stream velocity is much slower than wind, leading to lower blade and rotor speed. On the other hand, the density of sea water is 800 times greater than air [11] which increases the torque exerted on the tidal blades enabling them to produce significant amounts of power even at low rotor speeds, as the available power is dependent on the fluid density, and the cube of its velocity. It is calculated that if a tidal velocity of 10% of a given wind speed is applied to a tidal turbine; it would supply the same amount of power as the wind turbine of the same size. However tidal power harnessing devices are installed in significantly more hostile environments, typically submerged between 30 to 80 m deep in the sea, and up to 10 km from shore [12] [13]. As a result of the location, the pressure exerted on the tidal power device is much greater which could make the manufacture of tidal blades with sufficient strength both difficult and costly. Additionally, access for maintenance is much more difficult and costly with sub-sea tidal devices therefore more reliable components are required.

It should be noted that there is a mis-match between electricity generated by tidal stream currents and the grid demand as the power generated by a tidal stream power plant is variable due to variations in tidal currents. However although variable, tidal stream power is reliable because it can be predicted for decades ahead which means it could supplement the electrical power which would otherwise be generated by fossil fuel power plants, in turn decreasing greenhouse and acid gasses emissions into the atmosphere.

1.1 Background

1.1.1 Tidal currents

Tidal currents are generated from the interaction between the rotation of the Earth, the Moon and the Sun. This influences gravity acting on the oceans causing the rhythmic rising and lowering of water that results in tidal currents [14] as illustrated in *Fig 1.1* .
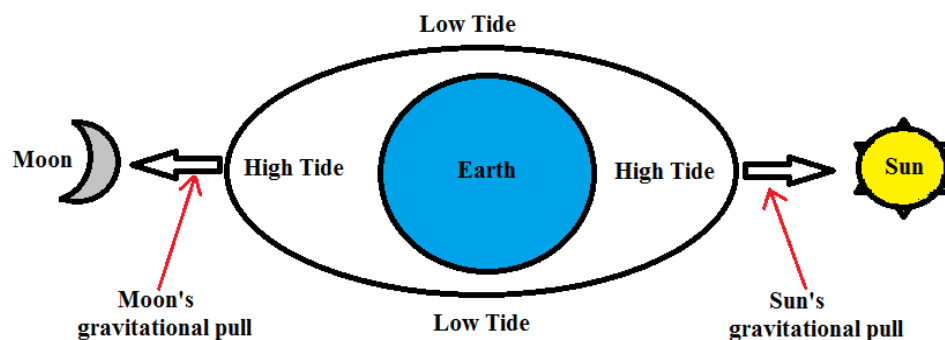
Fig 1.1: How tidal currents are occur

It is understood that the moon is much closer to the earth and has more influence on the amplitude of tidal velocity compared to the sun. Therefore, tidal current variations closely follow the moon as it rotates around the earth resulting in diurnal and ebb tide cycles at a given ocean surface. The velocity of the tidal currents is much less in the open waters measuring just a few centimetres in the centre of the wave distributed over hundreds of kilometres and increases intensely as the wave approaches continental shelves, carrying immense masses of water into narrow bays and river inlets along a coastline [15]. In depth information on tidal currents and the physics of their occurrences can be found in [1].

Tidal power is potentially infinite because it is generated from the flow of the sea water caused by gravitational interactions between the Earth, the Sun and the Moon, which also makes it a renewable energy source. It could be harnessed by either building barrages across estuaries or by tidal stream turbines [16]. The first technology employed to extract electrical power from the flow of ocean waters involved building a dam or a barrage where there is significant differences in height between high and low tides, typically across a bay [17].

The operation of a typical ebb-generating tidal barrage is as follows: The water retained behind the barrage at high tide creates a power head adequate to generate electrical power as the tide ebbs and water released from within the dam turns the turbine blades. Although this method of tidal power capture is durable, barrages are relatively expensive to construct in addition to causing all sorts of environmental problems like, build-up of silt inside the dam which would need regular and expensive dredging [17]. Therefore most tidal power developers no longer consider this type of technology feasible [18] thus, tidal stream turbines are now being developed.

1.1.2 Tidal stream turbines

A tidal stream turbine is similar to an underwater wind turbine where the flow of the moving water rotates the turbine blades as wind would in the case on a wind turbine *Fig 1.2* shows a typical horizontal axis tidal stream turbine.
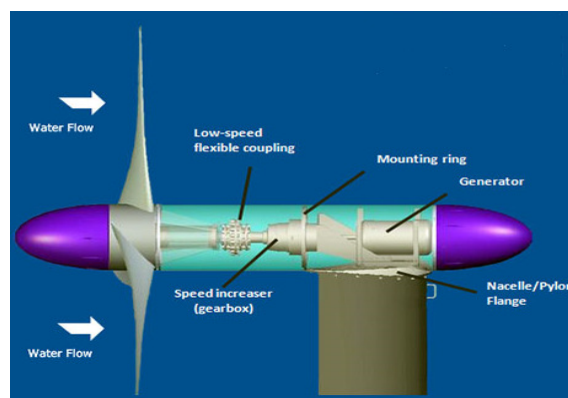
Fig 1.2: A typical horizontal axis Tidal stream turbine [19]

The first tidal stream turbine was proposed during the 1970s' oil crisis [11] although this technology was then considered both uneconomically and practically unviable.

Tidal stream power extraction devices are now gaining popularity and support as a result of the wind power industry's success. Moreover according to recent studies, the generation of tidal stream energy in the UK could potentially yield an estimated 94 TWh per annum of electrical power , generated from 36 GW tidal power extraction plant [21].

For this reason, various tidal stream turbine concepts have been proposed by tidal stream power developers [22]. As expected they are quite similar to wind turbines i.e. horizontal axis turbines and vertical axis turbines [23], others such as venturis and oscillating foils [16] are also being considered by some. Horizontal axis turbines are more commonly employed due to their operational experience observed over a number of years with primarily 3 blade turbines within the wind power industry. There are many approaches to horizontal axis turbine design which include ducts (open centre) shown in *Fig 1.3*, variable pitch blades and rim generators. All consisting of a turbine with a horizontal-axis of rotation aligned parallel to the current flow. Moreover, the theoretical efficiency for horizontal axis machines is much higher compared to other design concepts [16, 18, 24].
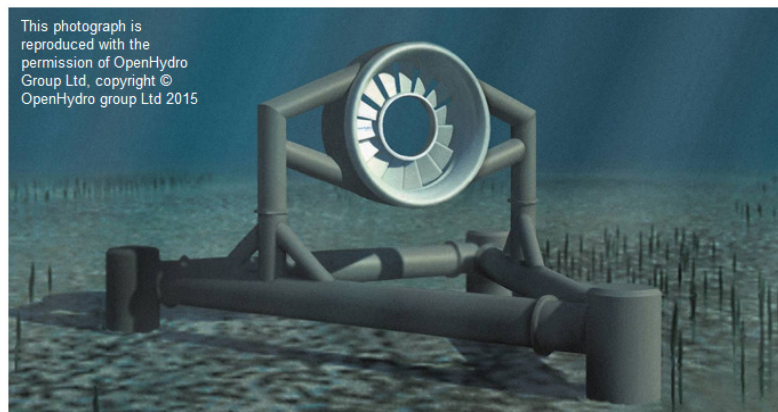
Fig 1.3: Open Centre (duct) Turbine, developed and manufactured by OpenHydro Group Ltd.

Fig 1.3 shows the open centre horizontal axis tidal turbine developed and manufactured by OpenHydro Group Ltd. This is one of the novel ideas being developed for tidal stream power extraction. It's lubricant free and its slow moving rotor would improve system reliability, in addition to minimising the risk to marine life [25].

The other designs also offer some benefits i.e. with vertical axis devices there is a possibility of locating the machine nacelle above water, therefore making access for maintenance much easier.

Engineering Business Ltd (EB) has created a prototype tidal stream generator termed "Stingray" shown in *Fig 1.4.*
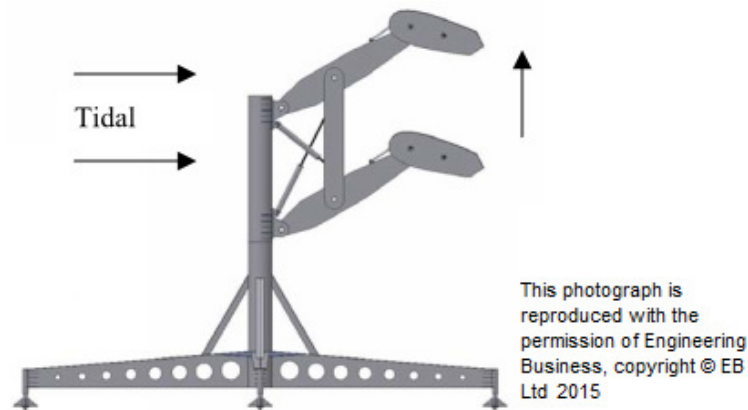
Fig 1.4: EB Stingray tidal generator.

The "Stingray" tidal harnessing device uses a set of hydroplanes to convert the kinetic energy from the tidal currents into hydraulic power, which is then used to turn an electrical generator via a hydraulic motor [26]. A hydraulic device of this type could remove the need for mechanical gearboxes, therefore leading to a less complex, increased reliability tidal-system with lower component count, consequently lowering operational costs. Nonetheless a hydraulic solution is likely to be inefficient compared to a electro-mechanical system i.e. hydraulic systems are reported to be around 10% to 30% less efficient than an equivalent mechanical system in transferring energy from the turbine blades to the generator input shaft, in addition to other losses incurred when the hydraulic fluid is moved through the pipe-work [27].

In [22] King and Tryfonas analyse a number of conceptual and prototype tidal power devices from different marine developers for the purpose of underlining the technology's state of the art. This study shows that tidal power is in its infancy, as developers are collectively investigating a wide variety of systems including those proved inefficient and uneconomical by the wind industry. Tidal power industry

development is following the same path taken in the early stages of wind power development. Therefore it seems likely that it is going to take some time before a standard architecture can be achieved.

Tidal stream power harnessing devices are installed in inhospitable sites, therefore having a dependable method of installation and maintenance is paramount given that the associated labour costs and the risk of delay could potentially be very high. As a consequence, achieving a relatively easy installation method for the tidal power harnessing devices is one of the major objective for tidal power developers. *Fig 1.5* below shows the most considered seabed preparation configurations.
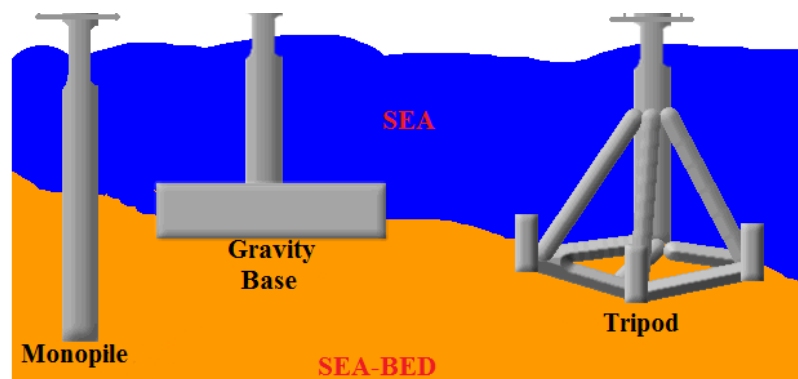
Fig 1.5: Seabed preparation methods

Some tidal stream power developers such as Lunar energy are opting to use a gravity base foundation [28]. E.on are currently developing a 3000 tonne turbine [29] which eliminates the need for sea-bed preparation however, a very large vessel would be needed to get this device into the sea, consequently making installation and maintenance much more difficult.

The component with the highest installation cost is the monopile [30], which would explain why Tidal Generation Ltd and Swan Turbines are trying to eliminate the need for the monopile by opting for a fairly lightweight tripod support structure[31-32] similar to the one shown in *Fig 1.5*

Other methods such as seabed anchoring via a gravity base as shown in *Fig 1.6* are also being considered by some developers [16].

Fig 1.6 presents a seabed anchored Kuroshio tidal stream power harnessing devices developed by Tokyo University, Toshiba IHI, and the Institute of Global Strategic Studies Mitsui [33]
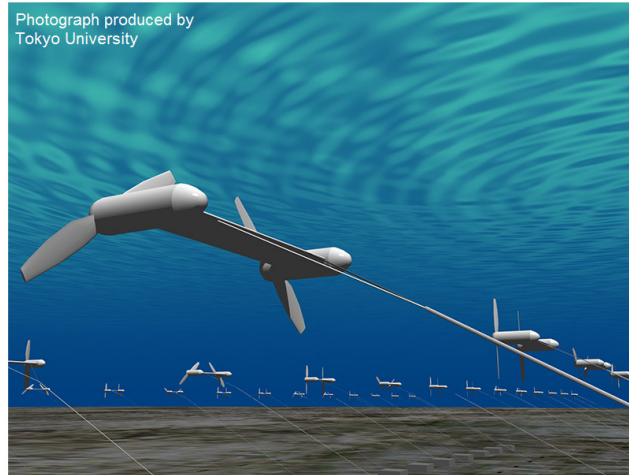
Fig 1.6: Seabed anchoring via a gravity base

Cable moored devices are usually employed for seabed installation given that little work is required after the cable fixing points are installed onto the sea bed leading to lower installation costs for the turbines.

1.1.3   Electrical power generation

Tidal blades convert kinetic energy from water flow into mechanical energy in the rotor shaft. The generator is the component of the tidal turbine system that converts mechanical energy in the tidal rotor into electricity which would then be fed onto the utility grid. There are number of generator types that can be employed for tidal power extraction and these include: doubly-fed induction generators (DFIG), permanent magnet synchronous generators (PMSG), electrically excited synchronous generators (SG) and Induction generators (IG) [34]. However, the selection of the most cost effective generator solution for a large scale tidal device is not straight forward given that all these generator types have their advantages and disadvantages.

IGs generate electrical power once their rotor is rotating faster than the synchronous speed for the device. At steady state a prime mover drives the rotor above synchronous speed generating negative slip and inducing current in the rotor equivalent to slip. IGs

are perhaps the choice for most electrical power applications throughout industry [35-36], and they could be used for fixed-speed tidal turbines because of their damping effect. However they require reactive power to energize the magnetic circuits which in most cases is provided by the utility grid or parallel capacitor banks at the machine terminals to compensate for reactive power consumption. Additional components would increase system component count, and in turn increase both maintenance and capital installation costs for these systems.

In general the operation principle of a DFIG is the same as that of an IG, the difference is that the rotor active power can be controlled by the rotor side converter in DFIG [35]. DFIGs are the most employed generators in the wind power industry especially where high powered wind turbines are installed, this is because the rating of power converters can be down sized by approximately 30%. This is possible due to the fact that, just a fraction of the power generated is processed by the electronic power converter, thus the employed converter system power rating can be lower than the power rating of the turbine.

PMSG machines have been widely used for industrial applications mostly because of their high efficiency, since excitation is not required, and their high reliability since slip rings and brushes are not required. However, the magnetic flux air gap cannot be controlled because it is dependent on the permanent magnet properties, thus it is nearly constant. Therefore a full rated power converter would be required to regulate the generators output power given that its power output would be at variable frequency and voltage when connected to the tidal turbine, which is incompatible with a direct grid connection that requires a fixed voltage and frequency. This then leads to higher expense, as a power electronic grid interface is required.

SGs typically comprise of a rotor with a field coil magnetised by a DC excitation system, and a stator that has three-phase windings the same as those of the induction machine. The rotor can consist of salient or cylindrical poles. Salient poles are usually employed when the SG is to operate at low speed, thus Salient pole SGs would be most suitable for tidal turbine generator applications, especially if a gearbox is to be omitted

[35]. Compared to the PM, the SG flux can be regulated, moreover the cost of the machine is significantly reduced because no permanent magnets are required.

Electronic converters are vital to power generation because they enhance generator power output through various control schemes that in turn improve performance, grid compliance and network power quality.

1.1.4 Power control

Tidal velocity varies every six hours as well as over extended time periods like the bi-monthly tidal cycle "spring-neap" [1]. Varying tidal velocities give rise to generator shaft speed variation, which cause voltage variations at the generator terminals. Thakur in [37] analyses the dynamic aspects of a wind turbine power system at low frequencies and variable speed, controlled using a back-to-back converter. This publication is of interest because it analyses the non-linearity of the operating conditions of a wind turbine under the influence of wind turbulence which in principle would be similar to what would be seen in a tidal turbine. For example the findings show that if voltage variations at the rotor-side are not adequately regulated they could be transferred to the grid, leading to poor power quality. In the case of tidal generation, the variation in tidal velocity causes variations in tidal generator output voltage, which could lead to the same effect.

It should be noted that the quality of the power generated by the tidal turbine is very important, especially if it is to be fed into the utility grid. Increasingly so, as the grid continues to experience an ever increasing number non-linear loads connecting directly onto it, such as wind turbines for example.

For this reason, the following offshore grid connection requirements have been set out in the Grid code (issue 4, Revision 2) [38-39], published by the National Grid. These requirements apply to all non-linear loads generating power onto the grid. i.e.

- Active power control: active power control is required to avoid overloading the grid in addition to grid power generation.

- Frequency control: frequency control is required in order to keep the power generated onto the utility grid within acceptable limits and power quality standards.

- Frequency and voltage ranges: ranges of voltage amplitude and frequency are required to enable continuity in operation in case of grid voltage and frequency stability problems.

- Voltage control: voltage control is required in order to be keep the power generated onto the utility grid within acceptable limits and power quality standards. Some utility grid providers such as E.on Netz [38] require the use of tap-changing transformers in order to vary the voltage ratio between the power generator and the grid where necessary.

The control of non-linear power sources is very complex due to their unpredictable variations in resource availability. Although tidal power is predictable in magnitude it still requires adequate power control due to the variations in tidal currents, which in turn affect the turbine's output power quality, leading to a system that is not complaint to the Grid Code. Therefore tidal turbines connecting onto the grid must be equipped with a power control system.

A tidal power controller therefore would comprise of many different components combined together to form a more comprehensive system that ensures that the device to be regulated operates satisfactorily, as well as operating within the Grid Code requirements listed above.

Power electronic converters are envisaged to be the way forward to achieve better control, high efficiency and performance for tidal stream power generation due to the advantages observed by wind power generation, in addition to achieving the Grid Code requirements i.e. reactive/active power, voltage and frequency regulation.

There are mainly two forms of converter systems employed for wind power generation, which could also apply to tidal power i.e.

Line commutated systems which are usually thyristor converters capable of high power generation. They consume inductive power and reactive power control is not possible.

Line commutated converter systems are typically employed for very high power and voltage applications like HVDC systems [36].

The other system is the self-commutated converter. This type of converter system is typically used in combination with pulse-width-modulation (PWM) control methods. They utilise IGBTs which are capable of being switched off, and they are capable of regulating both reactive and active power in both directions via a PWM scheme [36, 40]. Although PWM produces electrical harmonics due to the high frequency switching, these harmonics can be minimised by employing filters.

In [41] Patin presents a controller for a hybrid excitation synchronous generator that supplies an isolated grid for an aircraft application. This system utilises a rectifier between the synchronous generator and the DC bus, and field excitation control is employed to regulate the generator's terminal voltage. Employing this technique provides a low cost and reliable regulation of the armature voltages. This could be a very sensible control methodology if SGs are employed for tidal power generation since they allow power regulation via excitation control as shall be discussed in chapter 2. However, the use of passive rectifiers creates difficulties with controlling the complete system due to only having a single degree of control freedom. Moreover, low frequency harmonics are experienced due to the diode rectifiers operating characteristics [42-43] especially if a 6-pulse diode rectifier is used.

The requirement to match the variable speed of the tidal stream to the fixed voltage and frequency demanded by the utility grid is usually achieved by employing variable pitch blades, variable ratio gearbox, power electronic converters, or a combination of these methods [44]. However these greatly increase capital installation and running costs, thus making existing/prototype tidal stream turbines to date complex and relatively expensive. These costs must be reduced if tidal stream power is to economically compete with conventional and renewable energy sources including wind and solar energy.

Induction Generators (IG)	Doubly-Fed Induction Generators (DFIG)	Electrically Excited Synchronous Generators (SG)	Permanent Magnet Synchronous Generators (PMSG)
Robust and Simple	Relatively Complex	Relatively Complex	Robust and Simple
Relatively Cheap	heavy and bulky	heavy and bulky	Relatively Expensive
Low efficiency	High efficiency	**High efficiency**	High efficiency
Narrow Speed range	Wide speed range	**Wide speed range**	Narrow Speed range
Control and Regulation			
Complex voltage control with static generator	Complex voltage control with static generator	**Ease of voltage and torque control**	Ease of voltage and torque control
VAR or capacitor required for active and reactive power control	VAR or capacitor required for active and reactive power control	**Easy control of active and reactive power**	Easy control of active and reactive power
Inverter Requirements			
Large scale inverter	Inverter for 25% to 50% of nominal power	**Large scale inverter**	Large scale inverter
One controlling inverter	Two controlling inverter	**One controlling inverter**	Two controlling inverter
Simple inverter control	Complex inverter control	**Simple inverter control**	Simple inverter control
One inverter and a rectifier required	Complex inverter control	**One field controller and a rectifier required**	One inverter and a rectifier required

Table1.1: *Comparison summary of the various generators power control requirements for variable speed tidal turbines*

Table1.1 shows the Comparison summary of the various generators and their power control requirements. SGs are considered to present the most advantages that closely match the envisaged tidal generation strategy compared to the other generators i.e. The advantages of using SGs for tidal stream power generation include, high efficiency, and elimination of capacitor banks . They are suitable for high capacity power generation since they do not consume reactive power. Excitation of the SG can be provided by a separate DC power source in comparison to induction generators that require magnetising current from the power network. Additionally, the terminal voltage, current

and power can be easily controlled at a wide speed range without the need for fully controlled inverters i.e. via field current regulation.

Therefore SGs will form the basis of the research in the remainder of the thesis as shall be discussed in **Chapter 2**.

Using a synchronous generator also allows for indirect generator torque regulation via field control. It will be shown in this thesis that field current control alone is sufficient to achieve both speed and torque regulation of the turbine without the need for mechanical governors.

1.1.5   Tidal farms

When comparing the capability of any single tidal power generator to the overall capacity of the power generated by a single conventional power station, it can be said that an individual tidal turbine is relatively insignificant, even though its own power rating may seem to be high. Therefore, if tidal stream power is to make a substantial contribution to the UK's energy future, tidal farms have to be considered. A tidal farm could provide a significant amount power to the grid/consumers, and as a result enhances the country's energy security whilst at the same time contributing towards a low carbon future. Therefore tidal power developers are now looking at moving from single tidal stream devices to a point where multiple tidal device arrays can be demonstrated/installed in UK waters [22].

As previously stated, tidal velocity is variable and linking two or more tidal devices together would mean operating multiple machines at diverse power, speed/frequency and voltage. As a result, complex and sophisticated systems are required for frequency and voltage control which makes tidal stream power extraction difficult and expensive. However, it is understood that a tidal stream farm with devices that employ power electronics can achieve both frequency and voltage control at each device, which enables the turbine to operate in variable speed mode for maximum energy capture.

1.1.6 Possible Tidal farm topologies

Various prototypes from tidal stream power developers have shown potential although none have operated continuously to fully analyse performance and turnover on investment [22, 45]. However, when considering a cost effective tidal stream power generation topology it should be noted that the overall cost of the system consists of more than the system´s components price. i.e. Installation, maintenance, footprint and hauling costs should also be considered as they could increase the overall system cost significantly.

It should be noted that no information has been found with regards to a fully functional tidal stream energy farm connected to the utility grid during the course of this research, however various studies have been conducted on onshore and offshore-wind farms. Therefore, it is suggested that the best way to analyse the performance of tidal stream power farms would be to exploit its synergy with wind farms while, taking into account the differences.

In [46] a recent review of wind farm topologies was carried out by A. Ragheb and M Ragheb. It was observed that wind turbines, and consequently tidal turbines, require a "drive train" that comprises of a generator attached to the turbine rotor shaft via a gearbox, in some cases coupled directly onto the rotor shaft to form a power take off mechanism capable of generating electricity. Both geared and gearless topologies are explored for tidal power devices, although some tidal developers are also investigating the hydraulic drivetrain concept [22] in an effort to even out the output power variations caused by turbulence. Due to the nature of the velocity of tidal currents, the geared drivetrain option is more attractive for tidal developers given that it has proven successful with wind power generation. In contrast a gearbox needs maintenance which would be difficult and expensive especially for devices fixed on the seabed, making the geared drivetrain option problematic [16], i.e., failure of the gearbox could lead to long down times. As a result, some tidal developers are looking to eliminate this component altogether and employ direct drive devices to improve system reliability. Although one should bear in mind that records show that these failures are rare compared to electronic/electrical failures as will be discussed in sub-section **1.1.7**.

Gearless drive-trains are employed on some commercial wind power generation systems [47] such as the Enercon Ltd 'E-series' direct drive wind turbines [48].   On the other hand, a direct drive wind turbine requires a larger generator due to the increased number of poles required to achieve the effective electrical frequency needed for grid standard power generation. The larger generator causes high tower-top mass, although this would not be much of a concern with tidal turbines. However due to the much lower speeds of tidal turbine blades compared to wind, a direct drive tidal turbine would need a 3-phase generator with approximately 200 pole-pairs to match the slow rotor speeds if it is to achieve electrical frequencies of 20-50 Hz [47], such a generator may not fit in a standard tidal device nacelle.

Hydraulic drivetrains have a lower overall efficiency compared to the aforementioned, however there is the possibility of them assisting in the smoothing of output power variations, which could be caused by tidal turbulence and low rotor inertia [22, 46].

Some of the wind farm topologies and drive trains investigated in [49] that could also be adopted for tidal stream power generation systems are briefly discussed below.

The configuration featured in **Fig 1.7** is the most used topology for wind power, implemented on a 160 MW off-shore wind farm in Denmark [49]. It is also one of the preferred topology for tidal power generation [22].
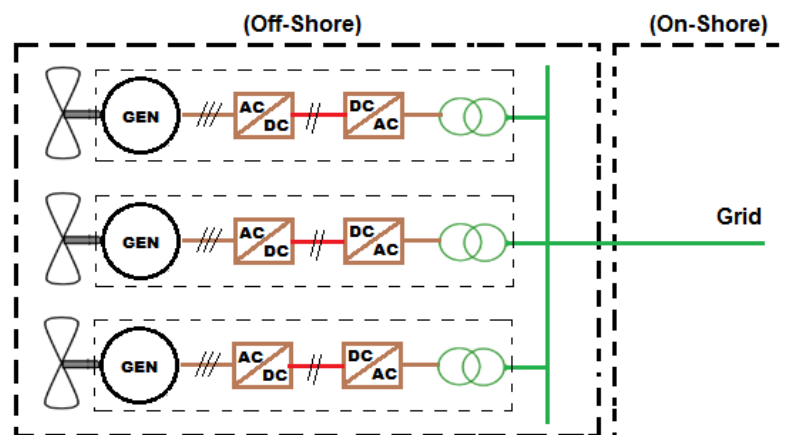
Fig 1.7*: Tidal power generation system coupled to a common AC grid via back-to-back converters*

The rotors have variable speeds over approximately a 3:1 speed range, from ~5 to ~15 rpm [50]. Either fixed or variable-pitch blades could be used given that power-

electronic converters can be used to determine the power (and torque) off-take at different speeds. The nacelles comprise of gearboxes, variable-speed 3-phase generators with 2 pole-pairs, and back-to-back power converters rated for the full power output. A transformer is also employed to step-up the generated voltage to match grid voltage.

This topology could be employed for tidal power capture because of the following reasons.

- It is a well-established technology (tried and tested within the wind power industry)

- Gearbox wear is minimal due to individual machine control

- Both active and reactive power control is possible as well as power factor control

- Loss of a single converter would only affect a single turbine, leaving the farm operable as the faulty turbine awaits repair.

- Auxiliary power in the nacelle is readily available thus the turbine doesn't require power from the grid.

Nonetheless this topology has its drawbacks i.e. depending on the distance to shore an offshore hub may be required, which would mean more system components offshore that would require maintenance. Given that the gearbox and converter are submerged 30-80m under the sea, failures of these components would be costly and time consuming to rectify which would lead to substantial loss of energy.

The configuration in *Fig 1.8* removes the need for converters in the nacelle leaving only the gearbox and generator. However, given that all devices are connected in parallel onto the grid this topology presents significant risk in terms of potential effects of tidal stream turbulence and velocity differences at the different turbine locations causing variations in frequencies and voltages generated by individual machines.
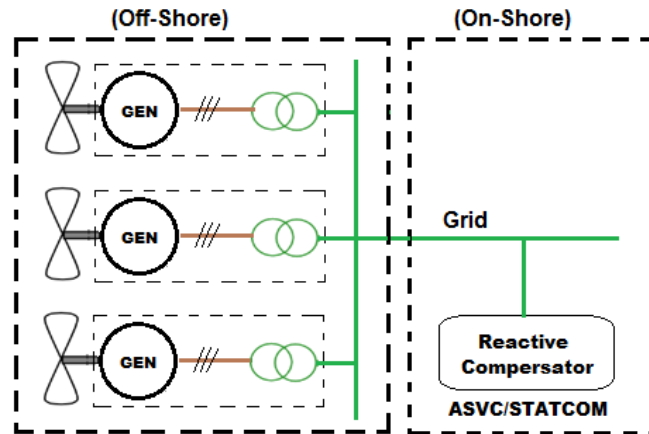
Fig 1.8: Pitch and reactive compensation controlled Induction generator with an AC grid

This topology would not work well with tidal stream power harnessing because of the following reasons

- It would not be possible to control both active and reactive power injected into the grid if fixed pitch blades were employed.

- Turbulence and tidal velocity variations across the array may cause torque ripples as the devices on the same array runs at a different speed.

The configuration in *Fig 1.9* removes the converters from the nacelles, leaving the gearboxes, induction machines and transformers. Back-to-back converter(s) are employed to interface the variable-frequency AC to grid-frequency AC.

Given that all the devices connected in parallel onto the grid are expected to have variable frequencies and voltages, the controllability of this topology for tidal power extraction is limited. Furthermore, system performance degrades when the rotor shaft speed differences at the various turbine locations become significant.
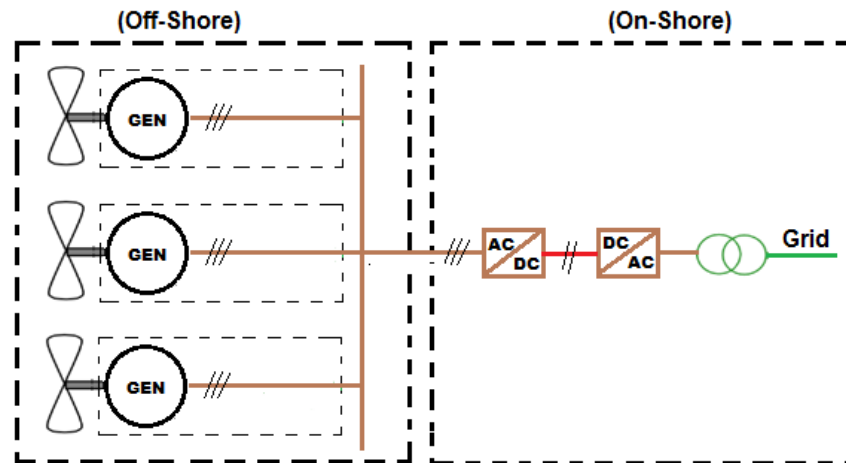
Fig 1.9: *Speed controlled induction generator with a common AC grid and DC transmission reactive power*

This topology would not work well with tidal stream power harnessing because of the following reasons

- Failure of the shared converter would disable the entire tidal farm

- Turbulence and tidal velocity difference across the array would affect power capture and may cause torque ripples.

- Auxiliary power needs to be taken from the AC supply which is at variable-frequency and variable voltage.

Nonetheless this topology does present some advantages that could be beneficial to tidal stream power development i.e. The Grid Code compliance is provided by a single pair of converters, which is situated onshore to provide easy access for maintenance consequently reducing downtime in case of converter failure.

The configuration in ***Fig 1.10*** removes some of the converter "halves" from the turbine nacelles (compared to ***Fig 1.7***) and instead places a larger, shared converter on shore for easy maintenance.
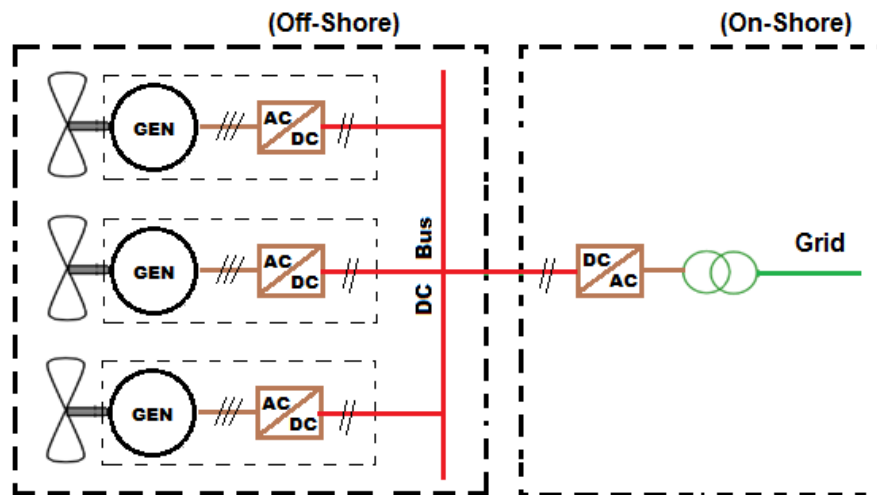
Fig 1.10: *Speed controlled induction generator with a common DC-bus and control of active and reactive power*

This topology could be employed for tidal power capture because of the following reasons.

- It is a well-established topology for wind farms.

- Gearbox wear is minimal due to individual turbine control

- Loss of a converter will only affect a single turbine, maintaining system operation as the failed turbine awaits repair

Nonetheless this topology has its drawbacks including;

- Depending on the distance to shore an offshore hub may be required, which would mean more system components offshore that would require maintenance.

- Failure of the shared converter affects all turbines sharing the DC bus disabling the entire tidal array leading to loss of power.

- Gearbox/converter failures will be costly and time consuming to rectify which may lead to substantial loss of energy.

- Auxiliary power in the nacelle has to be taken from the local AC supply which is at variable-frequency and voltage.

All the aforementioned possible tidal farm topologies could be best implemented with gearboxes; since employing a gearless tidal power generation system would significantly increase capital cost given that the development of a larger nacelle could be required to accommodate the enlarged generator.

1.1.7   Reliability

Since there isn't a fully functional tidal farm to date, reliability data of multiple turbines connected together to form an array of turbines can only be based on offshore and onshore wind farms. Nonetheless, reliability data in relation to wind turbines is limited, given that such data is often sensitive. Various publications with regards to wind turbines reliability were found [51-54] although the data presented varies extensively between these papers. Moreover some of the presented data is relatively old even for new publications such as [53].

Nonetheless, the information presented demonstrates some unexpected characteristics, for example it was envisaged that the failures of mechanical components including the generator were more frequent compared to electrical and control failures. However, the information presented shows that the Gearbox and generator failure rates are actually quite low although would still result in significant downtime as shown in and **Fig 1.11.**

Annual Failure Frequency

	Electrical System	Electronic Control	Rotor Blades	Mechanical Brake	Gearbox	Generator	Drive train
Percentage (%)	0.6	0.45	0.2	0.15	0.1	0.1	0.05

Down time per Failure

	Electrical System	Electronic Control	Rotor Blades	Mechanical Brake	Gearbox	Generator	Drive train
Days	1.5	1.8	4	2.5	6.2	7.5	5.8
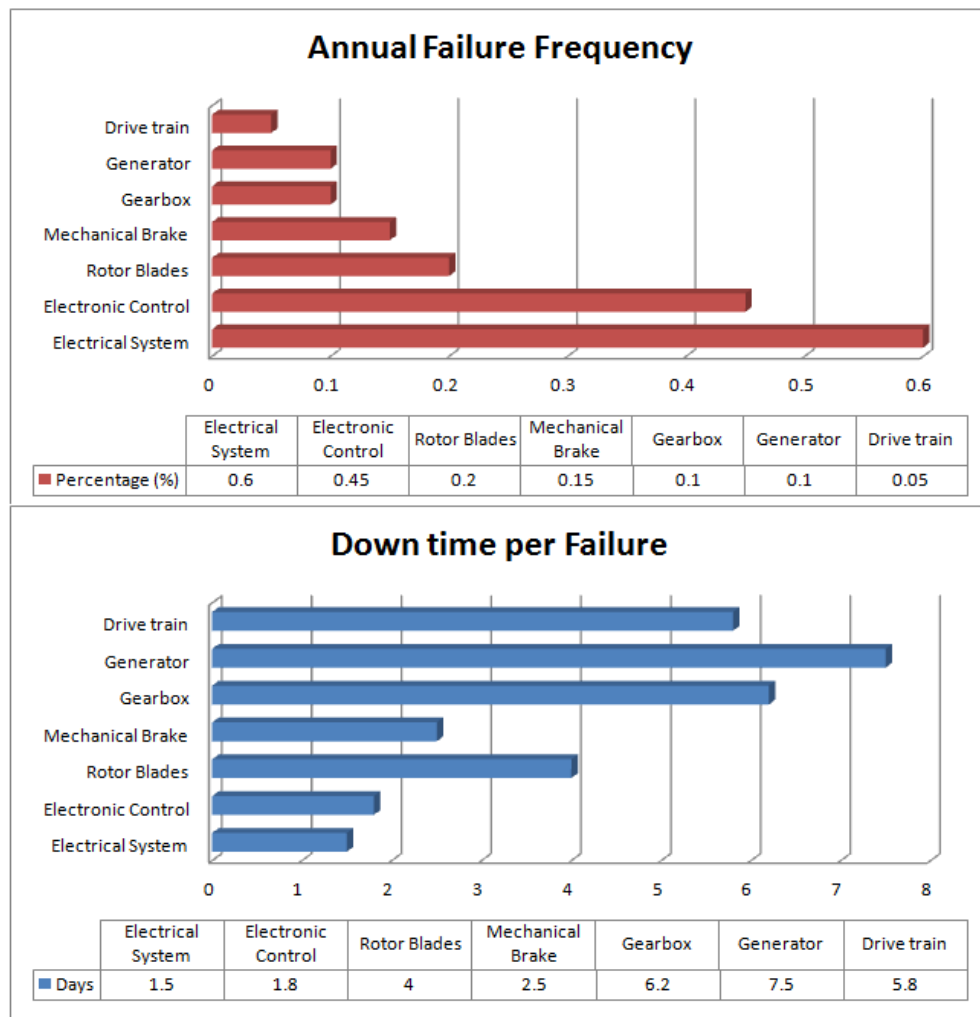
Fig 1.11: *Failure frequency and downtimes of components from [52]*

Electrical and control failure rates are much more common, but result in smaller downtimes per failure.

However, it could be said that many of the recorded electrical control faults may be due to inadequate software control resulting in over-currents during grid faults. The main reason for thinking along these lines is that within the wider low-voltage/low power AC machine drives community, motor control units do not have the same reputation for unreliability [55-56] suggesting that maybe the hardware is generally reliable, and perhaps the converter software could not deal with atypical grid situations.

The frequent electrical failures could also have happened due to the complexity of the electrical hardware at high power generation systems, given that electrical failures increase with the system's power rating.

1.1.8   Typical costs of existing wind farms

The cost breakdown given in this sub-section is to provide a viewpoint for tidal power generation. Only onshore and offshore wind power projects are considered given that these technologies are relatively mature compared to tidal power, in addition to the availability of data. Moreover, the challenges faced by the offshore wind energy industry are similar to those expected with tidal power production i.e. reliability is paramount because the device is harder to access for maintenance due to the environment in which they are installed, consequently repairs will take longer and cost more (both in actual terms and also in lost revenue).

An offshore installation of a wind turbine is relatively expensive compared to an onshore installation. i.e. An offshore installation could raise the typical capital cost of an onshore wind farm installation from ~€0.8-1M per MW (onshore) [57] to ~€1.2-2.2M per MW (offshore) [57-58], where between 10% and 30% [57-58] is grid connection cost. **Table1.2, Table1.3** and **Table1.4** give more of a breakdown of the costs.

	Installation cost share (%) (Onshore)	Installation cost share (%) (Offshore)
Turbine	74-82	30-50
Foundation	1-6	15-25
Installation	1-9	1-30
Grid Connection	2-9	15-30
Others	1-5	8
Total installation cost	800-1100 EUR/kW	1200-2000 EUR/kW

Table1.2: Comparison of onshore and offshore wind farm costs as per [57]

	Water Depth (m)				
	10-20	20-30	30-40	40-50	
Turbine	772	772	772	772	Cost (EUR/kW)
Foundation	352	466	625	900	
Installation	465	465	605	605	
Grid Connection	133	133	133	133	
Others	76	85	92	105	
Total instalation cost	1798	1921	2227	2515	
scale factor	1	1.067	1.237	1.396	

Table1.3: *Wind farm costs with increasing depths as per [57]*

Water Depth (m)	Distance to coast (km)							
	0-10	10-20	20-30	30-40	40-50	50-100	100-200	>200
10-20	1	1.022	1.043	1.065	1.086	1.183	1.408	1.598
20-30	1.067	1.09	1.113	1.136	1.159	1.262	1.501	1.705
30-40	1.237	1.264	1.29	1.317	1.344	1.464	1.741	1.977
40-50	1.396	1.427	1.457	1.487	1.517	1.653	1.966	2.232

Table1.4: *Wind farm cost multipliers with distance (from coast) and depth as per [57]*
Some very approximate breakdown costs of wind turbine components are given in [59]. XLPE cables cost in the region of $5000-$44000 per MWkm [60].

Therefore, an optimum tidal farm topology would be one with the lowest system capital, installation and maintenance cost scenario in addition to improved reliability, moreover these costs depend on site location. It should be noted that tidal stream power generation is an unproven technology with no large scale facilities to date continuously generating electricity onto the utility grid. Therefore there is currently no standard architecture, nonetheless a variety of conceptual and prototype designs are being explored with many close to practical large scale demonstration [22].

1.2   Summary

In the UK, tidal power is considered to be one of the most available and practically viable renewable power sources due to country's geographical location, although it still remains unexploited. Tidal stream turbines use the same principle as wind turbines to harness energy from tidal currents. A conventional horizontal axis turbine consists of

three or four blades fixed onto the shaft which turns an electrical generator, typically via a gearbox to attain the high speeds necessary for economic electrical power generation.

Due to much higher density of sea water compared to air, a single tidal stream device could generate relatively high amounts of power at much lower tidal stream speeds, i.e. at tidal speeds of approximately one-tenth of the wind speeds; a tidal stream turbine would supply the same amount of power as a wind turbine of the same size.

There are many advantages of using tidal power over other renewable energy sources and fossil fuel powered power plants, these include;

- Tidal stream power generation is highly efficient compared with other energy sources such as coal and oil at 30%, solar at 20%-30%, tidal energy efficiency is calculated at around 80%.

- Tidal stream power harnessing could aid in protecting the shoreline.

- Tidal stream power capturing devices have little or no visual impact.

- Tidal currents are generated all year round as a consequence it can be predicted.

Nonetheless, tidal devices have to be distributed over large areas and as a consequence the number of devices needed to generate electricity economically is high compared to those needed for conventional power stations. Moreover, given that tidal stream devices operate at depths of approximately 30-80m, access for maintenance is difficult.

In **Chapter 2** a novel tidal power generation system topology that aims at reducing the high costs associated with tidal power generation is proposed.

CHAPTER 2

2 PROPOSED RESEARCH

2.1 Introduction

In the previous chapter a brief review of the background of tidal power generation, the state-of-the-art technologies and costs for recent large offshore wind-farm deployments and their failures were discussed. Several possible tidal farm configurations adopted from existing wind farm deployments were presented, illustrating that some configurations were more favourable than others in suitability for tidal power farm deployment.

It was also perceived in **Chapter 1** that tidal power remains unexploited because of its high capital and operational costs that result from their underwater operating environment, and these costs must be reduced if tidal stream power generation is to be competitive with wind and conventional power sources. These high costs could be reduced by using simpler and cheaper components at the same time lowering component count, in particular those installed offshore and/or underwater.

2.2 Proposed system

This chapter presents a novel tidal stream power generation system referred to as "passive rectification to a common DC-bus", and describes the selection of components and control. The objective is to replace major cost components such as variable-pitched turbine blades and frequency converters in the nacelle with much simpler and cheaper components, in addition to locating as many components as possible onshore where costs are less. In particular the variable pitch blade mechanism is complex, has a large power demand, and has to operate day after day submerged in water at depths below 30 m. Moreover with current tidal stream prototype designs, variable speed gear boxes and power frequency converters are employed in the nacelle.

This thesis shows that variable pitched blades, variable speed gearboxes and frequency conversion in the nacelle may be replaced by a much simpler system that uses fixed pitch blades, a fixed ratio gearbox, generator excitation control system, and diode bridge rectifier. It is understood that all these components are generally cheaper, lighter, have a lower power demand and are more reliable than the components they replace. Also some of the voltage and frequency conversion is carried out onshore where costs are much less.

2.2.1   Turbine nacelle

The proposed turbine nacelle is intended to reduce the number of components installed under water and also simplify the control mechanism within the nacelle, in turn reducing both capital and installation cost. Moreover fewer components should lead to improved system efficiency.

Fig. 2.1 shows the proposed turbine nacelle configuration.
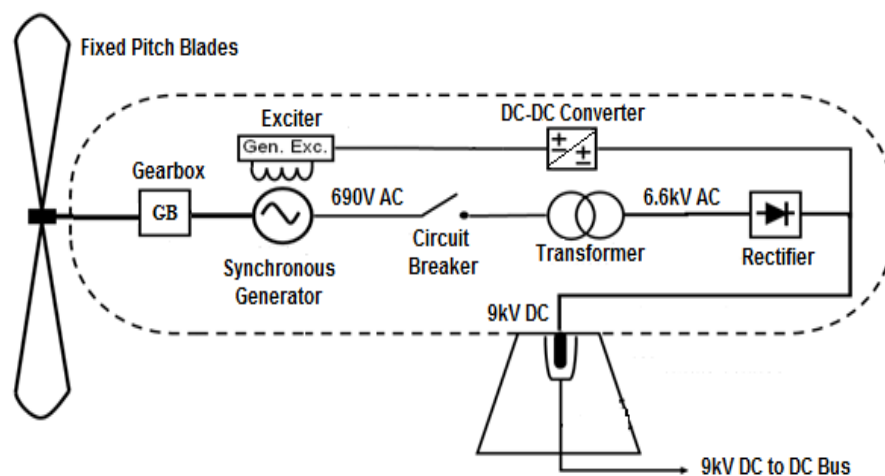
Fig. 2.1: Proposed Tidal turbine configuration schematic

From a design point of view, the proposed nacelle comprises of the following components as shown in *Fig. 2.1*:

- Fixed pitch Blades

- Synchronous generator with Exciter

- Diode rectifier

- Gearbox (optional)

- Transformer (optional)

2.1.1.1   Fixed pitch blades

Fixed pitches blades are proposed primarily due to their low capital cost and low maintenance. However, based on wind power studies in [61], fixed pitch blades would capture slightly less energy compared to a variable-pitch design. Nonetheless with a fixed pitch blade configuration the lost revenue in maintenance cost is less due to lower downtime [62] as there are no moving parts to fail. Moreover, capital cost is less because no blade control is required.

It should be noted however that in the wind power industry variable pitch blades are preferred because modern wind turbines are designed such that the turbine blades can turn slowly in low winds and/or turn much faster in high winds which is achieved when blade pitch is adjusted appropriately. The reason for this is that it lowers the cut-in speed of the turbines and optimises the energy capture by allowing a roughly constant tip-speed ratio. It also allows the turbines to shed excess energy but maintain optimum power output during the high winds.

Power regulation with the proposed tidal topology will be achieved via generator field excitation control that not only simplifies system controllability but also reduces capital and installation costs. It is expected that tidal power regulation can be achieved with a single degree of control freedom as shall be discussed in the following sub-sections.

2.1.1.2   Gearbox (Optional)

To achieve sensible AC frequencies (20-50Hz) with a direct drive configuration for tidal power conversion would require approximately 200 pole-pairs in the AC machine. This would be relatively expensive to build due to the resultant machine diameter and to

house such a large number of poles a bigger turbine nacelle would be required. This implies that in case such a device was to be built the costs associated with its installation and maintenance would be high. Therefore, the use of direct-drive within tidal turbines may simply not be economical for tidal power deployment.

To overcome the problems associated with direct drive, and to minimise capital and installation costs, a fixed ratio gearbox is proposed for this system to increase the speed seen by the rotor. A fixed ratio gearbox is simpler and cheaper than a variable ratio gearbox, leading to lower capital costs and lower maintenance costs.

2.1.1.3   Synchronous generator

A separately excited synchronous generator is proposed for this system, as compared to the other generators summarised in *Table1.1:   Comparison summary of the various generators power control requirements for variable speed tidal turbines*, the machine flux can be regulated, and it is less likely to suffer from performance loss in the harsh sub-sea environmental conditions. Moreover its cost is significantly lower than PM machines as no permanent magnets are required.

Using a synchronous generator also allows for indirect generator torque regulation via field control. It will be shown in this thesis that field current control alone is sufficient enough to achieve both speed and torque regulation of the turbine without the need for mechanical governors.

2.1.1.4   Transformer (Optional)

A transformer is employed for the purpose of stepping up the generator terminal voltage to a higher value to reduce transmission losses, for example if a low voltage 400Vrms generator was used a transformer could be employed to step-up the voltage to 6600rms, equivalent to approximately 9 kV DC. This would be adequate for transmission distances up to about 9 km based on a common estimation of 1kV per km used in electricity supply (either AC line voltage or maximum DC voltage between conductors). On the other hand, the transformer could be eliminated by employing a HV generator instead of the combination of a generator and a transformer. However, tidal generators further offshore would require higher voltages and for likely tidal generator ratings up

to 1 MW, it may be more economical to use an LV generator and an HV transformer instead of an HV generator alone.

2.1.1.5   Diode rectifier

It is shown in *Fig 1.11: Failure frequency and downtimes of components from [52]*, that failure rates of electronic converters for wind turbines appear to be relatively high. Although this data appears not to be consistent with the wider performance of motor control units, the data published by wind power developers suggest so. Therefore in spite of the cause of the frequent electronic control failures, getting rid of the requirement for a controllable converter in the nacelle and replacing it with a diode bridge rectifier is considered a sensible option in this case, as the maintenance of the tidal generator will be significantly more onerous than for a wind turbine. Moreover, generator output power regulation will be achieved via machine field control. Furthermore, diode rectifiers are lighter, relatively cheaper and more reliable [63] than active rectifiers (converters), and are therefore more appropriate for sub-sea installation.

2.1.1.6   Operation Principle

The proposed tidal configuration is to operate as follows: when the tide flows the kinetic energy in the water is transformed into mechanical energy by fixed pitch tidal blades, which is sequentially transformed into electricity by the synchronous generator and a transformer. The generated AC power is then rectified to DC via a diode bridge rectifier. The rectified output is connected onto a sub-sea DC bus alongside the outputs of other generators thus eliminating the need for AC synchronisation with the grid which would be complex and expensive given that tidal velocity is variable. Generator shaft power is regulated via field excitation in order to achieve optimum power generation.

Field excitation is considered for this system because it eliminates the need for active rectifiers which are normally installed in pairs (back to back converters), therefore reducing the number of components located in the turbine nacelle under water, which consequently lessens maintenance time/cost, in addition to improving efficiency.

However it should be noted that drawing excitation power from the DC Bus which is at high voltage to feed a low voltage generator could require a complex multi-stage DC-DC converter which could be relatively expensive and complex.

The other device on the market that employs a similar operational principle is the Enercon Ltd E-series direct drive wind turbines. These devices employ a synchronous generator with a diode rectifier [48] as illustrated in *Fig. 2.2*.
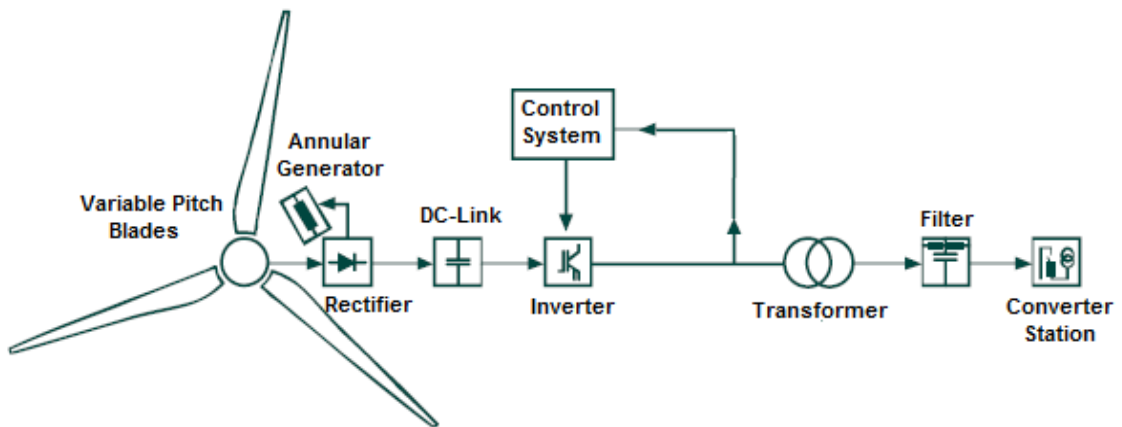
Fig. 2.2: Enercon DC wind turbine drive system topology

Although Enercon Ltd doesn't reveal in great detail how their devices power output is regulated it is envisaged that the field excitation technique is employed for the purpose of magnetising the annular generator and field current regulator. The use of variable pitch blades suggests that power regulation is achieved via pitched blade control. This topology differs from that proposed here as no blade pitch control is employed with the proposed topology, which utilises a single degree of control freedom i.e. via field current regulation alone.

2.1.2   Tidal stream power topology

Tidal stream power can only be profitable if low-cost electricity could be generated, thus the need for tidal farms i.e. tidal turbines have to be distributed over large areas to maximise resource utilisation and power generation.

Basically, the turbine nacelle in ***Fig. 2.1*** is used as a building block to form a tidal farm. The output DC power generated by each individual nacelle is fed in parallel onto a common DC-bus, and then a single cable from the DC-bus transmits the power to an onshore station where it is fed onto the utility grid via a DC-AC converter and transformer as shown in ***Fig. 2.3***
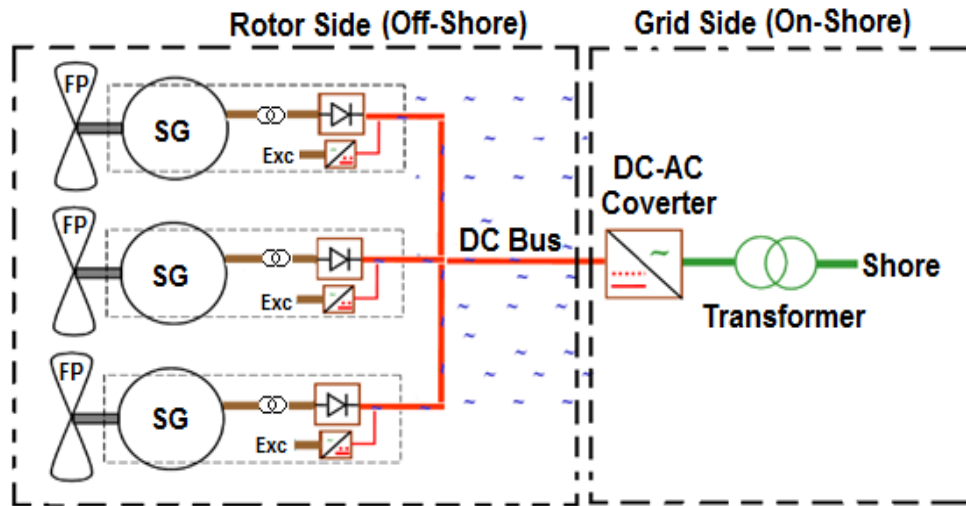
Fig. 2.3: *Proposed tidal farm topology with passive rectification to shore (nacelle transformers not shown for clarity*

The proposed tidal farm topology reduces the number of system components and therefore overall system complexity by effectively transferring much of the power conversion requirement from the individual turbine nacelles to the shore installation where costs are less and the conversion can be organised in bulk. Moreover, this method of installation makes maintenance easier in case of converter failure. Furthermore, the connection of several turbines together to a common subsea DC link reduces the number of cable runs to shore reducing capital and installation costs.

The choice of using a DC link circuit instead of an AC one can be justified as follows:

Implementing an AC link circuit would require all turbines on the same circuit to be synchronised together increasing the complexity of equipment in the nacelle. Moreover, additional system components such as variable pitched blades, variable ratio gearbox or

transmission, and power electronic frequency conversion could be required to generate grid standard electricity. This would in turn significantly increase both capital installation and maintenance costs.

A DC link circuit allows for the parallel connection of tidal turbines running at diverse speeds as only voltages need be matched. This can be done by fixing the DC-bus voltage given that tidal generators connect to the DC-bus via a diode rectifier the DC-bus voltage determines the terminal voltages of the generators connected to it.

2.1.3   Challenges

In view of the fact that multiple tidal turbines connect in parallel onto a common DC link circuit (DC-Bus), their terminal voltages must be equal at the point of connection. However, if the DC-bus voltage is fixed, all tidal generators that connect to it will inevitably have their terminal voltages equal to the DC-bus voltage. Moreover, if any of the tidal generators coupled to the DC-bus cannot generate a voltage higher or equal to the DC-bus voltage their associated diode rectifiers will remain reverse biased. Therefore power generation from the devices with the terminal voltages lower than the DC-bus voltage will be inhibited and they will not contribute to the overall tidal power generation on the DC-bus. It should be noted that local sea conditions will inevitably cause differences in the tidal stream velocities at different seabed locations, which could cause differences in terminal voltages generated by various tidal generators. In some of the cases terminal voltages could be less than the set DC-bus voltage.

The other challenge to be addressed is power regulation. Given that the proposed tidal turbine is composed of fixed pitch blades and connected to a bridge rectifier, power regulation cannot be undertaken in the conventional way i.e. via pitch blade control and/or electronic converter control. For that reason the proposed power regulation is to be achieved via generator field excitation control at individual machine level. This control method is implemented not only to achieve stable operation of interconnected turbine-generator systems, but also to maximise energy capture.

Tidal velocity is variable; therefore there may be situations where tidal velocity exceeds the design velocity. Therefore, due to the absence of blade pitch control typically used

to shed excess power in the wind power industry, the proposed tidal turbine will utilise field excitation control to shed excess power.

The operation of Diode rectifiers especially the 6-pulse rectifies generates high levels of low order harmonics in their input current. Nonetheless these harmonics can be minimised by employing filters. Additionally, other rectifier types could also be used to reduce harmonics i.e. a 12-pulse rectifier formed when two six-pulse rectifiers are connected in parallel onto a common DC bus link circuit [64] although such rectifiers have to be connected through a two secondary windings transformer to give a nearly ripple free current waveform compared to a single 6-pulse rectifier as illustrated in *Fig. 2.4*.
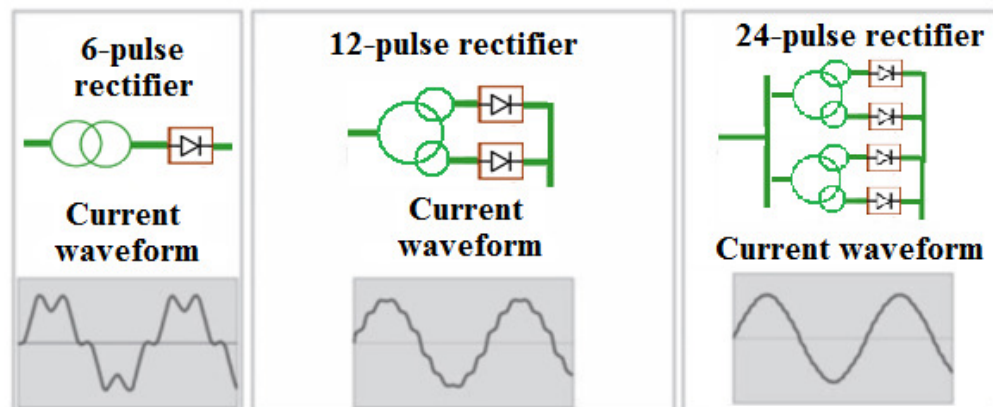
Fig. 2.4: Harmonics in line current with different rectifier constructions [43]

18-pulse and 24-pulse rectifiers could also be formed equally by linking multiple 6-pulse rectifiers [43]. The drawback for connecting multiple rectifiers together is that it would increases the number of components to be installed in the nacelle in addition to complicated cabling [65], which may raise capital installation and maintenance costs.

Tidal currents are extremely turbulent with a wide range of turbulent intensities of approximately 10% [66]. For that reason the effect of turbulence on turbine blades cannot be ignored. Turbulences are the main cause of gearbox wear and the core reason why gearboxes have the reputation for causing significant turbine down-time since the torque ripples caused by turbulence cause wear through variable stresses. Therefore the

effect of turbulence on the proposed fixed pitch blade tidal turbine with its power regulation carried out by field excitation alone must be investigated.

The proposed tidal topology is believed to be suitable for economical tidal power generation because of the following main reasons in addition to those discusses in previous subsections.

- No offshore hub is required because all power conversion is undertaken on shore.

- No fully-rated converters in the nacelle because power regulation is achieved via field current regulation

- Fixed-pitch rotor blades can be used which would simplify overall system controllability as well as reducing capital and maintenance costs.

Nonetheless this topology has its drawbacks/challenges that would need to be addressed and these include.

- Failure of the shared converter affects all turbines sharing the DC bus, however since the shared converter is located on shore, down time would be much less because the shared converter is easily accessible.

- Auxiliary power in the nacelle (for excitation) needs to be taken from a separate low-power DC-DC converter drawing power from the grid.

- Torque ripples due to 6-pulse rectification would be experienced; these could be managed by employing a suitable DC filter.

Therefore to address the above mentioned challenges the viability of this scheme was carefully examined with detailed electro-mechanical computer simulations to ensure that generator excitation can be controlled appropriately to achieve system power regulation.

2.3 Summary

This chapter described a novel cost effective tidal stream power generation system in which a group of 3-phase synchronous generators operating at diverse speeds are connected to a common DC bus via passive diode rectifiers. The proposed power topology reduces the amount of components required, while maximising efficiency, reliability and controllability, thereby facilitating a reduction in capital costs and in operational costs.

System power is regulated by controlling the field excitation of individual machines. Therefore, it is envisaged that generator field control alone is enough to achieve the required control.

The use of fixed pitch turbine blades instead of costly and more complicated variable pitch blades and fixed ratio gearboxes is also possible with the proposed tidal system configuration.

The proposed topology also reduces the number of cables to shore as only the single cable from the DC-bus runs to shore. Moreover, based on the reduction in system component count, size, weight and reliability, maintenance and capital installation cost are reduced compared to most reported prototype systems.

It should be noted that no other primary energy supply device (found during the course of this research) uses passive rectification onto a common stiff DC bus. Therefore the proposed tidal stream power extraction system viability was validated through computer and laboratory experimentation as discussed in the following chapters.

CHAPTER 3

3 TIDAL SYSTEM MODELLING

3.1 Introduction

In the previous chapters we discussed the generation and collection of power available at a distributed tidal generation site. Various tidal farm topologies together with their advantages and disadvantages were analysed in order to come up with the most economical grid connection methodology that could be adapted for a commercial tidal power installation. Based on this analysis a tidal farm topology termed "passive rectification to a common DC-bus" was proposed.

This chapter describes the development of an averaged model of the proposed tidal turbine topology as well as some aspects of its components selection. From a modelling viewpoint the proposed tidal system topology is composed of:

- Turbine rotor and blade assembly (prime mover).

- Synchronous Generator with diode rectifier (power generation).

- Shaft and gearbox unit (drivetrain);

3.1.1 Turbine Rotor and blade assembly

Just like wind turbines, tidal rotor blades operate by generating lift due to their shape as illustrated in *Fig 3.1*.
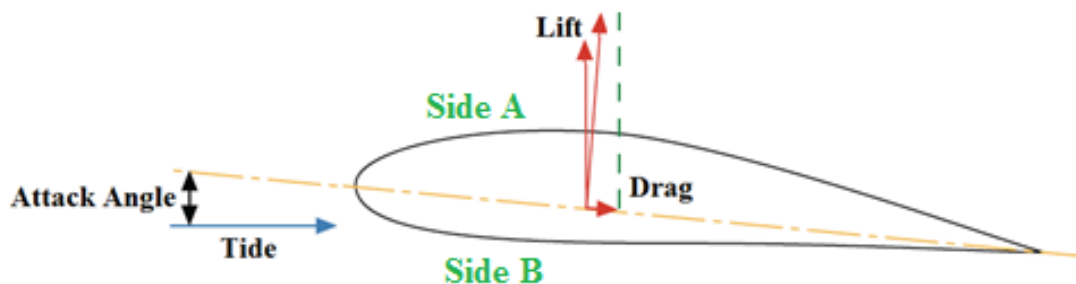
Fig 3.1: Tidal blade performance

"Side A" generates high flow across the blade surface which causes low water pressures, whilst high pressured slower moving water pushes on "Side B" resulting in a lift force perpendicular to the direction of the tide [67] consequently rotation.

The lift force rises when the blade centre line angle (attack angle) is greater than the tidal flow angle. However, when the attack angle becomes too large lift force decreases, which means that there is an optimum attack angle at which desired lift is generated. It is on this principle that blade pitch control operates.

When tidal blades are rotating the velocity of the tidal current is reduced just as it reaches the blades, thus the power available to the rotor also reduces. The theoretical maximum of the available tidal power that can be extracted from the tidal flow is 59%, commonly known as the Betz's limit illustrated in *Fig 3.2*. However, the Betz limit is a physical constraint, and when the other rotor design efficiencies are taken into account tidal rotor designs operate at less than Betz's limit. In practice the most sophisticated wind turbine designs can only operate at around 40-50% [68].
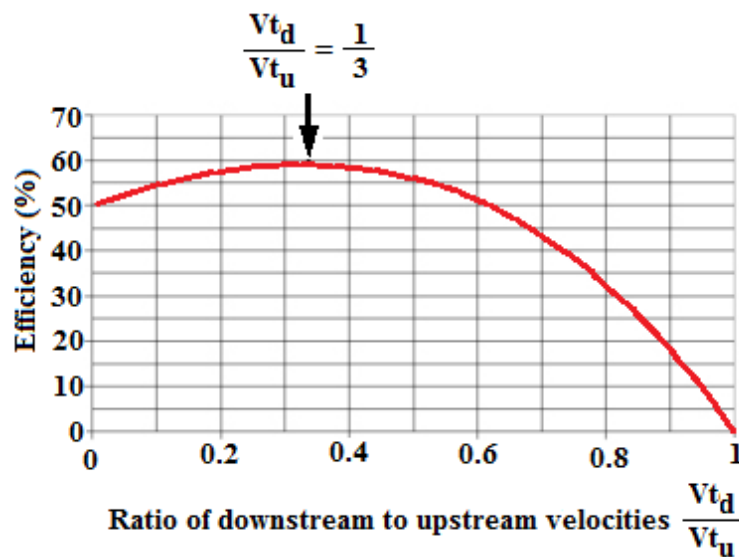
Fig 3.2: Maximum C_P [68]

3.1.1.1 Rotor design

When designing tidal blades it should be noted that tidal turbine blades are exposed to substantial pressure and torque that result from the high seawater density in which they are installed. These stress loadings create high bending moments at the blade root [69-

71], which could become a serious design limitation when manufacturing tidal blades with respect to system cost and blade dimensions.

The blade length/rotor diameter is determined by the desired tidal power to be harnessed at a given site bearing in mind the Betz's limit. The blade's hydrodynamic profile is due to its cross section area which enables it to create lift and rotate the turbine shaft as illustrated in *Fig 3.1*.

Another tidal rotor design consideration is the solidity (σ), defined as the fraction of the area swept by the turbine that is taken up by the blades. The solidity of a horizontal axis turbine can be calculated as [72]:

$$\sigma = \frac{N_b c_b}{2\pi R_m} \qquad\qquad 3.1$$

where N_b is the number of blades, c_b the average blade chord length and R_m the radius of the blade. Choosing a design value for the solidity is a trade-off between several parameters. The speed at which the tidal blades rotate is determined such that the hydrofoil tips are moving at seven to ten times the tidal velocity [71], with typically three blades [22]. Higher tidal velocities and number of blades means that each hydrofoil needs be thinner, making them relatively complex to manufacture with sufficient strength. Moreover at very high rotor speeds the blades become hydrodynamically inefficient, prone to erosion plus possible effects to marine life [73].

It should be noted that tidal turbine rotor blades should primarily be designed to achieve maximum power extraction at a given tidal site. However, due to economic constraints the rotor's hydrodynamic requirements for maximum power extraction may in most cases have to be compromised to keep the cost of blade construction low [74].

3.1.2   Synchronous Generator

It has been stated in the previous chapters that the generator converts turbine shaft power into electricity that is supplied to the utility grid. Most grid connected power generators are run at constant speed, this is primarily because the grid demands a fixed frequency [75-76] which translates to fixed generator speed. However most tidal and wind power developers opt for variable speed generators [22].

The main reason for employing variable speed generators is their increased efficiency compared to fixed speed generators [77], thus increased energy production. Moreover with variable speed generators shaft speed is not restricted to the network frequency, that is to say 157 rad/s for a 50 Hz network. Therefore, since tidal velocity varies on the six-hourly cycle [1], and the rotor/generator speed varies with tidal velocity, variable-speed generators are preferred if maximum power extraction is to be achieved economically.

3.1.3   Shaft and gearbox unit

The generator is coupled to the rotor via a gearbox which is an essential component because it converts the low rotor speeds generated by the tidal turbine into the high shaft speeds demanded by the generator.

The interaction between the tidal device components defined in previous sub-sections determine how much of the available power is extracted from the tidal currents. *Fig: 3.3* illustrate component interactions at a system level.
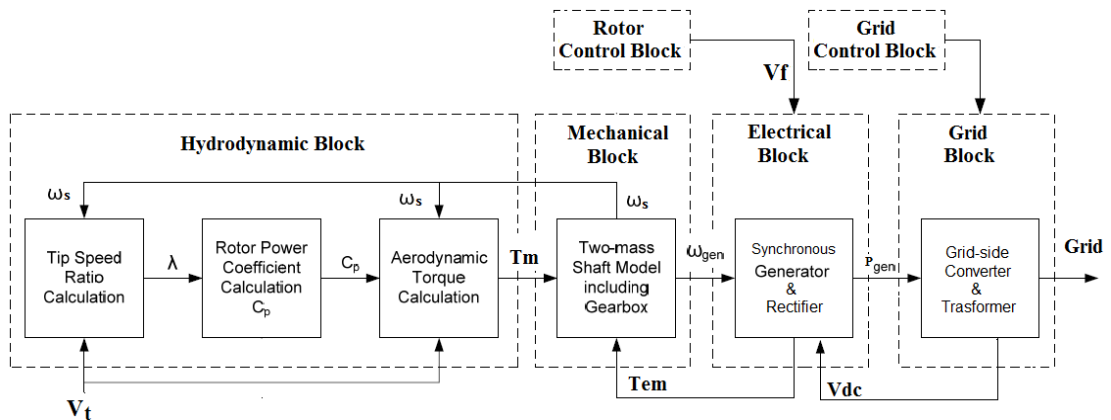
Fig: 3.3: Block Diagram of the implemented tidal turbine topology

The following sub-sections describe the modelling of these individual components with reference to the system's power transfer.

3.2 Hydrodynamic Block

The hydrodynamic block models the mechanical aspects of energy transfer from water flow into shaft torque. It comprises of three subsystems that include: tip-speed ratio calculation, rotor power coefficient calculation (C_p), and rotor torque calculation. Since

the primary objective for modelling the proposed tidal turbine topology is to analyse its dynamic system behaviour and given that generator/electrical transients are much faster than the mechanical transients, tidal velocity will be assumed constant at or during any electrical transient.

3.2.1   Tip speed ratio calculation

The percentage of the available power harnessed from the tidal current by the blades is determined by the tip speed ratio (TSR or λ). TSR is the ratio of the blade-tip linear speed to the tidal velocity and it can be realised as follows [78-79]:

$$\lambda = \frac{\omega_s . R_m}{V_t}$$ 3.2

ω_s = rotor angular speed [rad/s]

R_m= turbine blade radius [m]

V_t = Tidal velocity [m/s]

3.2.2   Turbine power coefficient (C_P) calculation

The TSR is used to determine the turbine power coefficient, denoted by C_p. The power coefficient is the efficiency of the turbine and can be realised as [78-80]:

$$C_p(\lambda) = C_1 \left(\frac{C_2}{\lambda_i} - C_3 \right) e \frac{-C_4}{\lambda_i} + C_5 \lambda$$ 3.3

$$\lambda_i = \frac{1}{\frac{1}{\lambda} - 0.035}$$ 3.4

In practice, there is a constant value of λ, which if maintained for all tidal velocities, will result in an optimal C_p as well as maximum power extraction from the given tidal velocity. C_1 to C_5 are turbine efficiency constants which in practice would be provided by the tidal rotor manufacturer identifying the efficiency of the rotor blades.

3.2.3   Hydrodynamic torque calculation

Tidal stream turbines transform the dynamic energy in flowing sea water into mechanical energy in the form of torque. The magnitude of the energy generated is dependent on the water density and the tidal currents speed. Therefore power available from the tidal currents (P_t) can be defined as [78-79, 81-82]:

$$P_t = \frac{1}{2}.\rho.A.V_t^3 \qquad\qquad 3.5$$

Where ρ is the density of sea water in kgm^{-3}, A is the area covered by the tidal blades as they rotate in m^2, and V_t is the velocity of the tidal currents in ms^{-1}. However, the tidal turbine blades cannot convert beyond 59% of the energy available in the flowing water into mechanical energy that turns the turbine shaft due to the Betz Limit [68]. Therefore there is a theoretical maximum power efficiency of any design of turbine referred to as the power coefficient C_p (λ). Thus, turbine mechanical power (P_{m_t}) [78-79] is defined as:

$$P_{m_t} = P_t.C_p(\lambda)$$

$$3.6$$

$$P_{m_t} = \frac{1}{2}.C_p(\lambda).\rho.A.V_t^3$$

Substituting (**3.2**) in (**3.6**) the turbine mechanical power equation becomes:

$$P_{m_t} = \frac{1}{2}.C_p(\lambda).\rho.A.\left(\frac{R_m}{\lambda}\right)^3.\omega_s^3 \qquad\qquad 3.7$$

The mechanical torque produced by the turbine (T_m) is defined as:

$$T_m = \frac{P_{m_t}}{\omega_s} \qquad\qquad 3.8$$

Thus,

$$T_m = \frac{1}{2}.\frac{C_{p(\lambda)}}{\lambda}.\rho.A.R_m.V_t^2 \qquad\qquad 3.9$$

3.3 Mechanical Block

The mechanical block is composed of the rotor shaft, generator shaft, and a gearbox. The shafts and the gearbox models can be represented as two-mass inertia rotational systems as defined in [83-85]. The mechanical model can be derived from a free-body disk with a moment of inertia **J,** damping **B** and shaft stiffness **K** as illustrated in **Fig 3.4**.
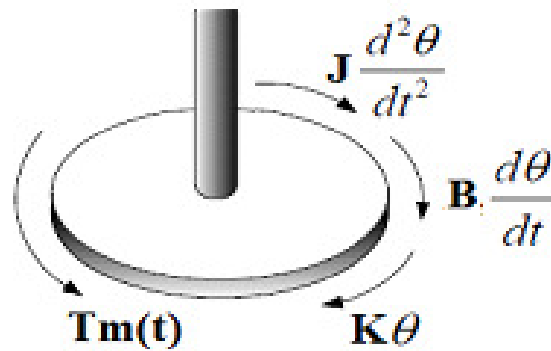
Fig 3.4: Block Diagram of the implemented tidal turbine model

The torque acting on the disk in *Fig 3.4* can be defined as in (**3.10**):

$$T_m(t) = J\frac{d^2\theta(t)}{dt^2} + B\frac{d\theta(t)}{dt} + K\theta(t) \qquad 3.10$$

The entire tidal configuration as a rotational system consisting of two sub-systems in *Fig 3.4,* can be represented as in *Fig 3.5*. The two sub-systems (Turbine and Generator) are coupled through a gear box, where T_m is the external torque applied to the Turbine system, T_{mT}, T_{mG} are transmitted torques. N_T, N_G are the numbers of teeth of the Turbine Gear and Generator Gear. J_T, J_G, B_T, B_G, K_T, K_G are the moments of inertia, damping, and stiffness of the Turbine and Generator respectively. The system is still time-dependent but the notation (**t**) is removed for clarity.
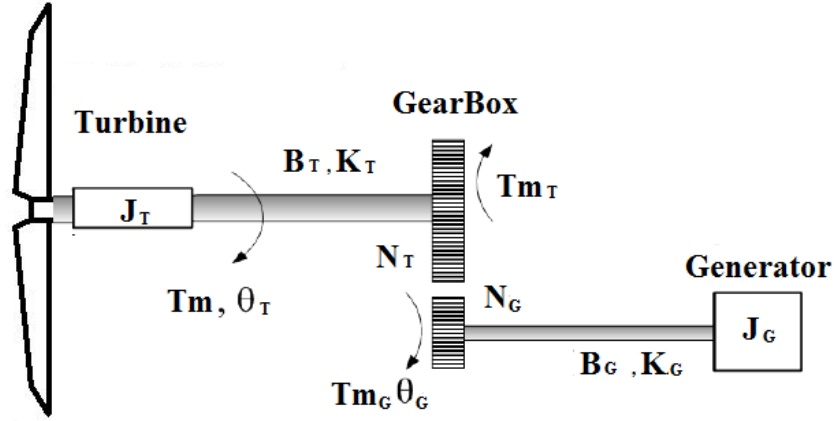
Fig 3.5: Turbine rotational system Block Diagram including Gearbox

Applying (**3.10**) to the system in *Fig 3.5* describes the torque equation at

J_T as (**3.11**),

$$T_{mT}(t) = J_T \frac{d^2\theta_T(t)}{dt^2} + B_T \frac{d\theta_T(t)}{dt} + K_T\theta_T(t) \qquad 3.11$$

J_G as

$$T_{mG}(t) = J_G \frac{d^2\theta_G(t)}{dt^2} + B_G \frac{d\theta_G(t)}{dt} + K_G\theta_G(t) \qquad 3.12$$

Since $T_{mT} = (N_T/N_G)T_{mG}$ and $\theta_G = (N_T/N_G)\theta_T$ due to the presence of the gearbox the quantities on the generator side can be referred to the turbine side as:

$$T_{mT} = \left(\frac{N_T}{N_G}\right)\left(J_G \frac{d^2\theta_G}{dt^2} + B_G \frac{d\theta_G}{dt} + K_G\theta_G\right) \qquad 3.13$$

$$T_{mT} = \left(\frac{N_T}{N_G}\right)\left|J_G \left(\frac{N_T}{N_G}\right)\frac{d^2\theta_T}{dt^2} + B_G \left(\frac{N_T}{N_G}\right)\frac{d\theta_T}{dt} + K_G \left(\frac{N_T}{N_G}\right)\theta_T\right| \qquad 3.14$$

$$T_{mT} = J_{refl} \frac{d^2\theta_T}{dt^2} + B_{refl} \frac{d\theta_T}{dt} + K_{refl}\theta_T \qquad 3.15$$

Where $J_{refl}, B_{refl},$ and K_{refl} are the quantities reflected on the Turbine's side. Substituting (**3.13**) into (**3.11**) and rearranging, we obtain (**3.16**) for the applied torque.

$$T_m(t) = J_{eq} \frac{d^2\theta_T(t)}{dt^2} + B_{eq} \frac{d\theta_T(t)}{dt} + K_{eq}\theta_T(t) \qquad 3.16$$

Where:

44

$$J_{eq} = J_T + J_G \left(\frac{N_T}{N_G}\right)^2 = J_T + J_{refl} \qquad\qquad 3.17$$

$$B_{eq} = B_T + B_G \left(\frac{N_T}{N_G}\right)^2 = B_T + B_{refl} \qquad\qquad 3.18$$

$$K_{eq} = K_T + K_G \left(\frac{N_T}{N_G}\right)^2 = K_T + K_{refl} \qquad\qquad 3.19$$

Therefore the system in *Fig 3.5* can now be reduced to an equivalent system shown in *Fig 3.6* where the gearbox is eliminated.
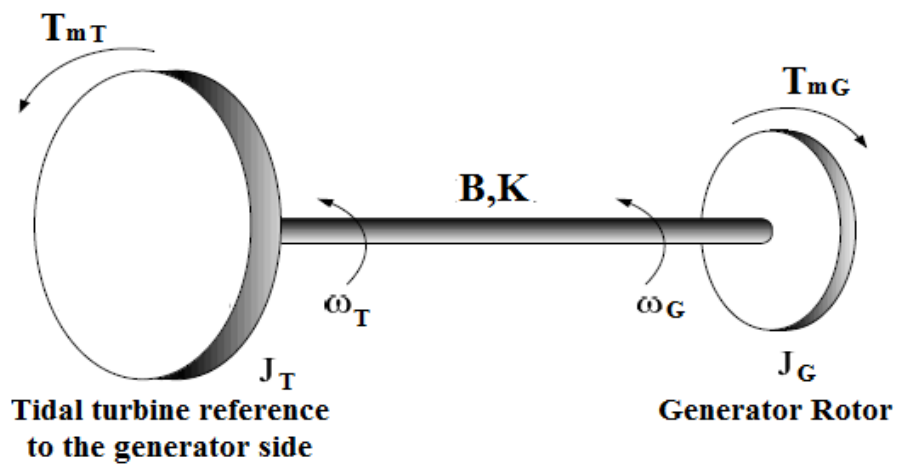
Fig 3.6: Turbine rotational system equivalent block diagram

(**3.11**) – (**3.19**) represents the model of the proposed tidal turbine, furthermore it simplifies the tidal turbine configuration as shown in *Fig 3.6* where the drivetrain is modelled as a two-mass system coupled through a gear train eliminating the gear ratio. Elimination of the damping, stiffness and inertia effects of the gearbox from the mechanical model is justified given that the tidal turbine rotor inertia is considerable when compared to that of the gearbox [84-85].

3.4 Electrical block

Electromechanical generators are required to convert the mechanical power from the turbine shaft into electricity.

From a modelling standpoint, the electrical block presented in *Fig: 3.3* consists of the following components:

- Synchronous Generator

- Diode rectifier

- Grid-side converter

3.4.1 Synchronous Generator (SG)

This section will focus on the realisation of a full mathematical representation of a synchronous generator, taking into account all relevant machine dynamic behaviour. However since this model is well known, only the generator characteristics relevant to this study will be presented.

3.4.1.1 SG Model

A 3-phase SG contains three identical armature windings each placed 120° electrical degrees apart around the air-gap, and a single field winding. The flux generated by the armature windings and the field winding is essentially sinusoidal. The armature windings are generally located on the stator, while the field windings are located on the rotor as illustrated in *Fig 3.7*.
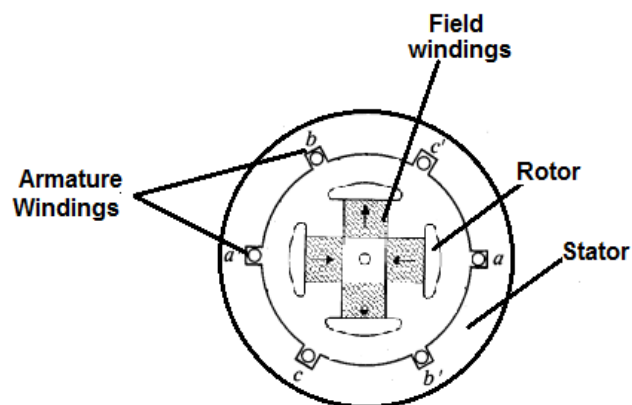
Fig 3.7: Salient-pole Synchronous generator section

However armature windings could be located on the rotor and field winding on the stator like in external rotor configurations. Nevertheless, this does not change the overall system dynamics, as the rotor and the stator behaviour remain unchanged.

The generator's electrical equations are realised through Kirchhoff's voltage law by equating the total of resistive and inductive voltage drops to the voltage across each winding [86]. For example:

$$V_a = R_a i_a + \frac{d\varphi_a}{dt} \qquad\qquad 3.20$$

For a symmetric 3 phase generator;

$$V_a = V_b = V_c \qquad\qquad 3.21$$

$$R_a = R_b = R_c \qquad\qquad 3.22$$

$$i_a = i_b = i_c \qquad\qquad 3.23$$

$$\varphi_a = \varphi_b = \varphi_c \qquad\qquad 3.24$$

where, V_a, V_b, V_c are the voltages across the windings, R_a, R_b, R_c are the windings resistances and $\varphi_a, \varphi_b, \varphi_c$ are the total flux linkages of the windings of phases *a b* and *c* respectively.

a b and *c* phase windings flux linkages can be defined as mutual and self-inductances as follows:

$$\varphi_a = \varphi_{aa} + \varphi_{ab} + \varphi_{ac} + \varphi_{af} \quad = \quad L_{aa} i_a + L_{ab} i_b + L_{ac} i_c + L_{af} i_f \qquad 3.25$$

$$\varphi_b = \varphi_{ba} + \varphi_{bb} + \varphi_{bc} + \varphi_{bf} \quad = \quad L_{ba} i_a + L_{bb} i_b + L_{bc} i_c + L_{bf} i_f \qquad 3.26$$

$$\varphi_c = \varphi_{ca} + \varphi_{cb} + \varphi_{cc} + \varphi_{cf} \quad = \quad L_{ca} i_a + L_{cb} i_b + L_{cc} i_c + L_{cf} i_f \qquad 3.27$$

where

$$L_{aa} + L_{bb} + L_{cc} = L_{aa0} + L_{al} \qquad\qquad 3.28$$

$$L_{ab} = L_{ba} = L_{ac} = L_{ca} = \frac{L_{aa0}}{2} \qquad\qquad 3.29$$

$$L_{af} = L_{afm} \cos(\theta) \qquad\qquad 3.30$$

$$L_{bf} = L_{afm} \cos(\theta - 120) \qquad\qquad 3.31$$

$$L_{cf} = L_{afm} \cos(\theta - 240) \qquad\qquad 3.32$$

For a balanced 3phase machine $L_{aa0} = \frac{\varphi_{aa0}}{i_a}$, $L_{al} = \frac{\varphi_{al}}{i_a}$, φ_{aa0} is the flux that links all three phase windings, φ_{al} is the flux that links only phase *a* winding and $\theta = \omega_t + \theta_0$

When the stator windings are excited by balanced 3 phase currents;

$$i_a + i_b + i_c = 0 \tag{3.33}$$

The total flux linkage of phase a could be further defined as follows:

$$\varphi_a = (L_{aa0} + L_{al})i_a - \frac{L_{aa0}i_b}{2} + L_{afm}i_f \cos(\omega_t + \theta_0) \tag{3.34}$$

$$= (L_{aa0} + L_{al})i_a - \frac{L_{aa0}i_b + i_c}{2} + L_{afm}i_f \cos(\omega_t + \theta_0) \tag{3.35}$$

$$= (L_{aa0} + L_{al})i_a - \frac{L_{aa0}i_a}{2} + L_{afm}i_f \cos(\omega_t + \theta_0) \tag{3.36}$$

$$= \left(\frac{3L_{aa0}}{2} + L_{al}\right)i_a + L_{afm}i_f \cos(\omega_t + \theta_0) \tag{3.37}$$

$$= L_s i_a + L_{afm}i_f \cos(\omega_t + \theta_0) \tag{3.38}$$

$$\text{where } \varphi_f = L_s i_a + L_{afm}i_f \tag{3.39}$$

where

$$L_s = \frac{3L_{aa0}}{2} + L_{al} \tag{3.40}$$

referred to as the synchronous inductance.

This allows for the three windings to be decoupled, thus for symmetric generator windings only the equation of one of the phase needs to be realised. Substituting the flux linkage equations into (**3.20**), (**3.41**) can be realised

$$V_a = -R_a i_a - L_s \frac{di_a}{dt} + \frac{d\varphi_{af}}{dt} \tag{3.41}$$

It should be noted that (3.41) is derived for a generator thus phase current is flowing to the negative terminal.

Based on the model equations defined above it was concluded that modelling a SG in the *abc* reference frame would be more complex, resulting in bulky and lengthy equations. This is mainly because the machine parameters in the *abc* frame are time variant and affected by the continuously increasing rotor position **(θ)**. Therefore transforming the generator parameters to the rotor reference frame *(dq)* in which the machine parameters are seen as constant creates more manageable model equations.

The *dq* and *abc* transformations can be obtained from the *Park's transformations*[1] defined below in (**3.42**) and (**3.43**) [87]:

$$\begin{bmatrix} v_d \\ v_q \end{bmatrix} = \sqrt{\frac{2}{3}} \cdot \begin{bmatrix} \cos(\theta) & \cos(\theta - 120^\circ) & \cos(\theta + 120^\circ) \\ -\sin(\theta) & -\sin(\theta - 120^\circ) & -\sin(\theta + 120^\circ) \end{bmatrix} \cdot \begin{bmatrix} v_a \\ v_b \\ v_c \end{bmatrix} \qquad 3.42$$

$$\begin{bmatrix} v_a \\ v_b \\ v_c \end{bmatrix} = \sqrt{\frac{2}{3}} \cdot \begin{bmatrix} \cos(\theta) & -\sin(\theta) \\ \cos(\theta - 120^\circ) & -\sin(\theta - 120^\circ) \\ \cos(\theta + 120^\circ) & -\sin(\theta + 120^\circ) \end{bmatrix} \cdot \begin{bmatrix} v_d \\ v_q \end{bmatrix} \qquad 3.43$$

The transformation Eqns (**3.42**) and (**3.43**) are magnitude invariant and apply equally to currents, voltages and flux linkages. Thus at any time instant, the variables in *abc* reference frame can be transformed to *dq* reference frame.

Fig 3.8 shows the *dq* axis and the rotor angle **(θ)**, which is measured between the magnetic axis of the armature's phase *a* and the rotor's d-axis which corresponds to the magnetic axis of the rotor.

---

[1] Direct–Quadrature (dq) transformation in the case of balanced three-phase circuits, reduces the three AC quantities to two DC quantities simplifying the calculations
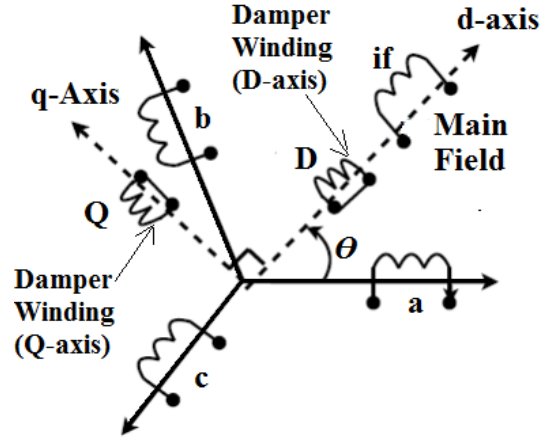
Fig 3.8: Synchronous generator winding with dampers

Therefore assuming, at $\theta = 0$ the rotor flux axis (*d*-axis) is in phase with the armature's phase (*a*) axis, the flux linkage of each phase due to the field/rotor winding current is given by:

$$\varphi_{af} = \varphi_f . \cos\theta \qquad\qquad 3.44$$

$$\varphi_{bf} = \varphi_f . \cos(\theta - 120^\circ) \qquad\qquad 3.45$$

$$\varphi_{cf} = \varphi_f . \cos(\theta + 120^\circ) \qquad\qquad 3.46$$

The SG model can be defined as described in (**3.47**)-(**3.57**) below in the *dq* reference frame [86, 88]:

Armature equations

$$v_d = -R_s . i_d - \omega\varphi_q - L_d \frac{di_d}{dt} + L_{md}\left(\frac{di_f}{dt} + \frac{di_{kd}}{dt}\right) \qquad\qquad 3.47$$

$$v_q = -R_s . i_q + \omega\varphi_d - L_q \frac{di_q}{dt} + L_{mq}\frac{di_{kq}}{dt} \qquad\qquad 3.48$$

Where;

$$\varphi_d = -L_d \cdot i_d + L_{md}(i_f + i_{kd}) \tag{3.49}$$

$$\varphi_q = -L_q \cdot i_q + L_{mq} \cdot i_{kq} \tag{3.50}$$

$$L_d = (L_{ls} + L_{md}), \quad L_q = \left(L_{ls} + L_{mq}\right) \tag{3.51}$$

Field equation

$$v_f = R_f \cdot i_f + L_f \frac{di_f}{dt} + L_{md}\left(\frac{di_{kd}}{dt} - \frac{di_d}{dt}\right) \tag{3.52}$$

Where:

$$L_f = (L_{lf} + L_{md}) \tag{3.53}$$

Damper winding equations

$$0 = R_{kd} \cdot i_{kd} + L_{md}\left(\frac{di_f}{dt} - \frac{di_d}{dt}\right) + L_{kd} \cdot \frac{di_{kd}}{dt} \tag{3.54}$$

$$0 = R_{kq} \cdot i_{kq} - L_{mq} \frac{di_q}{dt} + L_{kq} \cdot \frac{di_{kq}}{dt} \tag{3.55}$$

Where;

$$L_{kd} = L_{lkd} + L_{md}, \tag{3.56}$$

$$L_{kq} = L_{lkd} + L_{mq} \tag{3.57}$$

Parameters and variables in the above equations have the following meanings:

- ω: $\omega = p\,\theta$, angular velocity of rotation (in electrical rad/Sec.);
- v_d – armature terminal d axis voltage;
- v_q - armature terminal q axis voltage;
- i_d - armature terminal d axis current;
- i_q - armature terminal q axis current;
- v_f – terminal voltage of the field winding reflected to the stator;
- i_f – terminal current of the field winding reflected to the stator;
- i_{kd} - d axis damper winding current reflected to the stator;
- i_{kq} - q axis damper winding current reflected to the stator;
- L_d - d axis total armature flux;
- L_q - q axis total armature flux;
- R_s - phase resistance of the armature;
- L_{ls} - phase leakage inductance of the armature;
- L_{md} - coupling inductance of the a axis;
- R_f – resistance of the field winding reflected to the stator;
- L_{lf} - leakage inductance of the field winding reflected to the stator;
- R_{kd} - d axis damper winding resistance reflected to the stator;
- L_{kd} - d axis damper winding leakage inductance reflected to the stator;
- L_{mq} - q axis coupling inductance;
- R_{kq} - q axis damper winding resistance reflected to the stator;
- L_{kq} - q axis damper winding leakage inductance reflected to the stator.

The electromagnetic torque can be presented in the *dq* reference frame is shown below:

$$T_{em} = \frac{3}{2}\cdot p\cdot\left(\varphi_d\cdot i_q - \varphi_q\cdot i_d\right) \qquad 3.58$$

From the *dq* voltage equations shown above, the SG equivalent circuits are derived as illustrated in *Fig 3.9* below:
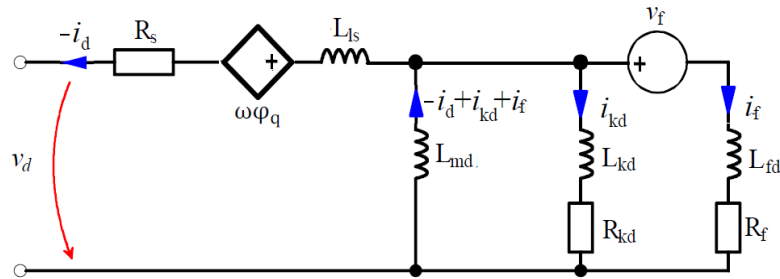
a): SG rotor equivalent circuit in the dq reference frame.
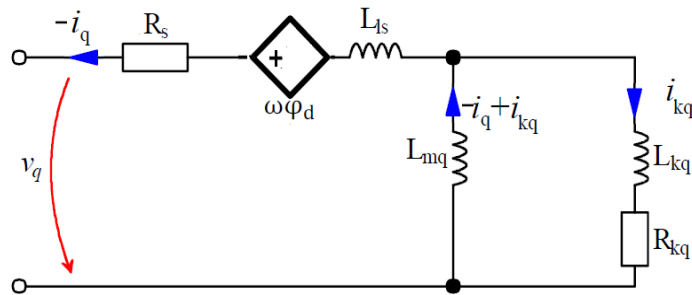
b): SG stator equivalent circuit in the dq reference frame.

Fig 3.9: SG stator equivalent circuits

(**3.19**) – (**3.58**) describe the electrical dynamics of the SG system, the mechanical dynamics models (**3.10**) – (**3.19**) are presented in the previous sub-section.

3.4.2   Diode rectifier

In renewable power generation systems, AC-DC converters are extensively employed, these converters include controlled and uncontrolled rectifiers. System operation and configuration is dependent on which type is employed. Therefore one should consider the cost, size, power quality, reliability and weight during their selection. Compared to active rectifiers, passive rectifiers are relatively cheaper, lighter, and more reliable [63] though their application generates low level frequency harmonics [89] [42-43], particularly in cases where 6-pulse diode rectifiers are used which would lead to poor power quality if not properly filtered.
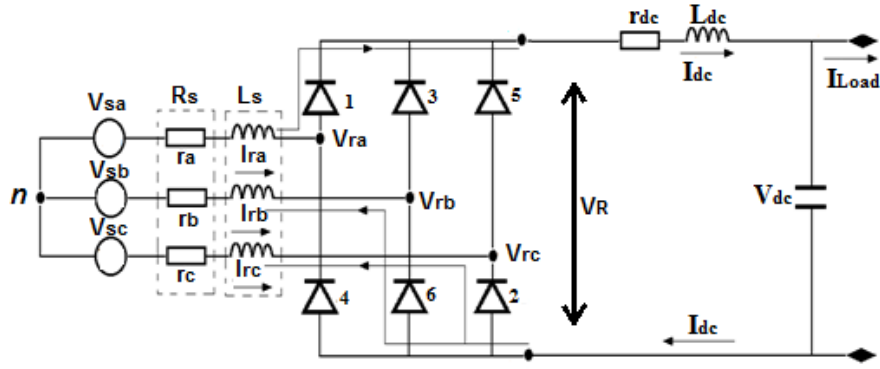
Fig: 3.10: Proposed 6-pulse diode rectifier arrangement
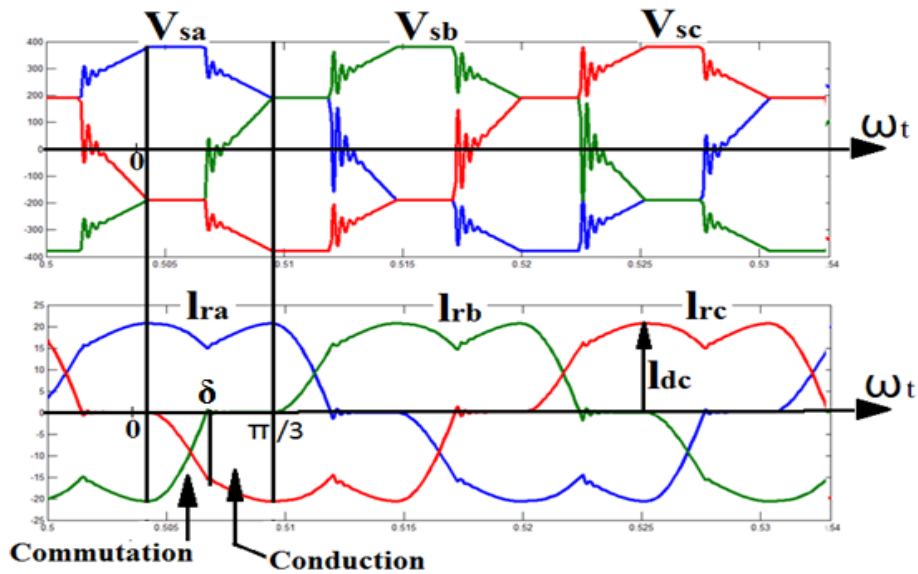
Fig. 3.11: *AC Voltage and Current Waveforms for a rectifier loaded generator*
*connected to a stiff DC voltage (simulation model shown in Appendix A, **Fig 8.3**)*

Fig: 3.10 illustrate a conventional three-phase, 6-pulse diode rectifier circuit, where **L$_s$**
and **R$_s$** stand for the collective effect of the cable and generator inductances and
resistances respectively. The resistances and inductances of the DC-bus are represented
by **r$_{dc}$** and **L$_{dc}$** respectively, and **V$_{dc}$** represents the DC-bus voltage.

It can be observed that the line-to-line voltage waveforms in ***Fig. 3.11*** have a 'flat' top.
This is due to the connection of the bridge rectifier to a fixed DC-bus voltage. The DC
voltage source clamps the generator terminal voltage therefore it does not change during
the commutation period. During the conduction period, three diodes are conducting in

the diode bridge, which implies that one of the generator's line-to-line voltages is equal to zero and the other two are equal to V_{dc} and $-V_{dc}$. where V_{dc} is equivalent to the DC-bus voltage source.

if it is presumed that the AC input voltages are equal and sinusoidal they can be realised as follows [64]:

$$V_{sa} = V_m \sin \left(\omega_t + \frac{\pi}{2} \right)$$

$$V_{sb} = V_m \sin \left(\omega_t - \frac{\pi}{6} \right) \qquad\qquad 3.59$$

$$V_{sc} = V_m \sin \left(\omega_t - \frac{5\pi}{6} \right)$$

where V_m is the peak phase voltage and ω_t represents the angular speed of the generator shaft with time. Current commutation is the most critical diode rectifier operation characteristic which is illustrated in **Fig. 3.11**, where a pair of diodes from the same set ie. Diodes (1, 3, 5) or (2, 4, 6) are forward biased, due to the input inductance L_s, as the load current increases the commutation period also increases. For the 6-pulse diode rectifier, current-commutation and conduction periods are repeated every after 60 electrical degrees [64].

3.4.2.1 Rectifier switching behaviour
The equations that represent the relationship between the rectifier input current (I_{ra}, I_{rb}, I_{rc}) and its output DC-bus current (I_{dc}) during the commutation interval ($0 \leq \omega_t < \delta$) and conduction interval ($\delta \leq \omega_t < \frac{\pi}{3}$) (see **Fig. 3.11**) can be defined by (**3.60**) and (**3.61**), respectively [64]. During commutation the DC current passes through one commutation inductance and a parallel connection of two commutation inductances

$$L_s \frac{dI_{ra}}{dt} = -R_s I_{ra} + V_{sa} - V_{ra}$$

$$I_{ra} \cong I_{dc}$$

$$L_s \frac{dI_{rb}}{dt} = -R_s I_{rb} + V_{sb} - V_{rb} \qquad\qquad 3.60$$

$$L_s \frac{dI_{rc}}{dt} = -R_s I_{rc} + V_{sc} - V_{rc} \qquad I_{rb} + I_{rc} \cong -I_{dc}$$

$$L_s \frac{dI_{ra}}{dt} = -R_s I_{ra} + V_{sa} - V_{ra} \qquad I_{ra} \cong I_{dc}$$

$$I_{rc} \cong -I_{dc} \qquad 3.61$$

$$L_s \frac{dI_{rc}}{dt} = -R_s I_{rc} + V_{sc} - V_{rc}$$

$$I_{rb} \cong 0$$

I_{dc} can be realised from (**3.62**) [64]:

$$L_{dc} \frac{dI_{dc}}{dt} = -r_{dc} I_{dc} + V_R - V_{dc} \qquad\qquad 3.62$$

where V_R is the rectifier DC terminal voltage

3.4.3   Tidal system averaged model

The proposed tidal turbine system mathematical components models were discussed in the previous sub-sections. However, to fully understand the proposed system dynamics i.e. how all components operate together, the proposed tidal system's averaged model was realised by analysing the turbine's power transfer behaviour in relation to its input variables such as tidal velocity, shaft speed, generator field current and DC-Bus voltage.

Fig 3.12 illustrates the system's schematic from which the averaged model is derived.
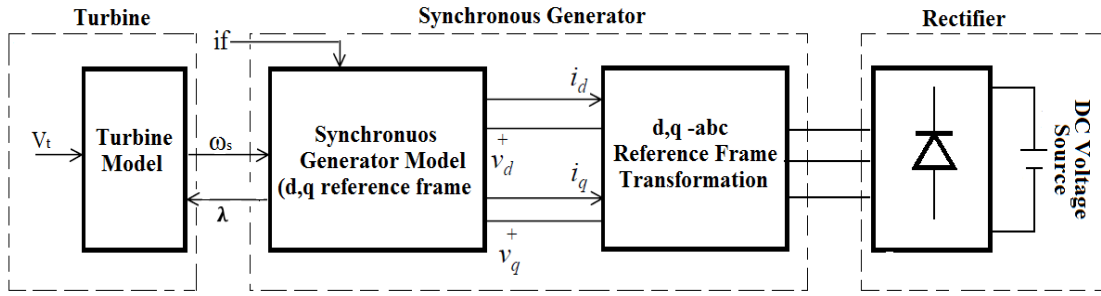
Fig 3.12: Tidal system Model

It should be noted that by employing a diode rectifier within this system its operation generates harmonics at the generator's output terminals at steady state. However, although high current and voltage harmonics are present at the generator's AC terminals [89] [42-43], for a standard generator it's only the fundamental component that produces useful shaft torque. Moreover, in practice a suitably sized DC link filter would be employed to reduce these harmonics. Therefore, active power associated with these harmonics will be neglected in the average model realisation i.e. system's power transfer will be determined primarily by the fundamental harmonic.

Although the diode rectifier operation is non-linear, it is believed that when its output DC voltage and current is averaged the resultant values are proportional to the phase current and voltage of the generator via constants k_i (AC-DC current constant) and k_v (AC-DC voltage constant). These values can be realised numerically as follows:

$$k_v = \frac{V_{dc}}{\sqrt{v_{d\,av}^2 + v_{q\,av}^2}}$$

3.63

$$k_i = \frac{i_{dc\,av}}{\sqrt{i_{d\,av}^2 + i_{q\,av}^2}}$$

3.64

Where, $i_{dc_{av}}$ and V_{dc} are the averaged DC output current and voltage variables respectively and $i_{d_{av}}$, $i_{q_{av}}$ and $v_{d_{av}}$, $v_{q_{av}}$ are the averaged/fundamental AC generator output current and voltage variables in the rotor reference frame (*dq*) respectively.

The averaged model shall be based on the AC-DC voltage and current constants relationship in (**3.63**) and (**3.64**), thus it accounts for only the fundamental harmonic of the AC variables and the average value of DC output.

The term 'average' refers to the 'moving average' which, for a generic periodic variable 'X' of period 'T', can be expressed as [90]:

$$X_{av} = \frac{1}{T} \int_{t-T}^{t} X(\xi) d\xi \qquad\qquad 3.65$$

Eqn (**3.65**) averages quantities over one electrical cycle and therefore the rotor reference frame variables ripple is removed leaving a 'ripple free' variable that represents the instantaneous value of the real variable that can only be affected by transients characterised of frequencies less than $\frac{1}{2T}$, where $T = \frac{1}{6f}$, f being the AC frequency of the generator. Transients occurring at frequencies higher than $\frac{1}{2T}$,are ignored through the averaging method.
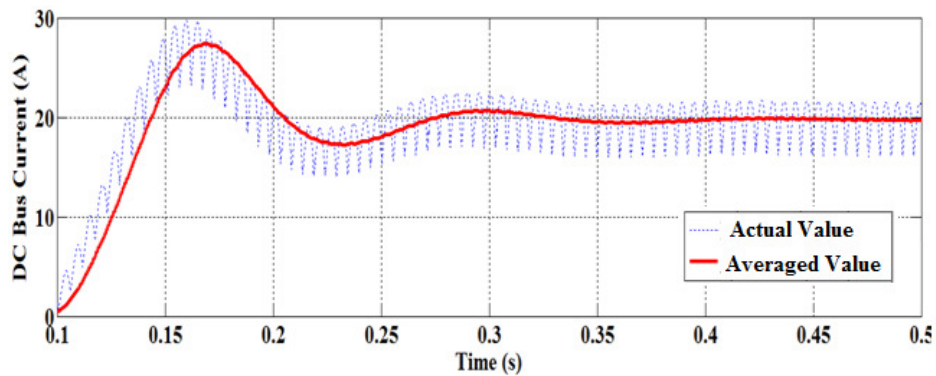
Fig 3.13: Averaged value of DC-bus Current
*(simulation model shown in Appendix A, **Fig 8.3**)*

Fig 3.13 shows a simulated example of the averaged output DC current variable illustrating both the actual value waveform and the averaged value wave form. It can be

observed that the averaging process introduces a phase shift due to the moving average filter defined in Equation (**3.65**). A transient can also be noticed, this is caused by the inrush current, nonetheless this does not affect the system controllability because a delay is introduced between turbine and controller operation start-up times. Moreover with tidal power generation sharp transients are uncommon.

Therefore based on simulation in *Fig 3.13* it is expected that when the averaging technique is applied to the system variables all the important system dynamic characteristics are preserved. Moreover, most conventional synchronous generators have their dominant characteristic frequencies well below $3f$ [91].

In [92], a wind power generation system averaged model comprising of a synchronous generator, 6-pulse diode rectifier and a converter is realised. The synchronous generator model was realised in the *abc* reference frame with its rotor, then converted to the rotor reference frame (*dq*) through the rotor angle ($\boldsymbol{\theta}$). The same technique shall be adopted in the derivation of the proposed tidal system averaged model.

The synchronous generator's space vector diagram is illustrated in **Fig 3.14** representing the averaged (*dq*) variables, and the AC variables fundamental quantities.
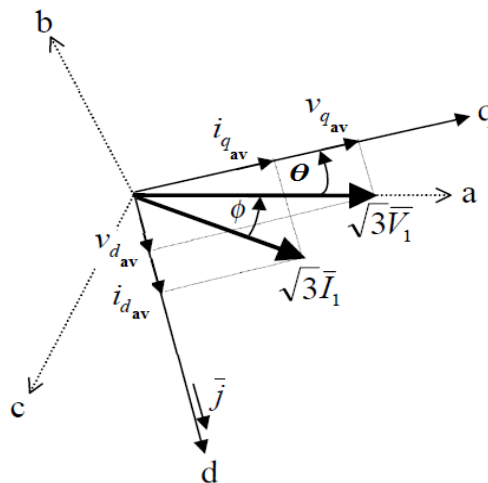
Fig 3.14: Space vector illustration of the generator's for non-sinusoidal steady state.

With reference to (**3.63**) and (**3.64**), substituting space vectors $\sqrt{3}\,\overline{V_1}$ and $\sqrt{3}\,\overline{I_1}$ in **Fig 3.14** with vectors whose lengths are $\frac{V_{dc}}{k_v}$ and $\frac{i_{dc_{av}}}{k_i}$, respectively, the tidal systems space

vector diagram can then be represented as in **Fig 3.15**. Axes *a, b* and *c* are not shown for clarity.
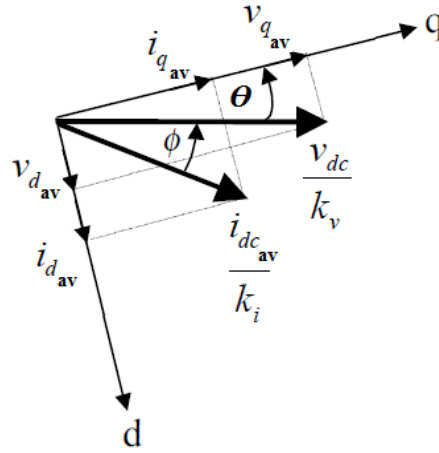
Fig 3.15: Generator/rectifier space vector diagram

The following expressions can then be obtained from the **Fig 3.15.**

$$V_{dc} = k_v \left(v_{d_{av}} \sin \theta + v_{q_{av}} \cos \theta \right) \qquad 3.66$$

$$i_{dc_{av}} = k_i \left[i_{d_{av}} \sin(\theta + \emptyset) \right] + \left[i_{q_{av}} \cos(\theta + \emptyset) \right] \qquad 3.67$$

$$v_{d_{av}} = \frac{V_{dc}}{k_v} \sin \theta \qquad 3.68$$

$$v_{av} = \frac{V_{dc}}{k_v} \cos \theta \qquad 3.69$$

$$i_{d_{av}} = \frac{i_{dc_{av}}}{k_i} \sin(\theta + \emptyset) \qquad 3.70$$

$$i_{q_{av}} = \frac{i_{dc_{av}}}{k_i} \cos(\theta + \emptyset) \qquad 3.71$$

where, $\emptyset$ is the phase shift between voltage and current of the generator's fundamental harmonics.

Assuming the rotor speed is constant and therefore the rotor angle ($\boldsymbol{\theta}$) can only be affected by the electrical transients; ($\boldsymbol{\theta}$) could be realised straight from the armature voltages in the rotor reference frame as shown in (**3.72**). The phase shift ($\emptyset$) can also be evaluated as in (**3.73**) [92].

$$\theta = tan^{-1}\frac{v_{d\,av}}{v_{q\,av}} \qquad\qquad 3.72$$

$$\emptyset = tan^{-1}\frac{i_{d\,av}}{i_{q\,av}} - tan^{-1}\frac{v_{d\,av}}{v_{q\,av}} \qquad\qquad 3.73$$

It can be noticed that the generator's output variables in the *dq* reference frame and the rectifier DC output variables of the averaged model equations possess transformer-like characteristics. For example, in (**3.66**) – (**3.71**), DC-bus voltage could be equated to the armature *d* and *q* axis voltages, and DC output current could be realised from the armature currents of the generator in the dq reference frame. Nonetheless, the occurrence of angle $\boldsymbol{\theta}$ in (**3.70**) and (**3.71**) makes the armature voltages reliant on the armature currents in the rotor reference frame. This suggests that the generator is not an ideal voltage source.

The tidal system rotor side can now be represented by either a current or a voltage source, however since it is assumed to be connected to a fixed DC voltage source, it will be considered as a current source as shown in **Fig 3.16.**
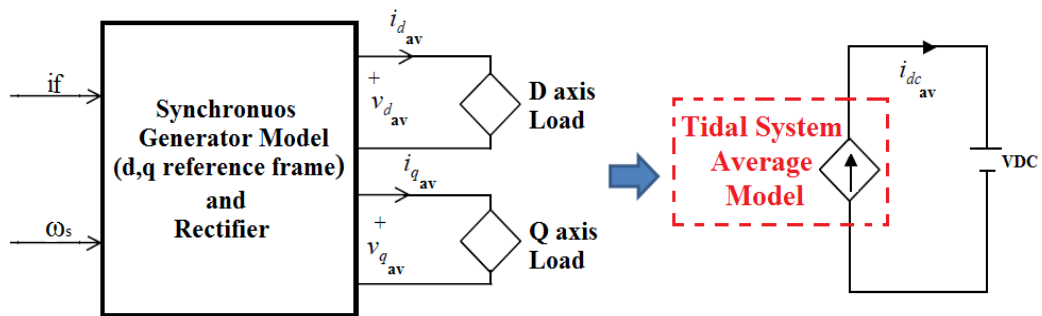
Fig 3.16: Equivalent tidal system average model (Electrical schematic)

(**3.66**) – (**3.71**) can be re-written in a different format when we incorporate (**3.72**) i.e. by

expanding $\sin(\theta + \emptyset)$ and $\cos(\theta + \emptyset)$ and replacing $\sin\theta$ with $\dfrac{k_v V_{d_{av}}}{V_{dc}}$ and

$\cos\theta$ with $\dfrac{k_v V_{q_{av}}}{V_{dc}}$ giving:

$$V_{dc} = k_v \sqrt{v_{d_{av}}^2 + v_{q_{av}}^2} \tag{3.74}$$

$$i_{dc_{av}} = k_i \sqrt{i_{d_{av}}^2 + i_{q_{av}}^2} \tag{3.75}$$

$$i_{d_{av}} = \left(K_{cos} v_{d_{av}} + K_{sin} v_{q_{av}}\right)\frac{i_{dc_{av}}}{V_{dc}} \tag{3.76}$$

$$i_{q_{av}} = \left(K_{cos} v_{q_{av}} - K_{sin} v_{d_{av}}\right)\frac{i_{dc_{av}}}{V_{dc}} \tag{3.77}$$

$$K_{sin} = \frac{k_v \sin\emptyset}{k_i} \tag{3.78}$$

$$K_{cos} = \frac{k_v \cos\emptyset}{k_i} \tag{3.79}$$

(**3.74**) – (**3.79**) now represent the dynamic tidal averaged model governing DC-link current and voltage, as well as the DC-link voltage and current analytical expressions in relation to the synchronous generator's AC output voltages and currents in the *dq* reference frame.

3.4.3.1 Averaged model simulations

The average model was simulated in Matlab/Simulink environment in conjunction with the SimPowerSystem[TM] Toolbox to analyse system behaviour and effects under various modes of operation such as variation in shaft speed, field current and DC-bus voltage on its output values such as phase voltage, current and power.

During simulation the following assumptions were made:

- Tidal velocity V_t and shaft speed ω_s were assumed constant at steady state so that tidal turbine blade behaviour can be eliminated from the analysis, given that electrical transients are much faster than mechanical transients.

- Field current was also assumed constant at steady state to enable a separate analysis of the effects of the diode rectifier on the generator's output voltage and current waveforms.

- The diode rectifier was coupled onto a fixed DC voltage source allowing for an independent analysis of rotor side from the grid side. In practice a DC link capacitor would be employed to decouple the rotor dynamics from the grid.

A standard Matlab Simulink four-pole, 157rad/s, synchronous generator model equipped with an integrated exciter and a rotating rectifier was used complete with ABB Ltd 0.91MW synchronous generator type AMG 0400ES04 parameters. The Matlab Simulink model used to obtain the following results is presented in Appendix A, **Fig 8.3**

All computer simulations in this thesis are based on the ABB Ltd 0.91MW synchronous generator type AMG 0400ES04 in order to give an indication of the proposed tidal system performance when an actual off-the-shelf generator is used.

*Simulated generator parameters (*ABB- AMG 0400ES04*)*

Nominal Power	- 0.91MW	L_{fd}	- 11.3mH
Nominal Frequency	- 50Hz	R_{kd}	- 3.142Ω
R_s	- 1.62Ω	L_{kd}	- 7.3mH
L_{ls}	- 4.52mH	R_{kq}	- 4.772Ω
L_{md}	- 108mH	L_{kq}	- 10.15mH
L_{mq}	- 52mH	Pole Pairs	- 2
R_f	- 1.208Ω	Nominal Voltage	- 400Vrms

Table 3.1: Proposed Generator Parameters

At the DC side of diode rectifier the current consists of an averaged value ripple and the voltage is ripple-free due to its connection to stiff DC voltage source. During simulation the power associated with the current ripple at the DC link was neglected by applying the averaging technique defined in Eqn (**3.65**), given that it's only the fundamental component of the currents that produces useful power. Moreover in practice a DC link Filter would be employed to minimise this ripple.

It is demonstrated in the following sub-section that the tidal system's output current, voltage and power can be accurately estimated from a set of input variables as described by the average model. The transients simulated are in the form of a ramp change rather than a step change. This is because tidal system's variables cannot change instantaneously due to the very high inertia of the system.

It should be noted that although a ramp change is assumed an overshoot is noticed in the following simulation results. This is due to the rate of change of the assumed variable (ramp), and can be eliminated by increasing the slope of the ramp change, which in turn would lead to higher simulation times. Nonetheless the system primary operation dynamics remain unchanged

3.4.3.2 DC Bus voltage (V_{dc}) increase after 20s

This scenario could occur when a tidal device connected onto a diode rectifier cannot generate voltage higher or equal to the DC-bus voltage i.e. if the DC-bus voltage is higher than the voltage the generator is capable of generating, field current would have to be raised for the terminal voltage to match the DC-bus voltage. However in some cases this may not be possible because the field current required to raise the voltage to the desired value may be higher than the generator's rated value. Therefore, DC bus voltage regulation could be required, given that tidal velocity is variable which would lead to variation of turbine rotor speed. It should be noted that variations in rotor speed would therefore cause variation of the tidal generator terminal voltage.
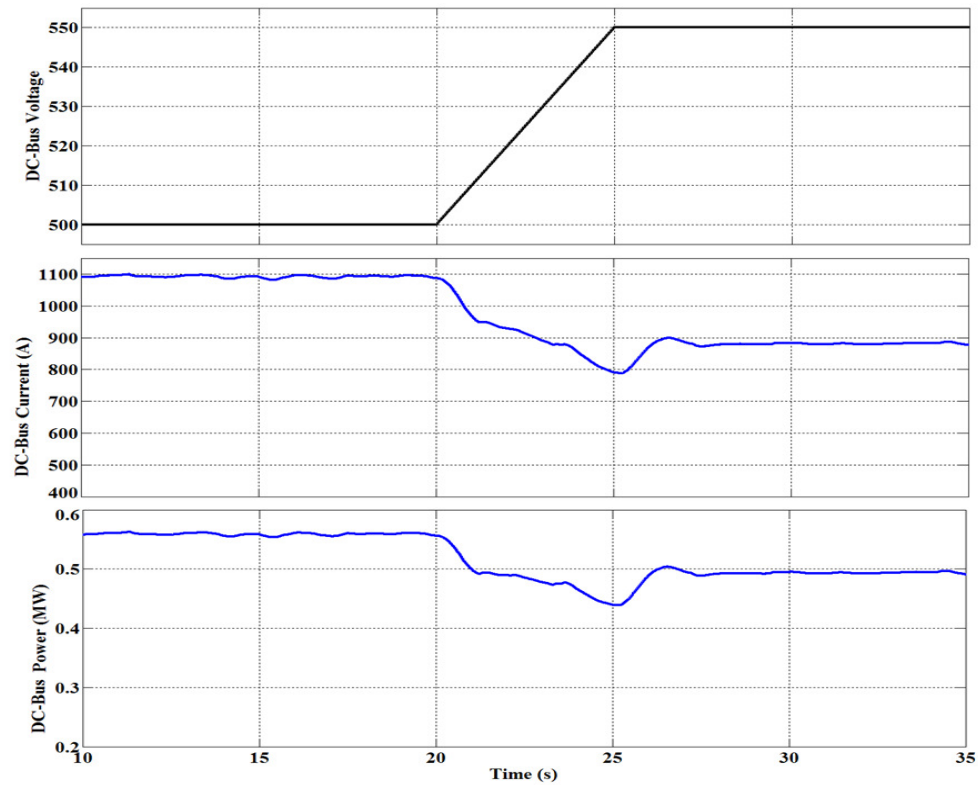
Fig 3.17: *DC-bus current and power waveforms*

Therefore, given that the generator is loaded with a diode rectifier, the generator's terminal voltage should vary with change in DC-bus voltage. This principle shall be discussed further in **Chapter 4**.

Fig 3.17: *DC-bus current and power waveforms*; shows the waveforms of the DC-bus current and power of tidal system average model when a DC-bus voltage increase of 500VDC to 550VDC occurs after 20s at 60rad/s rotor speed ($\boldsymbol{\omega_s}$) and 96A field current $(\boldsymbol{i_f})$

It can be observed in *Fig 3.17* that an increase in DC-Bus voltage leads to a higher generator terminal voltage requirement, which would require an increase in field current excitation if the power balance is to be maintained. However, by keeping the field constant as the DC-bus voltage increases, there would be a consequent decrease in the generator phase current I_m which would in turn lead to a drop is electromagnetic torque, resulting in a decrease in power. Therefore in order to maintain a constant output power as the DC-bus voltage increases, the field current (i_f) would have to be increased in turn in this case.
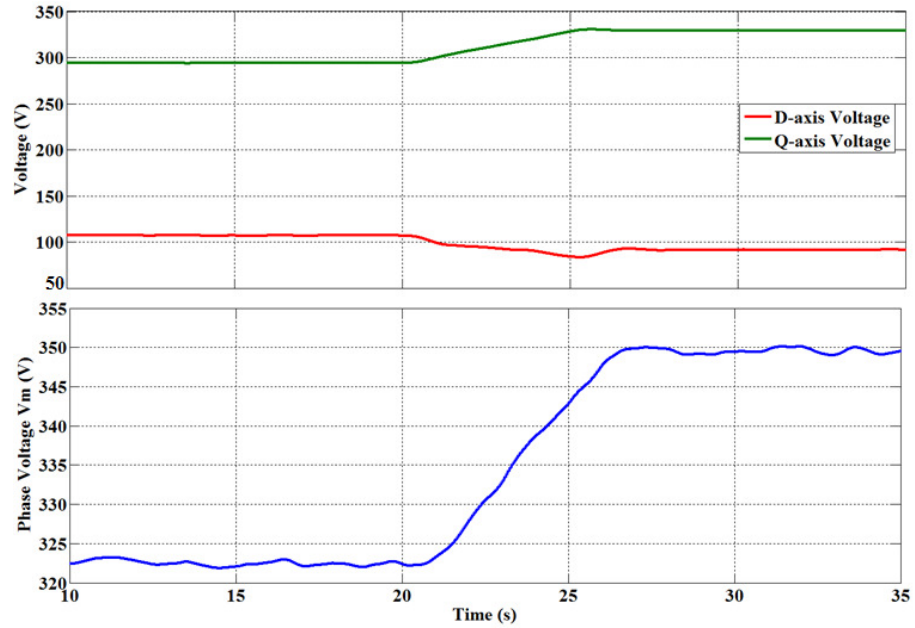
Fig 3.18: D and Q axis voltages and the equivalent phase voltage waveforms for when DC-bus voltage is increased at fixed shaft speed (60rad/s) and field current (96A)
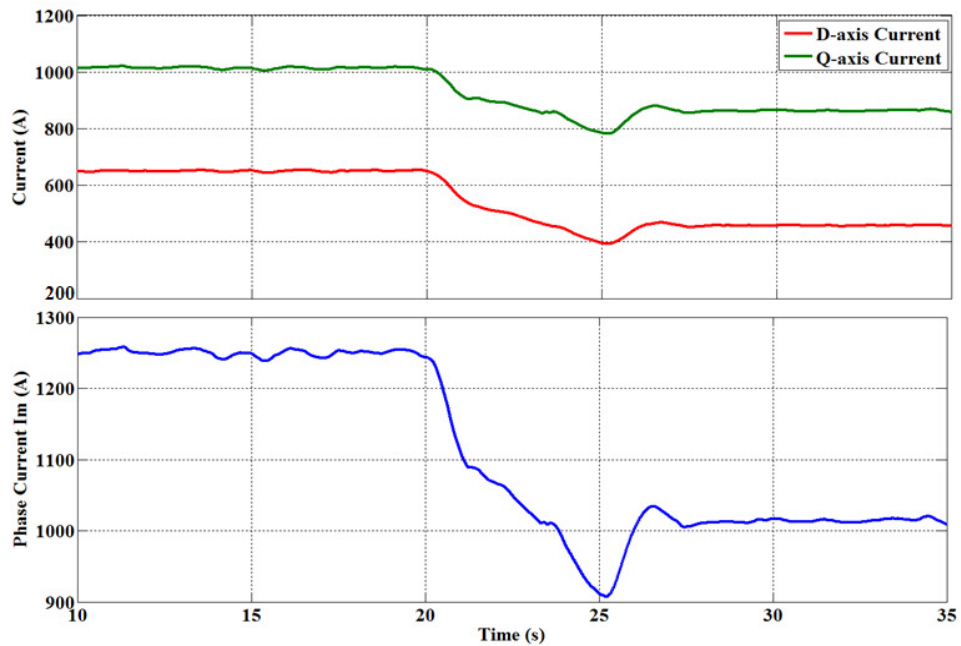
Fig 3.19: D and Q axis currents and the equivalent phase current waveforms for when DC-bus voltage is increased at fixed shaft speed (60rad/s) and field current (96A).

The waveforms in *Fig 3.18* and *Fig 3.19* illustrate the effect of DC bus voltage variation on the generator's output terminals. These waveforms were realised via computer simulation as described by the averaged model Eqns **(3.74)** and **(3.75)** respectively.

3.4.3.3 Field Current (i_f) change after (20s)

When the field current increases, torque is expected to increase, therefore if the speed is kept constant the power increases as a result. Moreover, given that the DC-bus voltage is kept constant, the increase in power consequently means an increase in the DC-bus current.
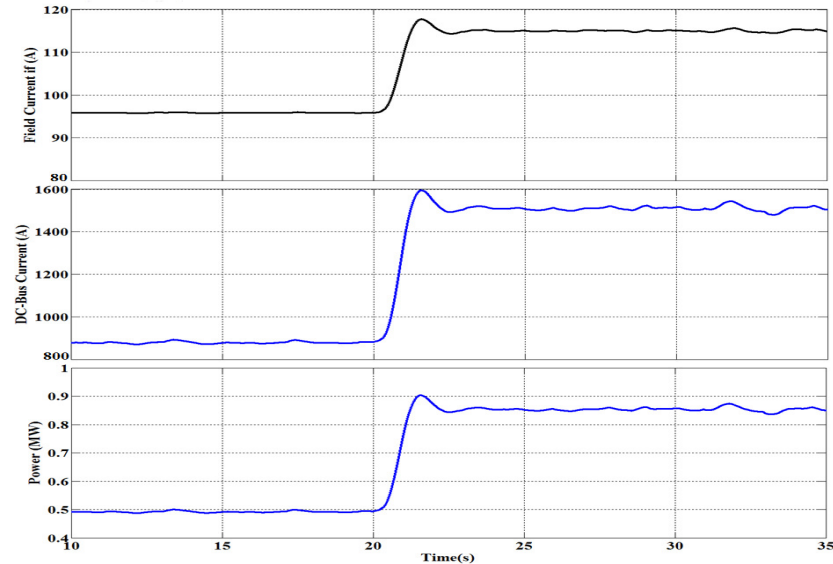
Fig 3.20 *DC-bus current and power waveforms of the tidal system model when the field current is varied at 60rad/s rotor speed and 550VDC*

Fig 3.20 shows the DC-bus current and power of tidal system average model when a variation in field voltage occurs after 20 seconds. ***Fig 3.20*** illustrates that the generator's power is directly proportional to its field current when both the shaft speed and DC-bus voltage are kept constant, thus input power could in principle be regulated by controlling field current. This principle forms part of the proposed tidal system control strategy and shall be discussed further in the following chapter.
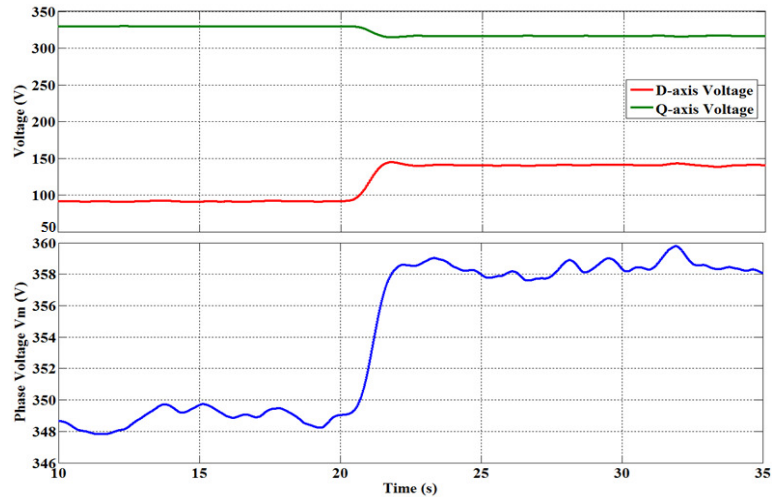
Fig 3.21: D and Q axis voltages and the equivalent rms phase voltage waveforms when the field current is varied at 60rad/s fixed rotor speed and 550VDC

When the field current is increased the dq-axis voltages are affected as shown in *Fig 3.21,* which in turn affects the rotor angle as defined in (**3.72**). *Fig 3.22* shows the D and Q axis currents and the equivalent phase current waveforms when the field current is varied at 60rad/s fixed rotor speed and 550VDC, as defined by the averaged model Tidal systems power is determined by both the shaft speed and torque, thus when the speed is kept constant the shaft power is proportional to shaft torque as well as field current.
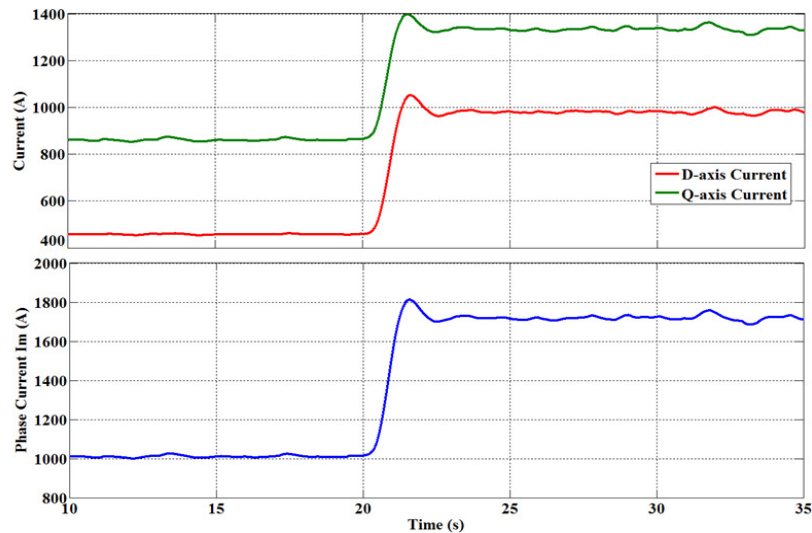
Fig 3.22: D and Q axis currents and the equivalent phase current waveforms when the field current is varied at 60rad/s fixed rotor speed and 550VDC
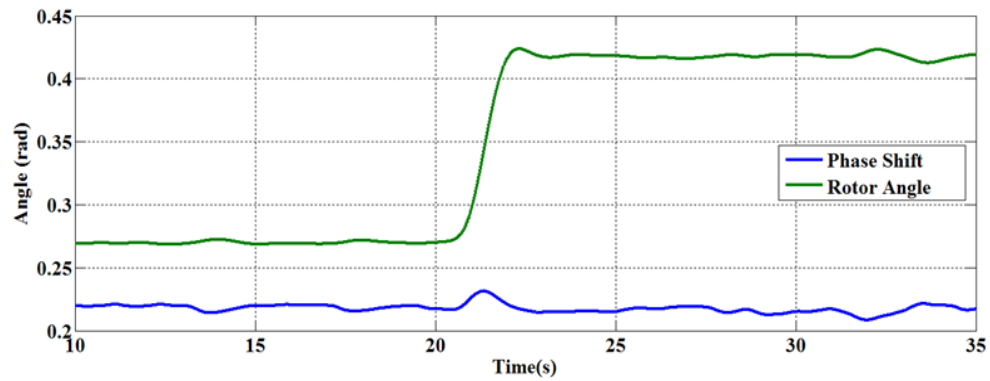
Fig 3.23*: Rotor and phase shift angle calculation of the tidal system model for when the field current changes at fixed rotor speed (60rad/s) and VDC=550*

Fig 3.23 shows the resultant rotor angle and phase shift as defined by the averaged model. It should be to note that by regulating field current, the torque applied to the shaft is also varied which in turn affects the shaft speed to maintain the power balance with reference to kinetic energy presented to the turbine by the tidal stream. As a result shaft speed could somewhat be indirectly regulated by field current control (also referred to as stall control). This principle will be discussed further in Chapter 4 as it forms part of the proposed system control strategy.

3.4.3.4 Rotor speed (ω_s) change after 20s

If the shaft speed was to be varied, shaft power would vary as a consequence therefore to properly validate the averaged model described above the effects of shaft speed variation to the systems power transfer cannot be ignored. Shaft speed variation can be caused by changes in tidal velocity, turbulence and field current.
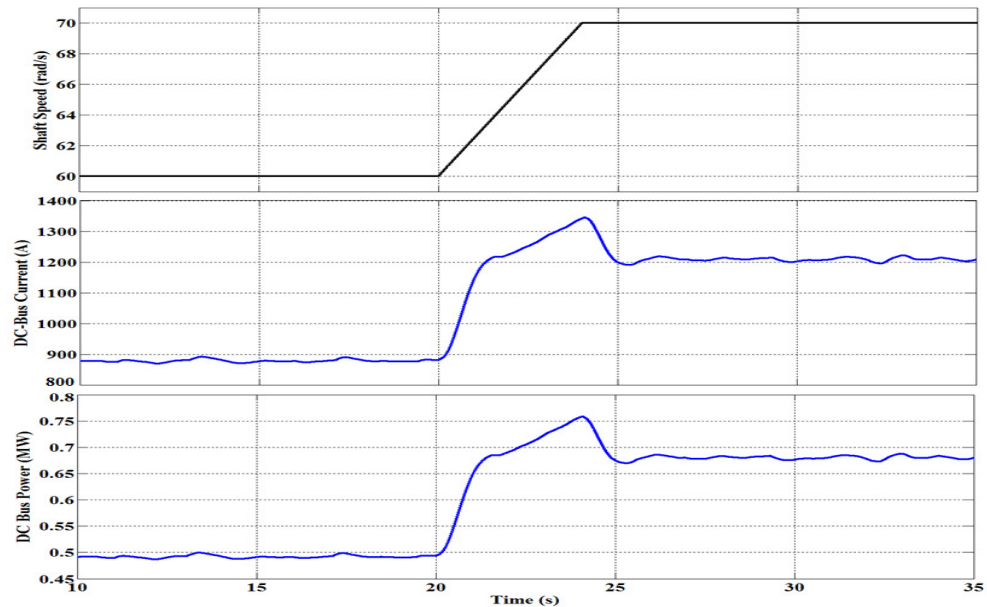
Fig 3.24: Generator phase current output waveform and rotor speed

Fig 3.24 shows DC-bus current and power waveform as the rotor speed increases from 60rad/s to 70rad/s after 20s. It can be seen that as generator speed increases both the DC-bus current and Power increases. This is because field current and DC-bus voltage are kept constant as speed increases. It is also illustrated that, the generator's power is directly proportional to shaft speed when both the field current and DC-bus voltage are kept constant, thus input power could in principle also be regulated by controlling shaft speed. This is the other a principle the will be explored further when discussing the proposed system control methodology the following chapter.

Based on the system averaged model realisation and simulation results presented in this chapter, if tidal system power extraction and transfer is to be successfully regulated, field current and/or shaft speed regulation is paramount. However due to the fact that a tidal system's shaft speed is mainly determined by the tidal stream velocity acting on the turbine blades, and given that the tidal stream velocity cannot be directly controlled, field current control will be employed to achieve power regulation for the proposed system as will be discussed in Chapter 4.

3.5 Summary

The proposed tidal system model components have been realised in this chapter, illustrating how they all connect and operate together analytically.

The averaged-value model for the proposed system topology has also been presented with simulations in the Matlab/Simulink environment in conjunction with the SimPowerSystem™ Toolbox analysing its utility and accuracy. It is also shown that the derived averaged model equations are computationally efficient, and faithfully represent the main dynamic characteristics of the proposed tidal system power transfer. The averaged system model will be employed in the following chapter to analyse the performance and control of proposed tidal power topology.

It should be noted that the following conditions must be satisfied for the derived tidal system's averaged model to accurately represent real system's behaviour:

- It is only the generator's fundamental harmonics that that deliver active power.

- The DC side of the diode rectifier is sufficiently filtered with for example a large capacitor.

In typical applications, both of these conditions are met, given that nearly all synchronous generators have their internal impedance "reactive part" dominant compared to the internal resistance "resistive part" which causes negligible active power associated with the rectifier harmonics. Furthermore, in practice as a rule the output of the rectifier is fitted with a filter of some kind, so that both the DC voltage and current have a negligible ripple.

All computer simulation carried out to analyse the proposed system models employ an off-the-shelf standard ABB Ltd Synchronous generator type AMG 0400ES04 parameters.

Detailed performance and control of the proposed system's power transfer shall be discussed in the following chapter.

CHAPTER 4

4 TIDAL SYSTEM PERFORMANCE AND CONTROL

4.1 Introduction

As described in the introduction, tidal turbines work by converting the kinetic energy in flowing sea water into rotational energy in the turbine rotor. Rotational energy is then converted into electrical energy via an electrical generator, which is then supplied to the utility grid. The power available for conversion mainly depends on the tidal velocity and the swept area of the turbine. However, energy conversion relies entirely on the control and performance of the tidal generation system. Therefore when designing a tidal stream power extraction device it is important to know the expected power and energy available at a given tidal site, as well as the control and performance of each tidal system component to determine the turbine's economic viability.

Following on from the development of an averaged system model of the proposed tidal turbine power system in **Chapter 3,** this chapter analyses its control and performance using a 0.91MW tidal device via computer simulations to demonstrate system viability.
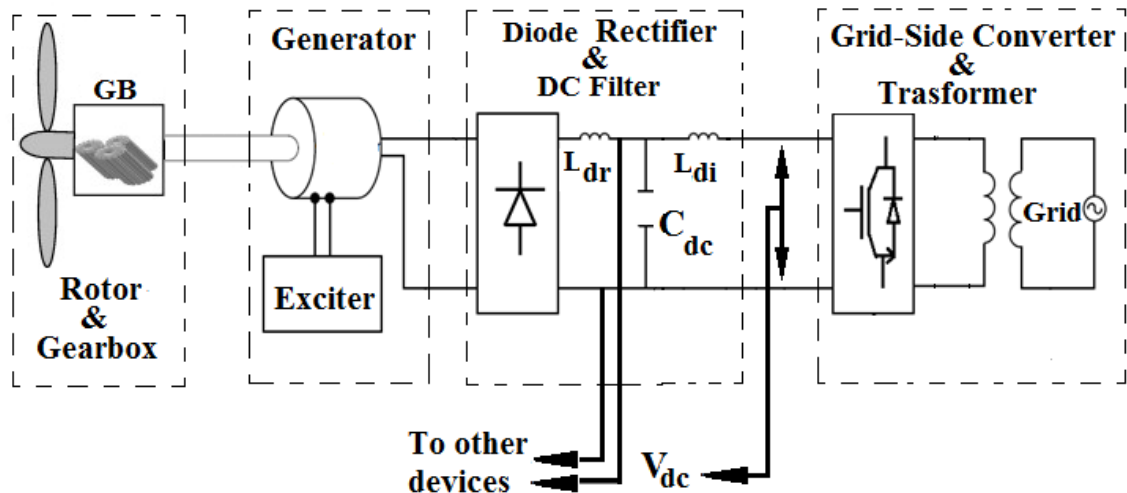
Fig 4.1: Tidal turbine electrical configuration

From the computer simulation view point the proposed tidal topology consists of the following components, as shown in *Fig 4.1*:

- Turbine rotor (blades)
- Synchronous generator
- Diode rectifier and DC filter
- Power electronic converter (grid side power control).

An understanding of tidal flow characteristics is fundamental to tidal turbine components selection since the rotor hydrodynamic efficiency depends on tip speed ratio (*TSR)* and the cube of the tidal velocity (as discussed in **Chapter 3)**. Furthermore it is beneficial during the selection of potential tidal power collection sites. For example; very low tidal velocities will not provide sufficient power to be useful. On the other hand very high velocities would provide extremely high levels of power. However, it would be uneconomical to employ a machine that can extract power at the highest possible site tidal velocity because this would mean that the device will be generally oversized, and would operate below its rated capacity most of the time. An ideal device would be one that is able to extract maximum power at low tidal velocities whilst surviving the highest.

The following sub-sections will provide an understanding of the proposed tidal turbine performance and control.

4.2 Tidal rotor

To understand the operation of the proposed tidal stream power generation systems, its rotor hydrodynamic profile was simulated in Matlab / Simulink, the simulation model is shown in Appendix A, *Fig 8.1: Simulation model of the implemented tidal turbine*. The simulations were made for a 20 meter diameter tidal turbine device, with the optimum power coefficient assumed to be 0.48 in line with a typical tidal turbine efficiency [22], thus the efficiency constant variables in (**3.3**) were selected to be : $C_1 = 0.5176$, $C_2 = 116$, $C_3 = 5$, $C_4 = 21$ and $C_5 = 0.0068$, to achieve this value of $C_{p_{(opt)}}$ and TSR ($\lambda_{opt} = 8$) as shown in Appendix A, *Fig 8.2: Turbine power coefficient Simulation model*. The simulated device was assumed to have three blades with fixed pitch control, thus its

73

rotor speed increases with tidal velocity. The assumed site average rated tidal velocity was 3.0 m/s and the turbine rated shaft speed was 157rad/s with a gearbox of 1:40 ratio. It should be noted that in practice, gear speed ratios over 1:25 between the generator and the turbine rotor speed are not used with a single-stage gear ratio [93-94], therefore a two stage gear would be needed for the simulated system. Each extra stage in gear ratio presents additional power losses of between 0.5 to 1 % [93, 95].

The tidal turbine rotor model defined in **Chapter 3** was used to determine the rotor shaft power output characteristics as function of various tidal velocities (1.4m/s – 3.0m/s) and the rated shaft speed for the device described above, as shown in *Fig 4.2*.
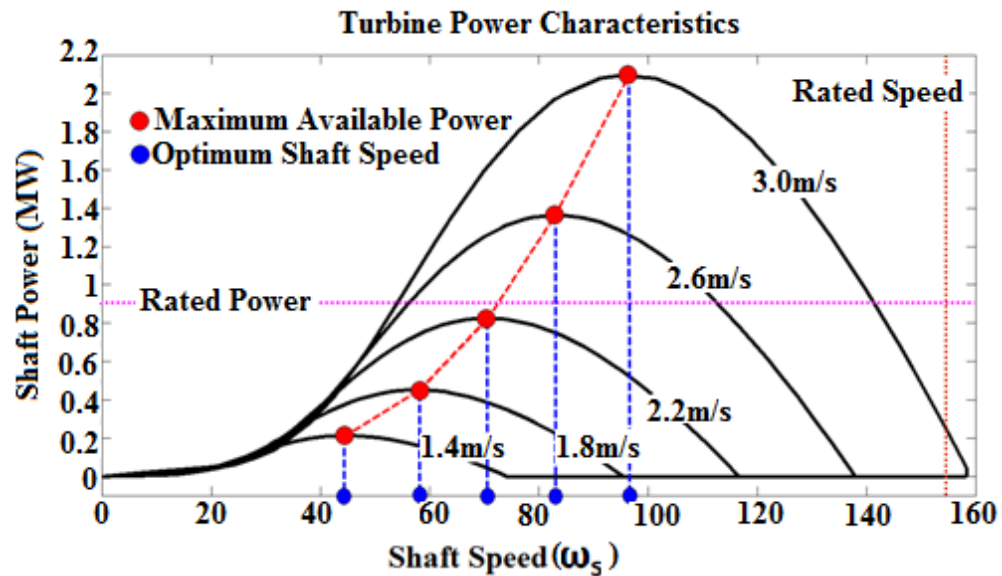
Fig 4.2: Speed Vs Power turbine characteristics

Fig 4.2 presents the power curves of the simulated tidal stream turbine showing variations of its shaft power as a function of the tidal velocity and rotor speed. It can be seen on the graph that for a given tidal velocity, there is an optimal turbine rotor speed (shown by the blue dots) that yields maximum power (shown by the red dots). Maximum power at a given tidal velocity is realised in practice by tracking the rate of change of the slope, identifying the point when the slope is equal to zero, which would equate to the peak point. this method is known as maximum power point tracking. The simulation model used to obtain the results in *Fig 4.2* is presented in Appendix A, *Fig 8.1: Simulation model of the implemented tidal turbine.*

Shaft speed determines how much of the available kinetic energy from the tidal flow is converted into mechanical shaft power for a given tidal velocity, orientation of the tidal blades ('attack angle') and blade arrangement [96]. Therefore, if maximum power extraction is to be achieved the tidal turbine shaft should be run at the optimum speed shown by the blue dots in *Fig 4.2*.

The tidal turbine was then coupled to a separately excited synchronous generator which converted shaft mechanical power into electrical power.

4.3 Generator

The proposed tidal turbine electrical to mechanical power conversion and transfer is organised as shown in *Fig 4.3*, where power transfer from the generator to the DC bus is via a passive diode rectifier which converts the generated AC power into DC power.
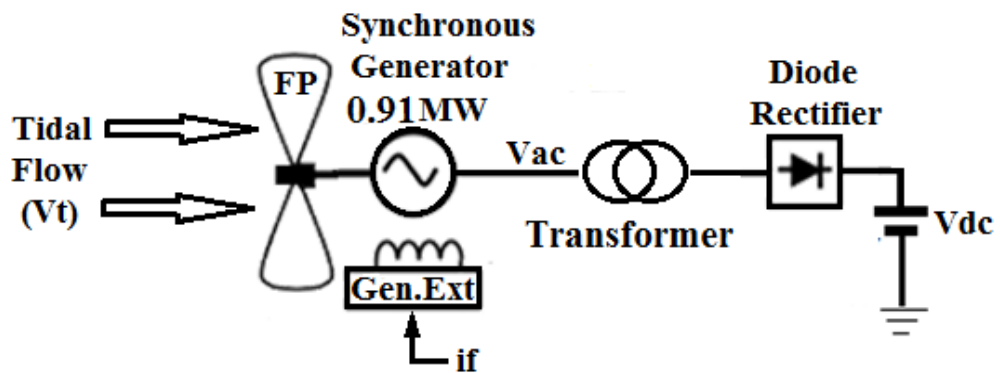
Fig 4.3: Tidal turbine equivalent electrical schematic

The tidal system simulation was configured as shown in *Fig 4.3*. a standard Matlab/Simulink generator simulation model shown in Appendix A, *Fig 8.3* was employed for this analysis

When generator loaded with a diode rectifier is converting mechanical power into electrical power, there is a minimum shaft speed at which sufficient voltage is generated to make the rectifier diodes forward biased, and hence for the generator to start generating power onto the DC bus. This speed will be referred to as the *"cut-in"* speed thought this thesis.
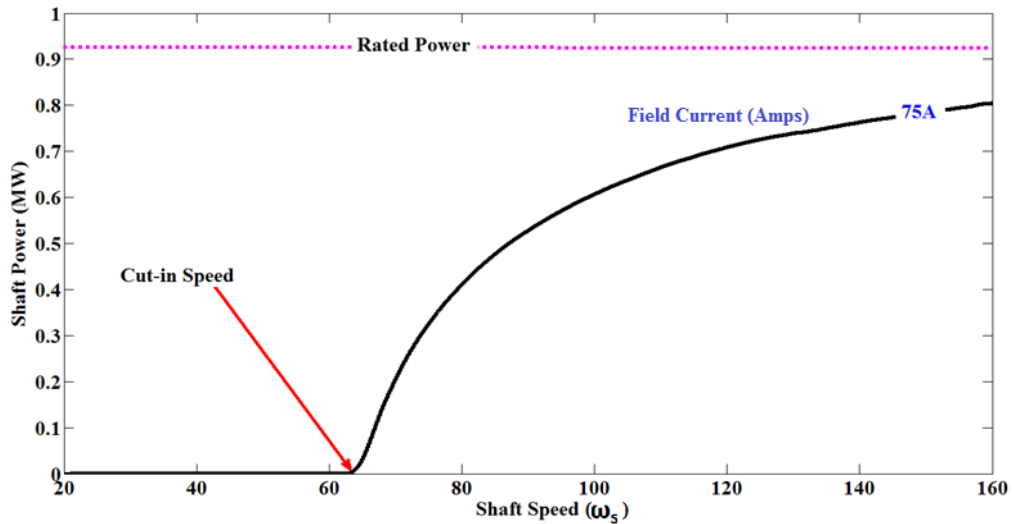
Fig 4.4: *Tidal Generator power curve at 8kVDC*

*(simulation model shown in Appendix A, **Fig 8.3***

Fig 4.4 shows an example of a tidal generator power curve; this figure indicates the expected power production as shaft speeds increases.

It can be noticed in equation **(4.1)** that at very low tidal velocities there is insufficient torque exerted on the tidal blades to make the rotor rotate at a speed higher than the cut in speed i.e. a speed of 65rad/s as demonstrated in ***Fig 4.4***. However, as the tidal velocity increases and the shaft speed increases beyond the cut-in speed of 65rad/s, the generator starts to generate electrical power. Generator *"cut-in"* speed is also dependent on other system characteristics such as generator parameters, field current, and DC- bus voltage, as will be discussed later in this chapter.

Another aspect to consider is commutation voltage drop. "Diode commutation is a short circuit of two armature phase windings during the time of commutation" [97]. This short circuit causes the rectified output voltage to be lower than the possible output voltage if the commutation was to happen instantly causing a lower efficiency.

4.3.1   Time domain simulations

The same generator parameters listed in ***Table 3.1*** were considered in the following simulations. The simulated generator was coupled to a three phase transformer in order to step-up its output voltage from 400Vrms to 6600Vrms, making the DC-bus rated

voltage $\approx$ 9kVDC to represent high voltage power transmission expected from a practical grid connected power generation system for efficient power transmission.

The DC bus voltage V_{dc} was considered as a constant voltage source under steady state conditions since in practice the DC capacitance C_{dc} would be large, in addition to the grid side converter maintaining a steady DC bus voltage.

The synchronous generator illustrated in **Fig 4.3:** *Tidal turbine equivalent electrical schematic* was simulated at various field currents i.e. between 75A and 135A to analyse the effects of field current on the generators shaft power. **Fig 4.5** shows the variations of the generator's shaft power as a function of its rotational speed and field current when connected to a stiff DC-bus voltage source of 9kVDC via a passive diode rectifier. When the field current was increased, generator shaft power increased as a consequence, and the "*cut-in*" speed reduced in turn.
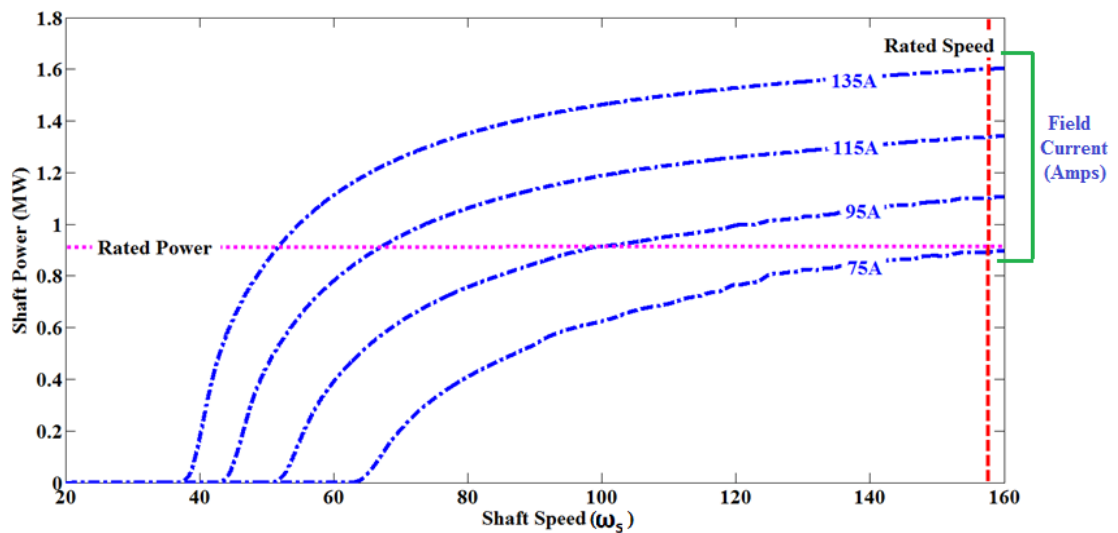
Fig 4.5: *Generator input power curve at 9kVDC*

it can be seen in **Fig 4.5** that for a given field current there is a minimum rotor speed below which power conversion is inhibited, "*cut-in*" speed decreases with an increase in the field current. The computer simulation model used to obtain the results in **Fig 4.5** is presented in Appendix A, **Fig 8.3:** *Tidal turbine Nacelle Simulation model.*

4.4 Turbine steady state operation

The turbine's steady state operation points were realised by superimposing *Fig 4.2: Speed Vs Power turbine characteristics* onto *Fig 4.5: Generator input power curve at 9kVDC* , and then identifying the intersection points of the two sets of curves as shown in *Fig 4.6: Steady state operation points at 9kVDC* below.
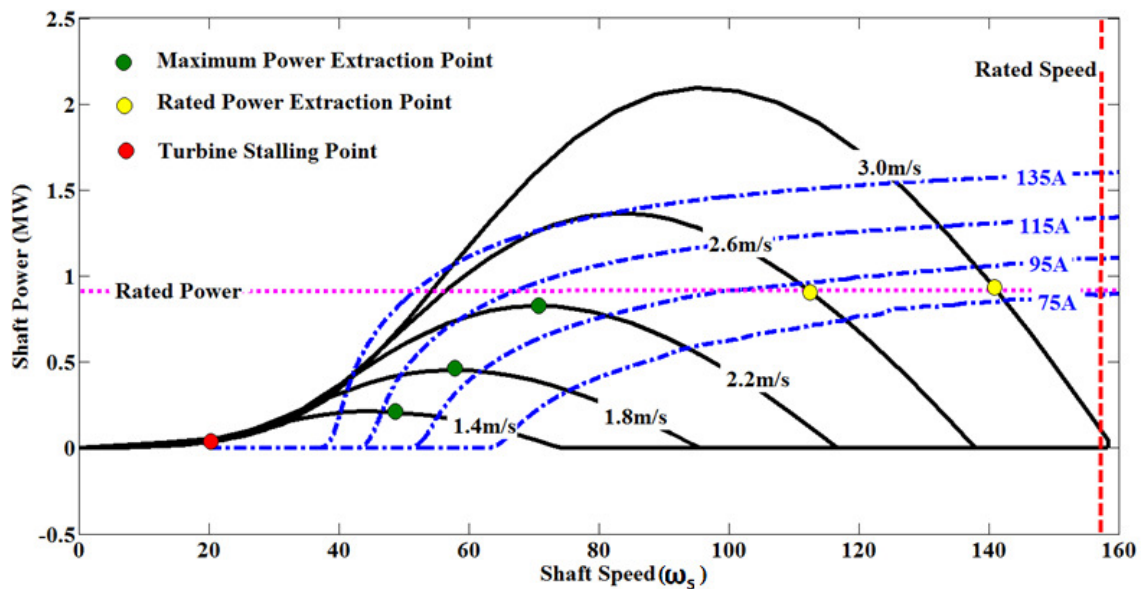
Fig 4.6: Steady state operation points at 9kVDC

Fig 4.6 can be interpreted as follows:

It can be observed that at 1.4m/s tidal velocity the peak maximum power extraction point marked by the green dot almost coincides with intersection point for when field current is set to 110A. Therefore, if maximum power extraction is to be achieved at this tidal velocity, field current should be set to approximately 110A. Similarly, at 1.8m/s tidal velocity the maximum power extraction point marked by the green dots almost coincides with the intersection point when the field current as set to 100A, again by setting the field current to approximately 100A, maximum power extraction can be achieved at this velocity. However as the tidal velocity increases further to 2.6m/s the peak power exceeds the generator's rated power represented by the pink line thus, to protect the generator from overload field current should be set to approximately 92A so that the intersection points at this tidal velocity coincides with the yellow dot to limit shaft power to the generator's rated power for the generator to operate within its rated

power envelope. Therefore it is understood that for a given tidal velocity there is a field current value that yields optimum/desired power. Similarly, for a given desired shaft power there is field current value that yields this power.

It should be noted however that over-excitation for the purpose of achieving maximum power extraction could heat-up the rotor and damage either the exciter or main rotor or both. For example if the generator field current in *Fig 4.6: Steady state operation points at 9kVDC*: was to be rated at 95A, achieving maximum power extraction at 1.4m/s would requires a field current of approximately 110A which would be higher than the rated value and may cause the rotor to overheat. Moreover in *Fig 3.22: D and Q axis currents and the equivalent phase current waveforms when the field current is varied at 60rad/s fixed rotor speed and 550VDC*: of the average model it was observed that at high field currents, generator phase current is also high, therefore if the field current is increased beyond its rated value the generators phase current required to maintain power balance could also exceeded the generator's rated value which could yet again cause damage to the generator.

Furthermore, the averaged model simulations presented in *Fig 3.17: DC-bus current and power waveforms*:, show that at low DC bus voltage, DC bus current is high. Therefore if the desired power is very high at very low DC bus voltage, the DC bus current required to maintain power balance could be higher than the systems rated current. Thus for the system to operate within its rated power envelope and at the same time achieve maximum power extraction from all devices connected on a common DC link circuit even at very low tidal velocities, DC-bus voltage regulation should also be considered.

It should be noted that, although multiple tidal generators are connected in parallel onto a common DC bus, field current regulation is undertaken at individual machine level. Therefore field current demand for each generator could be different depending on the tidal velocity acting on individual turbines i.e. field current can be regulated from 0 to the rated value for each device.

4.4.1   DC-Bus voltage variation

To analyse the effects of DC-bus voltage variation on the system steady state operation points hence power transfer. The same simulation process as in *Fig 4.6: Steady state operation points at 9kVDC:* was repeated at various DC-bus voltages i.e. 8kVDC and 7kVDC as illustrated in *Fig 4.7* and *Fig 4.8* respectively

 Fig 4.7 presents the steady state operation points for when DC-bus voltage is set to 8kVDC.
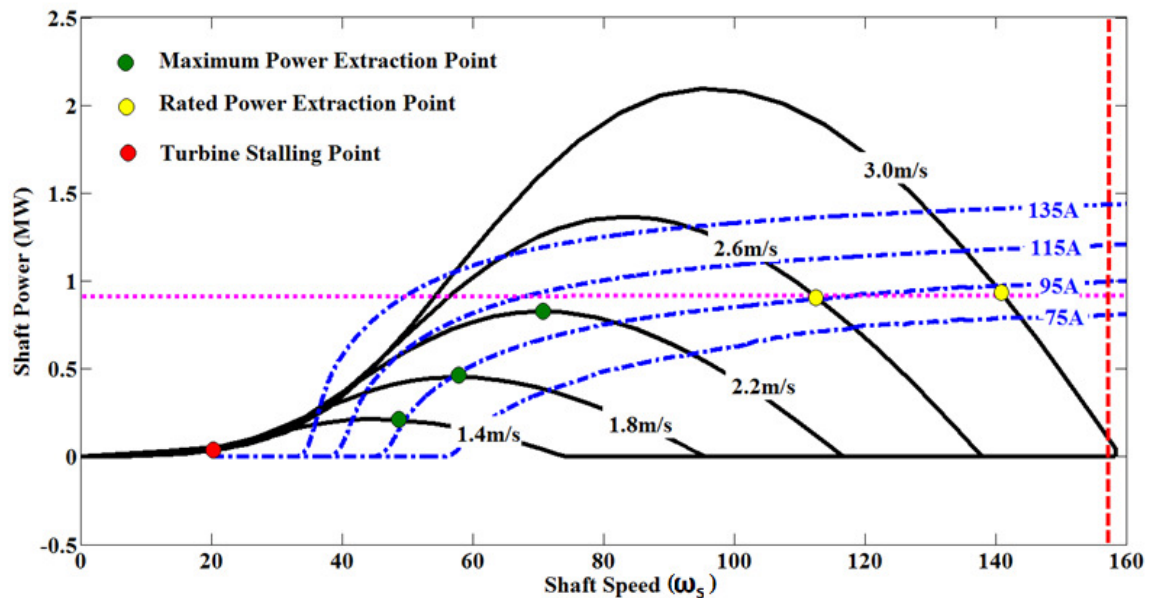
Fig 4.7: Steady state operation points at 8kVDC

It can be observed in *Fig 4.7* that when the DC-bus voltage was decreased the *"cut in"* speed at which the generator starts to generate power at a given field current also decreased as a consequence. Moreover, as expected the field current required to achieve maximum power extraction at lower tidal velocities is also lower than that observed in *Fig 4.6: Steady state operation points at 9kVDC* . For example it can be noticed in *Fig 4.7* that field current required to achieve maximum power extraction at 1.4m/s is now approximately 97A, lower than the 110A required when DC bus voltage was set to 9kVDC (*Fig 4.6: Steady state operation points at 9kVDC*). However, if the generator's rated field current was 95A, maximum power extraction at 1.4m/s could still not be achieved within the generator's rated power envelope at 8kVDC voltage set point.

80

This indicates that if maximum power extraction is to be achieved at 1.4m/s tidal velocity DC-bus voltage should be decreased even further.

In *Fig 4.8*, DC-bus voltage was decreased even further to 7kVDC again as you would expect the field current required to achieve maximum power extraction at 1.4m/s has further decreased to approximately 95A.
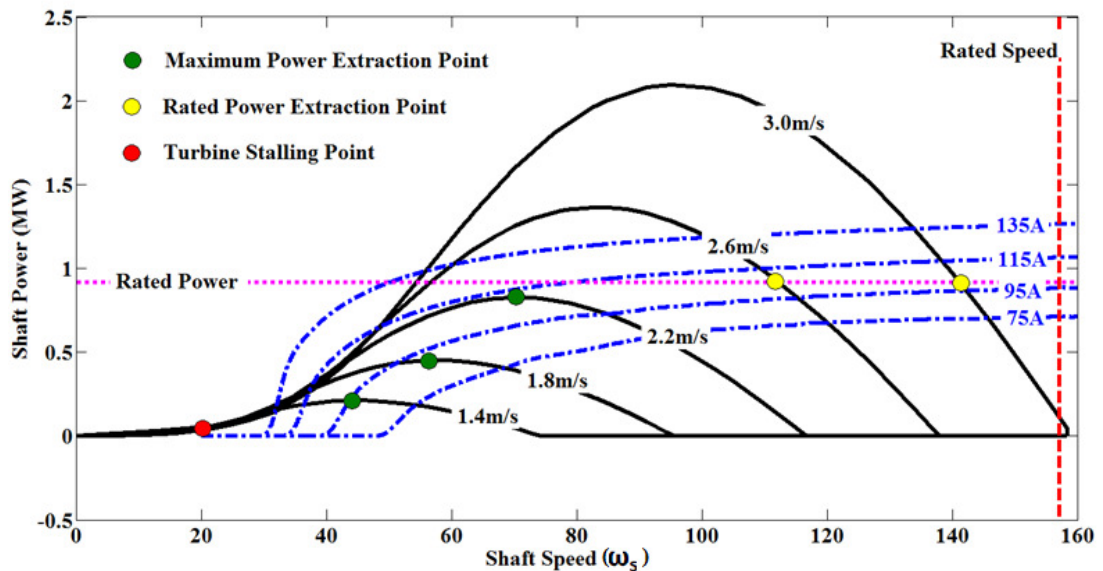
Fig 4.8: Steady state operation points at 7kVDC

This indicates that if the field current required for desired power extraction is higher than the systems rated field current value DC-bus voltage should be reduced to bring the field current demand within the generator's rated limits. As observed in *Fig 4.6: Steady state operation points at 9kVDC:*, *Fig 4.7: Steady state operation points at 8kVDC:* and *Fig 4.8: Steady state operation points at 7kVDC*.

However it can also be noticed that for 2.2m/s tidal velocity the required field current is increased to approximately 115A compared to the approximately 100A required in *Fig 4.6: Steady state operation points at 9kVDC*. This observation shows that if DC-bus voltage is set too low, desired power extraction at higher tidal velocities may not be possible within the generator's rated power envelope because a higher than rated field current may be required. Moreover, when the DC-bus voltage is set too low at a high shaft power, the generator output current could exceed the system's rated value damaging the generator. Therefore, to select an optimum DC-bus voltage set point, the

tidal velocities acting on all the devices connected onto the common DC bus should be taken into consideration so that the field current required to achieve optimum power extraction for any device on the same array is lower than the generator's rated field current value for all tidal devices to operate within their power envelopes. This observation validates the need for a DC-bus voltage set-point controller.

4.4.1.1 DC bus voltage set-point

The proposed DC bus voltage set-point controller is configured schematically in shown in *Fig 4.9*.
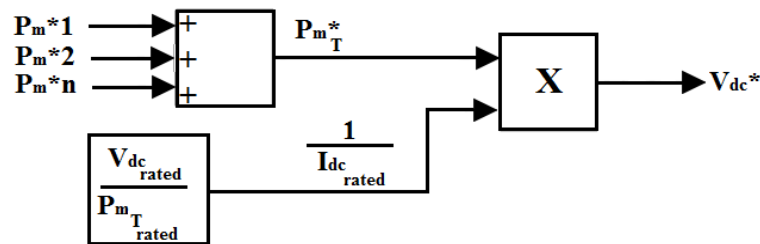
Fig 4.9: DC-bus voltage control schematic

The primary objective of the voltage controller is to select a DC bus voltage set point that would enable all the devices connected onto the same tidal array to extract optimum power from the tidal flow and at the same time operate within their rated power envelopes. In addition to maintain a constant DC-bus voltage during steady state and transient input power.

"Optimum power" in this thesis refers to the maximum power that could be extracted from the tidal currents without over loading the tidal generator .i.e. where the power available for extraction is greater than the generator's rated power, "optimum power" in this case would be equivalent to the generator's rated power.

DC-bus voltage is regulated with respect to the power generated by all devices connected onto the common DC-bus. The DC voltage value obtained from the controller is used to produce the reference current value required by each individual generator current controller as illustrated in *Fig 4.13: Rotor side power control schematic,* as shall be discussed later in the chapter.

Optimum DC-bus voltage can also be calculated from (**4.1**): "Optimum DC-bus voltage" refers to the voltage that could enable all tidal devices connected onto the common DC-bus circuit to generate optimum power.

$$V_{dc}{}^* = \sum_{i=n}^{i=0} P_m{}^* \cdot \frac{1}{I_{dc_{rated}}}$$ 4.1

Where $V_{dc}{}^*$, $P_m{}^*$ and $I_{dc_{rated}}$ are the desired DC-bus voltage, desired generators input power, and rated DC-bus current respectively.

Equation (**4.1**) is obtained from *Fig 4.9* i.e. Dividing rated total tidal farm power by the rated DC-bus current, optimum DC bus voltage set point can be realised. Rated DC-bus current is the system's rated output current, and the rated total tidal farm power is the sum of possible power available from all tidal turbines connected onto the common DC-bus generating at full power.

Voltage regulation is also important for thermal protection since it maintains the generator's field and phase currents within their rated limits preventing field saturation and overheating.

It should be noted that the DC bus voltage set point realised by (**4.1**) is the minimum possible DC- bus voltage set point. The minimum voltage is selected because when the generator DC-bus voltage is low the field current required by the tidal generators influenced by low tidal velocities is also low allowing for maximum power extraction even at low tidal velocities. However, if the voltage was to be reduced any lower than the voltage calculated in (**4.1**) the DC-bus current would exceed the system's rated value. Operating at the lowest DC Bus voltage means that the DC Bus cable operates at the maximum current most of the time which could introduce additional system/cable loses. Therefore investigation into the effects of these additional loses should be undertaken to validate its suitability.

It should be noted however that if the difference in tidal velocities between the highest power generating device and the lowest power generating device is significant, using the lowest DC-bus voltage set point may lead to generator current of the highest power

generating device to exceed its rated value. Nonetheless, the chance of having significant differences in tidal velocities at the same location site to cause this problem is unlikely in practice.

4.4.2 Stall control
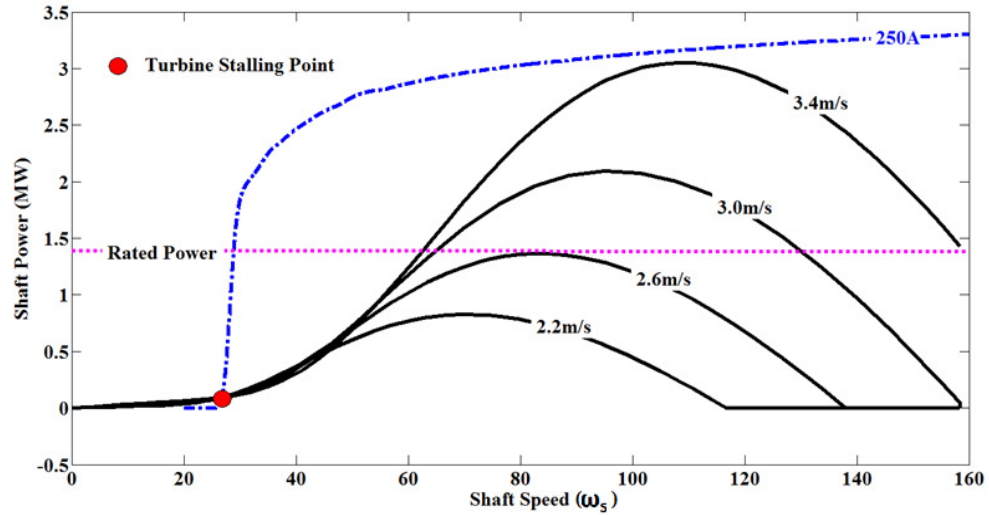
Fig 4.10: Stall control 9kVDC

It was noticed that, when the tidal velocity increased even further to say above 3.4m/s as illustrated in *Fig 4.10*, not only does the available peak tidal power exceed the generator's rated power value but also the speed at which rated power could be achieved safely without overloading the generator by applying too much torque also exceeds the machines rated shaft speed. Therefore to protect the generator from overload and over-speed, field current should be increased to the maximum field current value (rated field current), This is assumed to be 250A for the simulated system, achieving the intersection point marked by the red dot which equates to low shaft torque and speed and therefore low or no shaft power. As a result the turbine stalls protecting the generator from overload, over-speed and damage. However, it should be noted that in some cases the field current required to stall the turbine could be higher than the rated value and raising the field current beyond its rated value may heat up the rotor excessively leading to damage. On the other hand, if the DC-bus voltage was increased to a higher value the field current required to achieve stall control could be reduced as demonstrated in *Fig 4.6: Steady state operation points at 9kVDC*, *Fig 4.7: Steady state operation points at 8kVDC* and *Fig 4.8: Steady state operation points at 7kVDC*

Stall control will be discussed in more detail later in the Chapter.

4.4.3   Generator parameter variation

The other factor to consider when maximum power extraction, power limiting and stalling control is required is the generator parameters.
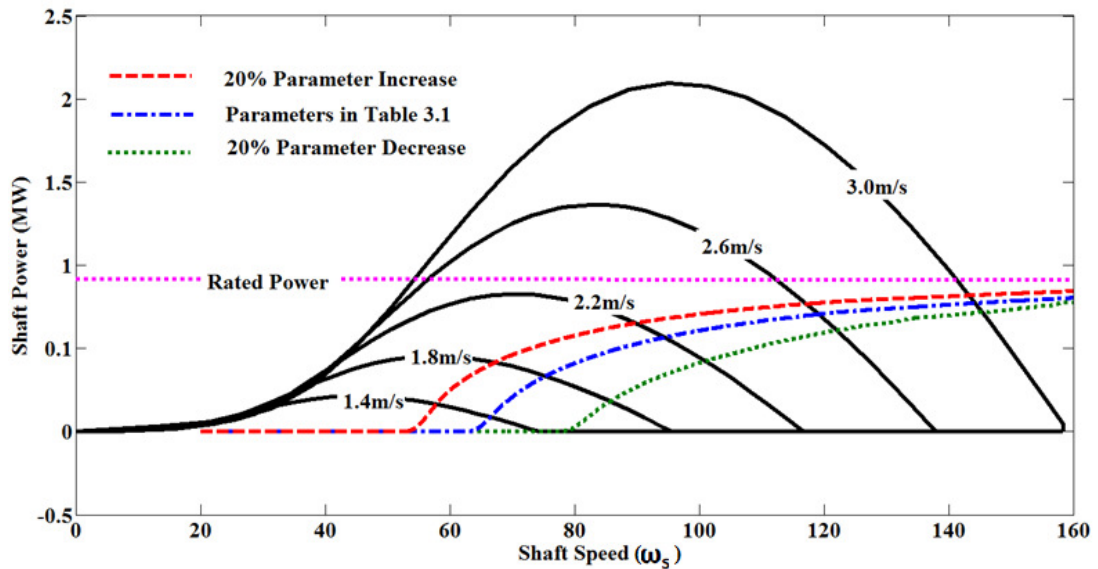
Fig 4.11: Steady state operation points when generator parameters are varied

Fig 4.11 shows the steady state operation points of the generator when its parameters were varied, for example the generator resistances and inductances shown in *Table 3.1: Proposed Generator Parameters* (shown by the blue line) were increased by 20% (shown by the green line) and again reduced by 20% (shown by the red line). This analysis showed that when the generator's parameters are decreased the cut-in speed is reduced, and increased when parameters were increased. Furthermore the shaft speed at which power extraction (intersection point) is achieved also changed. This indicates that the desired steady state operation points are also influenced by the generator parameters. Therefore when fine-tuning of the steady state operation points is required, generator parameter variation should be considered, for example in the case of stall control. The simulation results presented in *Fig 4.11* were achieved at 9kVDC DC bus voltage set point.

85

It should be noted that the lower the *"cut-in"* speed the better the tidal turbine design, because this allows for power extraction even at very low tidal velocities.

4.5 Tidal Turbine Control

The speed and torque at which a tidal stream turbine operates must be controlled for several reasons including:

- Optimising hydrodynamic efficiency of the rotor at low tidal velocities.
- Keeping the generator/system within its speed and power operation rated envelope due to the fact that exceeding the rated power production would result in high currents and hence overheating of the system.
- Keeping the rotor within its speed limits. i.e. the rotational speed of the rotor increases as the square of the tidal velocity which means that at high tidal velocity the rotor could over speed affecting the tidal device structure.
- Keeping the rotor within its strength limits, given that tidal power increases as the cube of the tidal velocity. For that reason, turbines must be able to survive much higher tidal velocities because the blades produce more tangential and perpendicular forces when they are producing torque so tidal turbines must be controlled to reduce torque in high tidal velocities.

Due to variations in tidal velocity, the proposed tidal turbine topology shaft power will be automatically controlled via generator field current control in order to achieve desired power extraction at various tidal velocities. A tidal power generation system is composed of two parts, the rotor-side and the grid-side, so to effectively operate the proposed tidal stream topology two separate levels of control are employed i.e. rotor-side control and grid-side control. The rotor side control is primarily responsible for maximum power extraction, power limitation and stall control. The grid-side controller is to achieve efficient power transfer to the grid, in addition to maintaining a stable DC-bus voltage and unity power factor. These control methods operate independent of one another. The proposed rotor-side controller will be discussed in more detail in this Chapter.

However, given that the grid side control is a mature technology employed by almost all power generation industries it will not be discussed in great detail within this thesis.

4.6 Rotor-side control

It should be noted that the proposed tidal farm topology consists of multiple turbines (rotors) connected in parallel onto a common DC-bus. Therefore the rotor control methodology described in this section applies to all devices coupled onto the same DC link circuit.

The proposed tidal rotor control strategy is configured as shown in *Fig 4.12*.
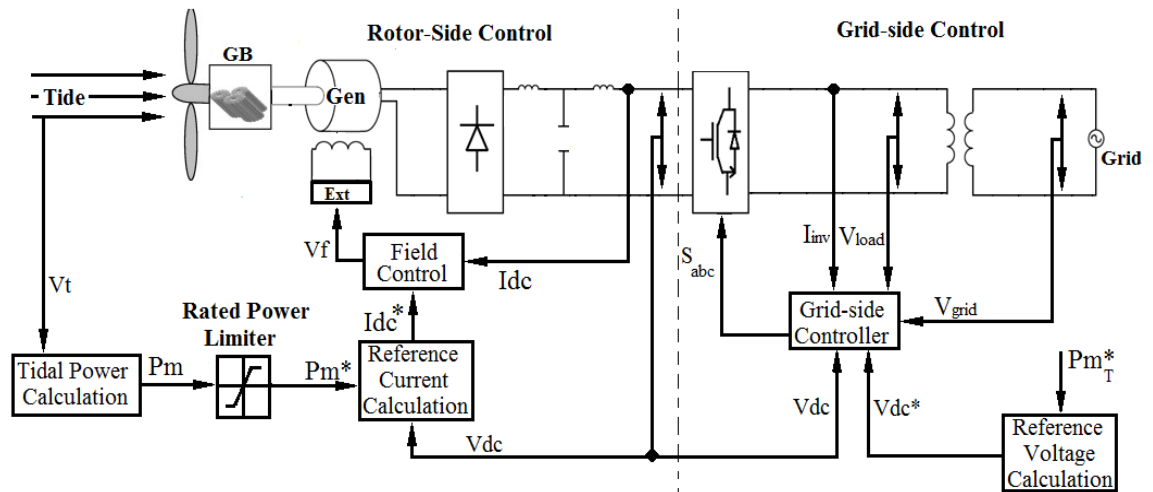
Fig 4.12: Tidal turbine control methodology

The proposed tidal turbine rotor is of fixed pitch blades therefore the power coefficient (C_p) is dependent only on the tip speed ratio (λ). The terminals of the tidal generators are connected onto a common DC-Bus circuit via a diode rectifier which clamps generator's terminal voltage. This indicated that only the output current from the generator can be regulated in order to achieve the desired shaft power. Current control is to be achieved via generator field current regulation, which indirectly controls torque, and as a consequence regulates generator shaft power at a given shaft speed/tidal velocity.

4.6.1.1 Operation principle

When the turbine blades start to rotate due to the kinetic energy within the tidal flow, tidal velocity (V_t) is measured (tidal current metres are commercially available on the market i.e. from Valeport LTD) and used to calculate the available tidal power (P_m^*) using Eqn (**3.7**), with the *TSR* (λ) set to its optimum value. A power limiter is included to avoid the desired power from exceeding the generator rated power. The calculated available tidal power is then divided by the DC-bus voltage set point (V_{dc}) realised by the voltage controller to determine the desired DC-bus current (I_{dc}^*).This is then used by the field excitation controller to determine the desired field voltage (current). The field current is then regulated to achieve optimum shaft power at a given tidal velocity.

In *Fig 4.13* the proposed rotor side power control schematic is presented.
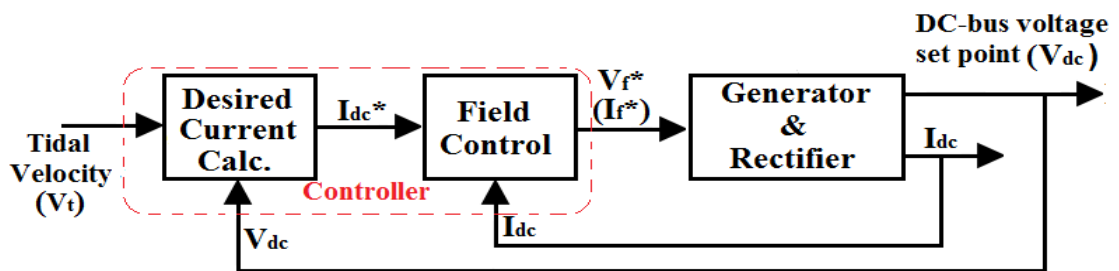
Fig 4.13: Rotor side power control schematic

The field control block is composed of two main parts, the power unit that provides DC current for the field windings and the automatic voltage regulator (AVR) that regulates the field voltage/current. Power required for excitation is drawn from the DC bus.
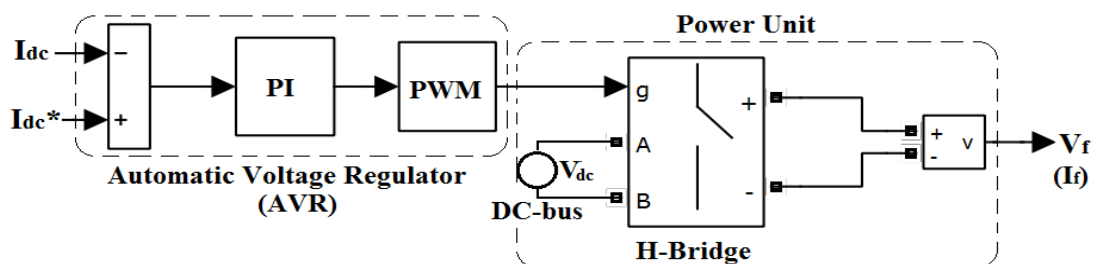
Fig 4.14: Field Controller

The principal input of the field controller is the generator's diode rectifier output DC current (I_{dc}) as shown in *Fig 4.14*, which is measured and compared to the reference

current ($I_{dc}{}^*$), and the obtained error signal is fed to a PI controller. The output signal of the AVR is used by the PWM module to determine the switching instants of the H-bridge, thereby regulating the generator's field voltage/current, in turn yielding desired torque at a given tidal velocity/shaft speed.

The field control loop forms part of the rotor-side current control loop as shown in **Fig 4.15**.
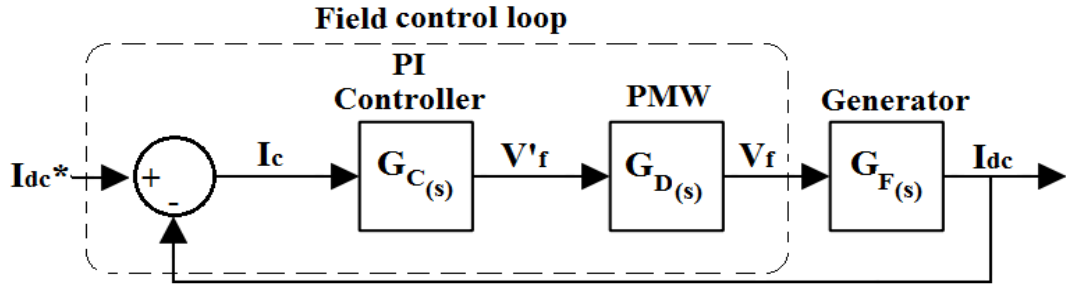
Fig 4.15: Rotor-side current loop control

The current control loop is described as follows:

$G_{c(s)}$ represents the PI controller and its transfer function can be defined as:

$$G_{C(s)} = \frac{K_P(T_i s + 1)}{T_i s}$$

4.2

Considering the time delay due to the PWM module between the control signal I_c and the output signal V_f, $G_{D(s)}$ represents the computational delay of the PWM module and its transfer function can be presented to be as follows:

$$G_{D(s)} = \frac{1}{1.5 T_s s}$$

4.3

where T_s is the PWM control module time constant.

$G_{F(s)}$ represents the plant which in this case is the synchronous generator. The transfer function of the synchronous generator is quite complicated; thus we will consider a scenario where the current flowing through the stator winding (i_G) is zero "no-load running condition". This means that only the effect of the excitation voltage (V_f) on the

generator's voltage (V_G) is taken in account. Given that the maximum voltage is approximately equal to the rated voltage, saturation shall not be taken into account. From the generator's no-load air gap line and the relations existing in the excitation circuit, we have [98];

$$V_{G0} = K'_G i_f \tag{4.4}$$

$$V_f = R_f i_f + L_f \frac{\partial i_f}{\partial t} = R_f \left(i_f + T_G \frac{\partial i_f}{\partial t} \right) \tag{4.5}$$

$$T_G = \frac{L_f}{R_f} \tag{4.6}$$

where i_f and V_{G0} are excitation current and the corresponding no-load of the generator voltage respectively, L_f and R_f are the reactance and resistance of the field winding respectively, T_G is the time constant of excitation circuit and K'_G is a coefficient with resistance dimension. When **(4.4)** and **(4.5)** are transformed into Laplace form in zero state, we obtain:

$$V_{G0(s)} = \frac{K_G}{1 + T_G s} \cdot V_f \tag{4.7}$$

where

$$K_G = \frac{K'_G}{R_f} \ (as \ a \ diamentional \ coeficient) \tag{4.8}$$

Thus, transfer function of the generator becomes;

$$G_{F(s)} = \frac{K_G}{1 + T_G s} \tag{4.9}$$

It should be noted that maintaining a safe and stable operation of the tidal rotor is the main function of the current control loop. This makes the PI controller the most important component in the loop because it's responsible for the generator field

regulation, therefore the stable and safe operation of the whole system. A PI controller has a relatively less complex structure, easy debugging, flexible and robust [98]. It is also one of the most employed control scheme for industrial applications to date [99]. However, it requires tuning, the values of the P and I components determine how well the controller reacts to system transients. A variety of PI controller tuning techniques are reported in literature [100-101]. The "Symmetric optimum" method is implemented for in this system. This is especially suitable for cases when the transfer function of an open regulatory circuit has a third degree multinomial polynomial in the denominator as illustrated above.

When the "symmetrical optimum" tuning method was applied, the P and I components were calculated as follows:

$$K_P = \frac{1.5T_S}{2K_G 5T_G} = 5e^{-5} \tag{4.10}$$

$$T_i = \frac{2}{K_G K_P} = 8.2e^4 \tag{4.11}$$

Assuming a fixed DC bus voltage (8kVDC), and constant tidal velocity (2.2m/s), gives a maximum power of 0.82MW as shown in *Fig 4.2: Speed Vs Power turbine characteristics:*, the desired DC-Bus current would be ($I_{dc} * = 104A$); The P and I controller values presented by (**4.10**) and (**4.9**) were incorporated into the controller and simulated to achieve the desired DC-bus current as shown in *Fig 4.16*.
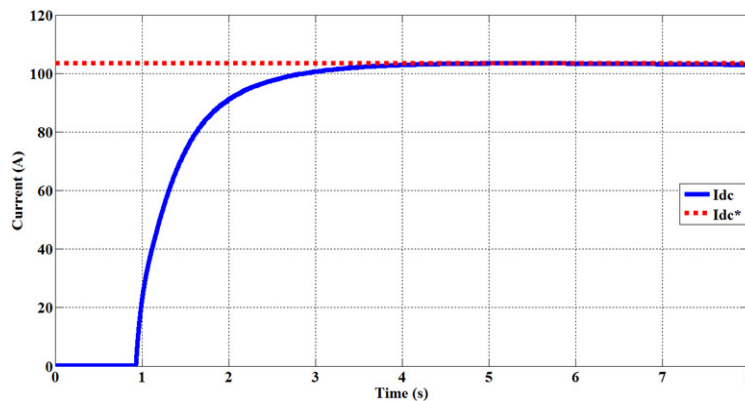
Fig 4.16: DC-bus current regulation using PI controller in (4.10) and (4.9)

(simulation model shown in Appendix A, Fig 8.3)

It can be seen in *Fig 4.16* that the controller is stable i.e. it took ≈3 seconds to achieve the desired DC bus current of 104A.

4.6.2   Stall control

As discussed in previous sub-sections, multiple generators are connected in parallel onto a common DC-bus. Therefore those with shaft speeds lower than the required *"cut-in"* speed will not produce enough back emf to make the rectifier diodes forward biased thus no power generation takes place from those turbines. To extract power from all devices connected onto the common DC-bus, even those with lower shaft speeds, DC-bus voltage would have to be regulated such that the back *emf* required by all the generators is low enough for the associated rectifier diodes to become forward biased. This as a consequence would reduce *"cut in"* speed, and in-turn allow for power generation even at very low tidal velocities and shaft speeds as illustrated in *Fig 4.9: DC-bus voltage control schematic*.

On the other hand, tidal turbines have to cope with the intermittent and seasonal variability of tidal currents. Therefore they begin to generate useful amounts of power when the tidal velocity is above the *"cut-in"* speed, and that is when power can be supplied to the utility grid. However, when the tidal currents are too high, control must be exercised to limit the turbine shaft speed to its rated value. Therefore, for cases where rotor speed cannot be maintained at its rated value, stall control is proposed. Typical tidal turbines stall regulation is achieved when the "angle of attack" at which the tidal flow strikes the blades is raised, as a consequence reducing the induced drag associated with lift stalling the turbine.

For the proposed system, stall control is to be achieved by indirect control of the turbine shaft torque so that it occurs when the tidal velocities exceeds a certain level. This means that the captured power can be automatically limited within the generator's rated power envelope. This method is believed to be simple, robust and cheap, as stalling is made to happen passively as described in section **4.4.1**

Proposed stall control is to operate as shown schematically in *Fig 4.17* below.
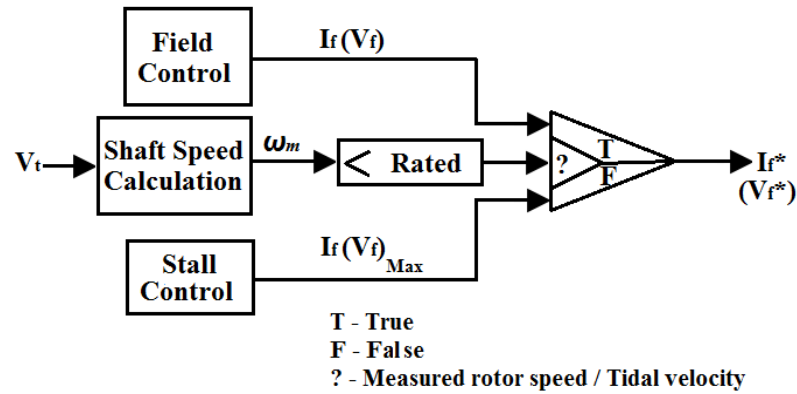
Fig 4.17: Stall control schematic

At very high tidal velocities both the available generator shaft power and speed could exceed the system's rated values, therefore to protect the generator from overload and over-speed, the field current is increased to the maximum possible value increasing torque, and as a consequence rotor speed is reduced resulting in the rotor stalling as illustrated in *Fig 4.10: Stall control 9kVDC*. However, if higher field current is required to stall the turbine i.e. more than the rated value, voltage regulation could be employed to reduce DC-bus voltage thus reducing the field current requirement as demonstrated in *Fig 4.6: Steady state operation points at 9kVDC*, *Fig 4.7: Steady state operation points at 8kVDC* and *Fig 4.8: Steady state operation points at 7kVDC*.

4.6.3   System Simulation Results and discussions

A Matlab/Simulink model of the proposed tidal control system was developed. A synchronous generator driven by variable speed constant-pitch tidal turbine together with a diode rectifier and field excitation controller was modelled and simulated to analyse the control methodology presented in *Fig 4.12: Tidal turbine control methodology.*

The primary objective of the control system is to regulate the generator's shaft power via field current control so that the system operates within its rated power and speed envelope as shown in *Fig 4.18*. For example field current should be controlled to achieve maximum available power for tidal velocities with peak power below the rated value as shown by the green dots. For the velocities with peak power above the

generators rated power, field current will be controlled to limit the shaft power to the rated power as shown by the yellow dots.

The purple dots show the speed at which optimum power is achieved at various tidal velocities.
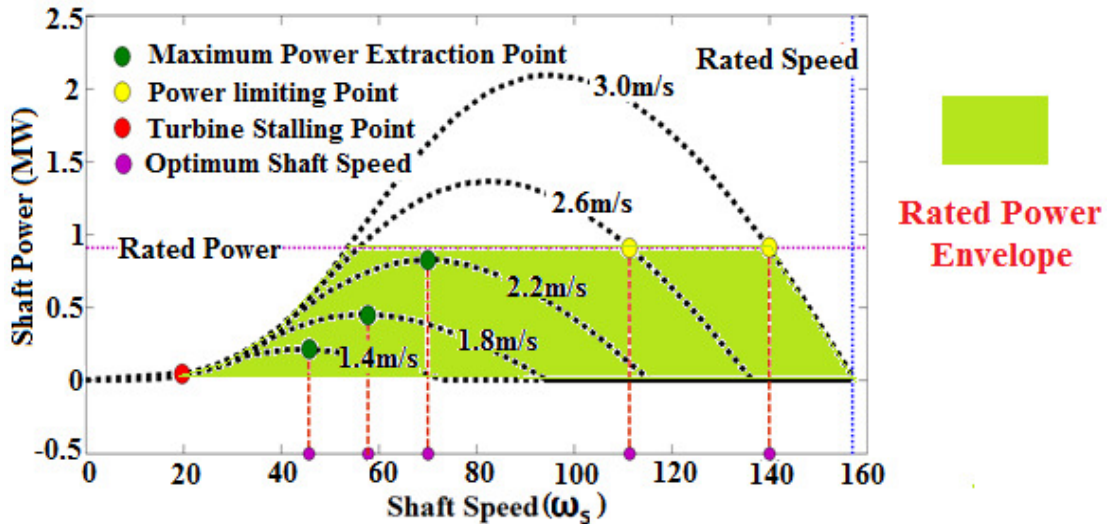
Fig 4.18: Rated Power Envelope

When the tidal velocity is too high such that the speed at which rated power can be achieved without exceeding the machines rated torque is greater than the machines rated speed, field current will be controlled to achieve the intersection point shown by the red dot stalling the turbine.

4.6.3.1 Time-domain simulation

The proposed tidal turbine was simulated together with the proposed controller to analyse its ability to achieve the steady state operation points predicted at various DC-bus set voltages as illustrated in *Fig 4.6: Steady state operation points at 9kVDC*, *Fig 4.7: Steady state operation points at 8kVDC* and *Fig 4.8: Steady state operation points at 7kVDC*. (Simulation model used to obtain the following results is presented in Appendix A, *Fig 8.3*).

4.6.3.1.1   Shaft Power control

When the rotor shaft is at steady state the control system starts to regulate the field current to achieve the desired shaft torque which in turn regulates speed achieving desired shaft power.

The reason why the control system is engaged at steady state is to enable power regulation to take place on the right hand side of the power curve where field current, and thus torque demand, is low as demonstrated in *Fig 4.19*.
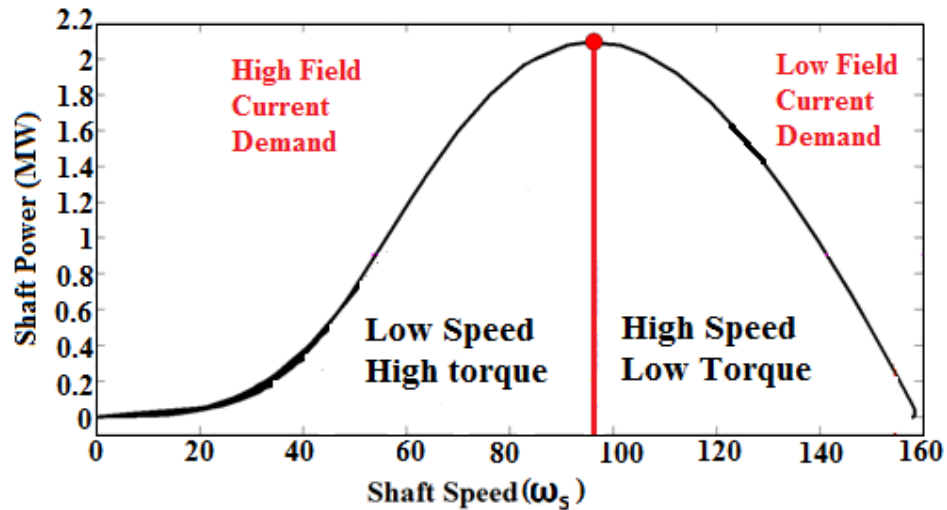
Fig 4.19: Field Current Demand

If the controller was to operate on the left hand side of the power curve there would be a higher chance of overloading the generator by applying too much torque and field current causing damage, especially for the devices influenced by tidal velocities whose peak power is greater than the system's rated power.

The proposed tidal turbine computer simulations where carried out at various DC-bus voltages i.e. 9kVDC, 8kVDC and 7kVDC analysing the control systems ability to regulate shaft power via field current control.

The simulation results in *Fig 4.20* and *Fig 4.21* show the regulated shaft power and speed respectively when the proposed controller described is employed. *Fig 4.22* shows how the field current was regulated to achieve the results in *Fig 4.20* and *Fig 4.21*
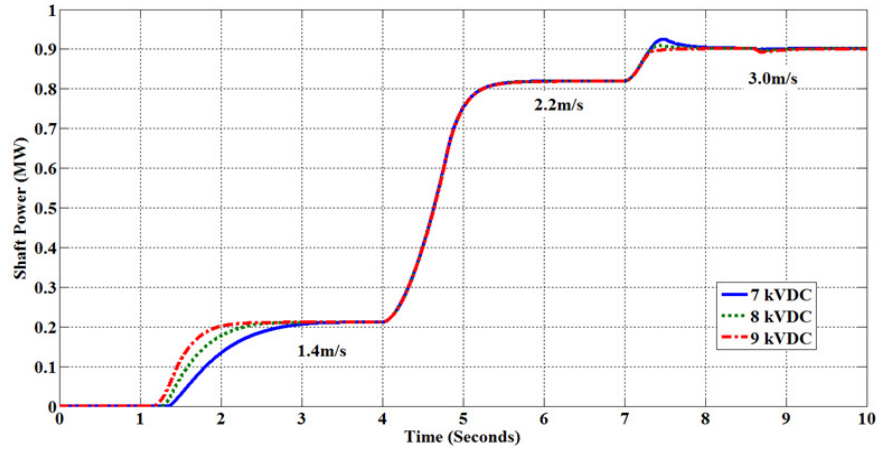
Fig 4.20: Regulated Shaft Power
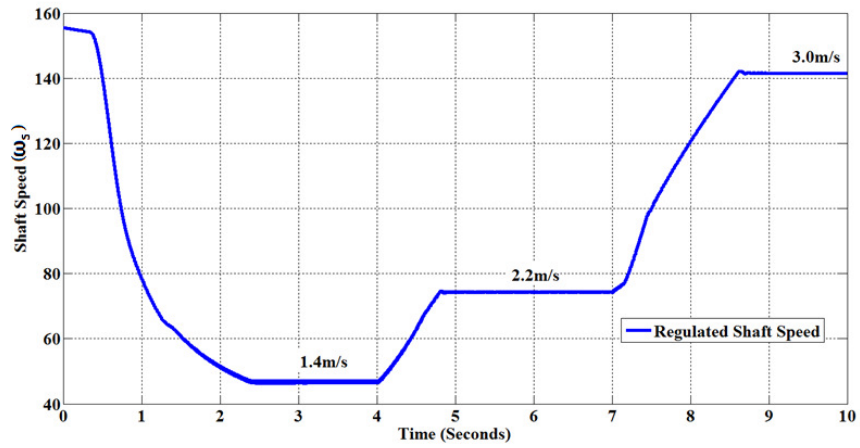
Fig 4.21: Regulated Shaft speed
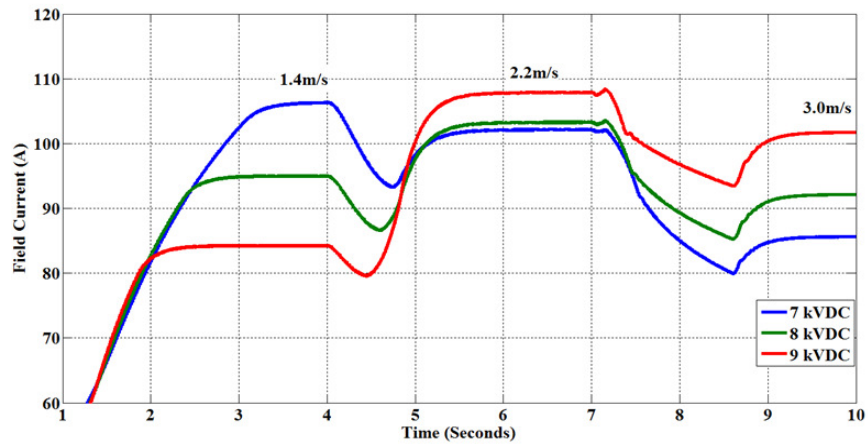
Fig 4.22: Regulated Field Current

It can be identified in *Fig 4.22* that the proposed control methodology successfully regulated the generator field current achieving desired shaft power as well as optimum

shaft speed at various DC-bus voltage set points. For example: when the tidal velocity was set to 1.4m/s maximum power extraction was achieved at all DC-bus voltages. Power limitation was also achieved for when the tidal velocity was set to 3.0m/s.

The results presented in ***Fig 4.20***, ***Fig 4.21*** and ***Fig 4.22*** when compared to the predicted steady state operation points presented in ***Fig 4.6:*** *Steady state operation points at 9kVDC*, ***Fig 4.7:*** *Steady state operation points at 8kVDC* and ***Fig 4.8:*** *Steady state operation points at 7kVDC*, it can be observed that the optimum/desired operation points are almost exactly the same. This confirms the proposed controller's ability to achieve desired system operation points via field current regulation alone.

Stall control could also be achieved by raising the field current to its rated value of 250A as illustrated below. ***Fig 4.23***
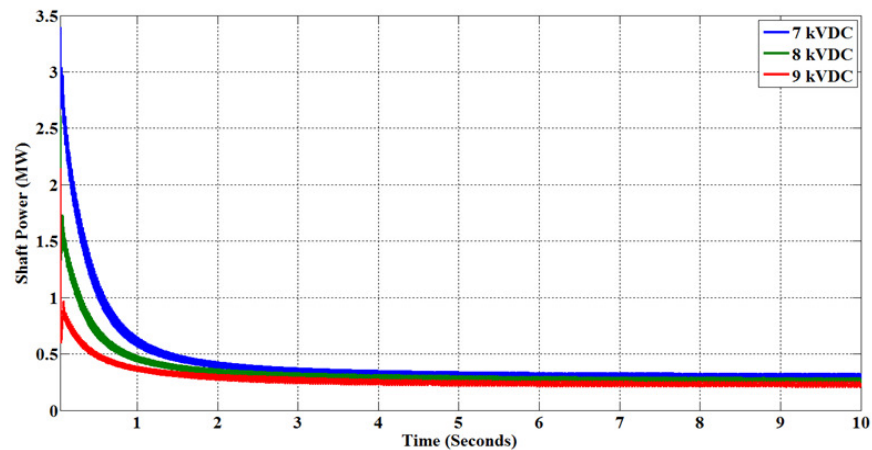
Fig 4.23: *Stall control Power Regulation*
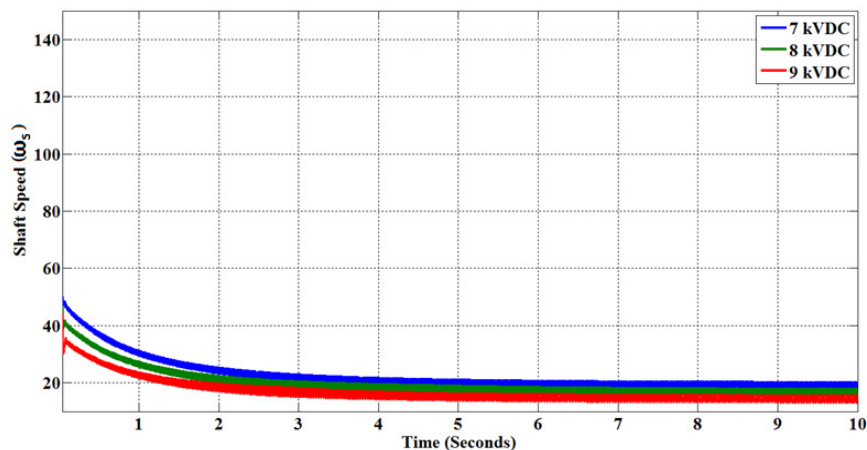
Fig 4.24: Stall control Speed Regulation

97
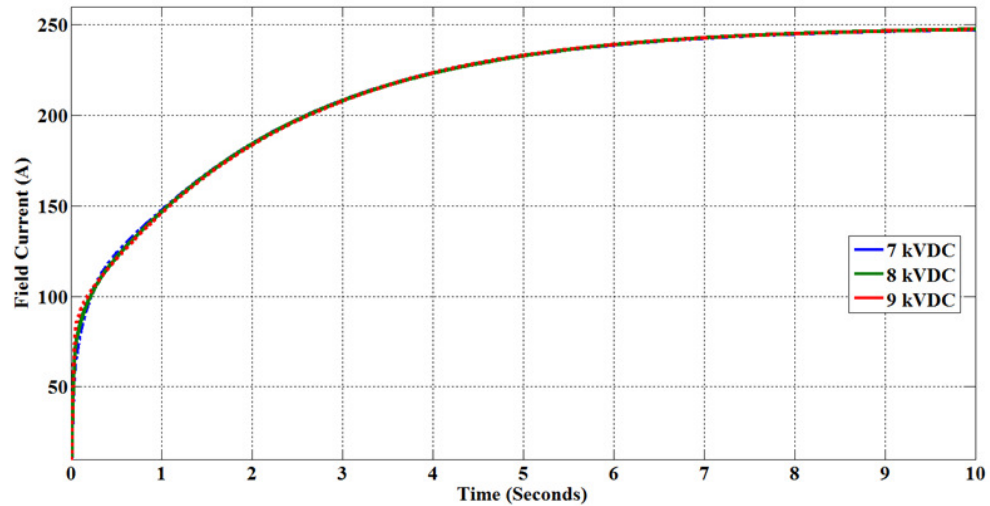
Fig 4.25: Stall control Field Current Regulation

Fig 4.23 and *Fig 4.24* show shaft power and speed when the maximum/rated generator field current is applied as illustrated in *Fig 4.25*. It can be seen that the proposed control methodology can successfully achieve stall control. However a brief overpower is attained as the excitation increased to its maximum value to reduce the shaft speed from over 157rad/s to ≈ 20rad/s to stall the turbine. In practice the tidal rotor would not run at such low speeds seen in *Fig 4.24* thus the turbine would simply stall. Nonetheless, when tidal velocity is higher than the systems designed velocity stalling the turbine is the desired effect because it would protect the rotor from over speed and the generator from over load.   It should be noted that stall control by field excitation is only possible if this surge in power is only brief and wouldn't burn out the generator or blow the protective device (Fuse).

It should be noted that the field current can only be raised to a value not greater than the generator's rated value. Therefore, instants where the field current required to stall the turbine is greater than the rated value, DC-bus voltage would have to be raised to a higher value in turn reduce required field demand.

4.7 Average model rotor control methodology

The averaged model realised in **Chapter 3** shows that power transfer from the tidal rotor side to the DC-Bus can be determined from the input variables such as, field current, rotor speed and DC-bus voltage. This implies that the system's input variables

98

required to generate desired power can be derived from the averaged model as illustrated below.

$$P_m = T_{em}.\,\omega_s \qquad\qquad 4.12$$

$$T_{em} = K_T.\,i_f.\,I_m \sin\vartheta \qquad\qquad 4.13$$

$$K_T = \frac{3P.\,L_f}{\sqrt{2}}$$

$$P_{dc} = (I_m K_i).\,(V_T K_V) \qquad\qquad 4.14$$

$$P_{m_t} \cong P_m \cong P_{dc}\,, \qquad \frac{1}{2}.\,C_p(\lambda).\,\rho.\,A.\,V_t^{\,3} \cong T_{em}.\,\omega_s \cong (I_m K_i).\,(V_T K_V) \qquad 4.15$$

$$I_m = \sqrt{i_{d_{av}}^2 + i_{q_{av}}^2} \qquad V_T = \sqrt{V_{d_{av}}^2 + V_{q_{av}}^2} \qquad \omega_s = \frac{\partial\theta}{\partial t}$$

Where L_f ,i_f and I_m are the field inductance, field current, and generator stator phase current respectively, P is the number of pole pairs. ϑ, P_m and T_{em} are the torque angle, generator output power and electromagnetic torque at synchronous speed ($\vartheta=90^o$).

From the average model, the generator terminal voltage (V_T) and current (I_m), can be estimated as follows for a given set of inputs, i.e. V_{dc}, i_f and ω_s.

when the DC-bus voltage is fixed, the generators output terminal voltage (V_T) can be realised as described in (**4.16**), which in turn determines the generator phase current (I_m) with reference to system's shaft power dictated by i_f and ω_s.

$$V_T = \frac{K_T . i_f . \omega_s}{K_i . K_v}$$

4.16

$$I_m = \frac{id_{av} . \omega_s}{i_f \left(K_T . K_{cos} \sqrt{\left(\frac{V_{dc}}{K_v}\right)^2 - V_{q_{av}}^2} + K_T . K_{sin} \sqrt{\left(\frac{V_{dc}}{K_v}\right)^2 - V_{d_{av}}^2} \right)}$$

4.17

K_v and K_i, are load dependent and their values can be realised as follows:

$$K_i = \frac{K_T . i_f . \omega_s}{V_{dc}}$$

4.18

$$K_v = \frac{K_T . i_f . \omega_s}{K_i . V_T}$$

4.19

Therefore the rotor side controller discussed in the previous subsection can be further simplified by using the system averaged model. For example if the tidal velocity and the DC-bus voltage were known or could be measured, the field current required to archive desired power extraction can be calculated as described in (**4.20**).

$$i_f^* = \frac{\left(K_{cos}V_{d_{av}} + K_{sin}V_{q_{av}}\right)\frac{I_{dc}}{V_{dc}} . \frac{V_t . \lambda_{opt} . G_B}{R_m} . K_i}{I_{dc} \left(K_T . K_{cos} \sqrt{\left(\frac{V_{dc}}{K_v}\right)^2 - V_{q_{av}}^2} + K_T . K_{sin} \sqrt{\left(\frac{V_{dc}}{K_v}\right)^2 - V_{d_{av}}^2} \right)}$$

4.20

where G_B is the gear ratio (assumed to be 1:40 in this case, thus $G_B = 40$)

During normal operation, maximum power extraction is usually desired, however operating at the maximum TSR (λ_{max}) with the tidal turbine is not necessarily the best operating state for the system as a whole. For instance at high tidal velocities it could be better to operate at a lower TSR to limit shaft power and to protect the generator from overload. Therefore in order to achieve power limitation with this simplified controller, optimum TSR(λ_{opt}) at a given tidal velocity has to be known and this could be realised

from the turbine characteristics shown in *Fig 4.18: Rated Power Envelope*, where the desired shaft speeds can be identified, thus by utilising equation **(3.2)** (λ_{opt}) can be calculated and incorporated into equation (**4.20**)**.**

Equation (**4.20**) can be used during component selection i.e. if the field current required to achieve desired output power can be calculated, the system model equations defined in **Chapter 3** can be used to determine the other system parameters allowing for the initial selection of the tidal system components without extensive simulations.

 The tables below show the calculated field current using (**4.20**)**.**

Tidal Velocity (m/s) $[V_t]$	*Shaft Power (MW)* $[P_m{}^*]$	*Shaft Speed (rad/s)* $\left[\omega_s = \left(\frac{V_t \cdot \lambda_{opt} \cdot G_B}{R_m}\right)\right]$	*DC-bus Current (A)* $\left[I_{dc} = \left(\frac{P_m{}^*}{V_{dc}}\right)\right]$	*Field Current (A)* ($i_f{}^*$)
1.4	0.21	46	23	**105**
1.8	0.45	56	50	**93**
2.2	0.83	76	92	**102**
2.6	0.91	113	101	**91**
3.0	0.91	141	101	**85**

Table 4.1: Field Current Calculation at 9kVDC

Tidal Velocity (m/s) $[V_t]$	*Shaft Power (MW)* $[P_m{}^*]$	*Shaft Speed (rad/s)* $\left[\omega_s = \left(\frac{V_t \cdot \lambda_{opt} \cdot G_B}{R_m}\right)\right]$	*DC-bus Current (A)* $\left[I_{dc} = \left(\frac{P_m{}^*}{V_{dc}}\right)\right]$	*Field Current (A)* ($i_f{}^*$)
1.4	0.21	46	26	**94**
1.8	0.45	56	56	**88**
2.2	0.83	76	104	**102**
2.6	0.91	113	114	**96**
3.0	0.91	141	114	**92**

Table 4.2: Field Current Calculation at 8kVDC

Tidal Velocity (m/s) [V_t]	Shaft Power (MW) [$P_m{}^*$]	Shaft Speed (rad/s) $\left[\omega_s = \left(\dfrac{V_t \cdot \lambda_{opt} \cdot G_B}{R_m}\right)\right]$	DC-bus Current (A) $\left[I_{dc} = \left(\dfrac{P_m{}^*}{V_{dc}}\right)\right]$	Field Current (A) ($i_f{}^*$)
1.4	0.21	46	30	**79**
1.8	0.45	56	64	**82**
2.2	0.83	76	118	**106**
2.6	0.91	113	130	**105**
3.0	0.91	141	130	**100**

Table 4.3: Field Current Calculation at 7kVDC

It can be noticed that the calculated values in *Table 4.1*, *Table 4.2* and *Table 4.3* almost coincide with the simulation results presented in *Fig 4.20*, *Fig 4.21* and *Fig 4.22* respectively. This also shows that the developed average models in **Chapter 3** are capable of capturing the key dynamic features of the proposed tidal system power transfer in addition to being analytically efficient.

From the *Table 4.1, Table 4.2* and *Table 4.3, Fig 4.26* can be realised as below.
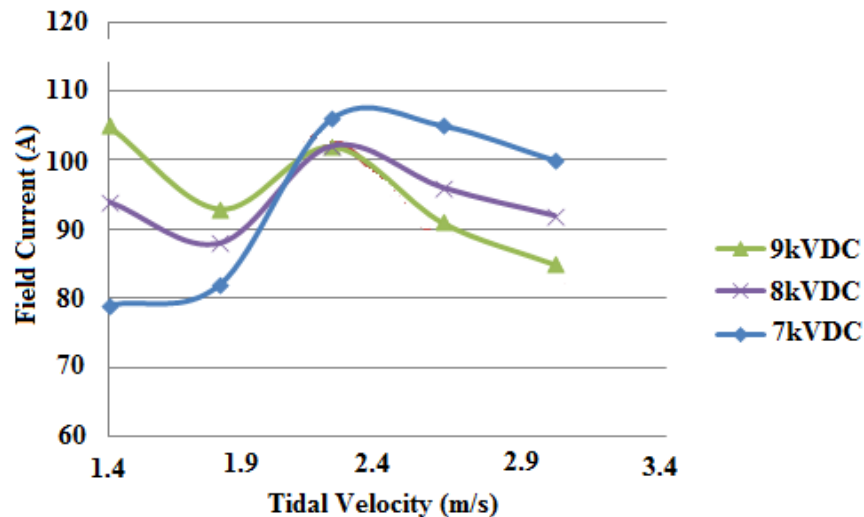
Fig 4.26: Steady state operation characteristics

Fig 4.26 shows the variation of generator field current with the tidal velocity at various DC-bus voltages.

Based on *Fig 4.26*, the tidal rotor controller illustrated in *Fig 4.12: Tidal turbine control methodology,* can now be re-organised as shown in *Fig 4.27*, replacing the automatic field control loop block with the system operation profile block containing the characteristics in *Fig 4.26*.
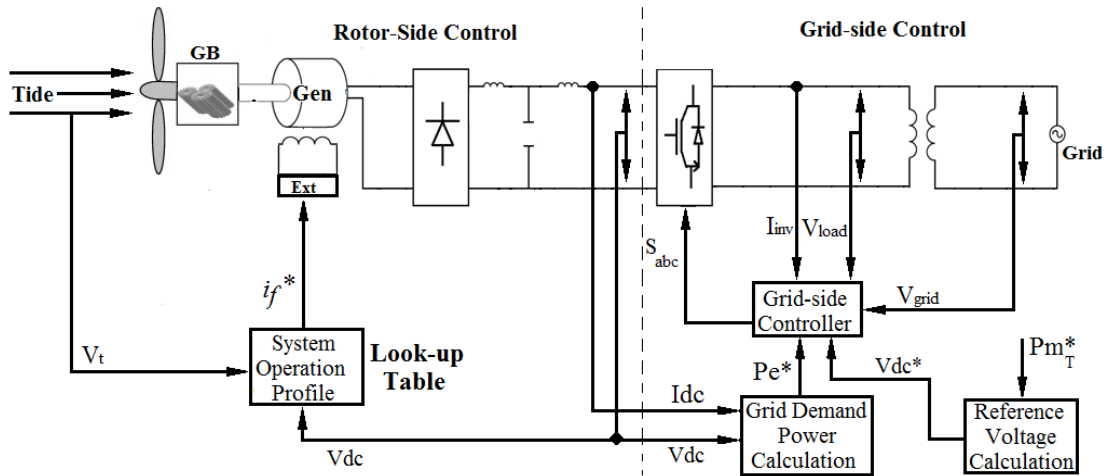
Fig 4.27: Average model rotor control Strategy

When the tidal turbine is at steady state, tidal velocity (V_t) and DC-bus velocity (V_{dc}) are measured and used by the system's operation profile in relation to *Fig 4.26* to determine the field current required to achieve desired shaft power at a given tidal velocity.

4.8 Tidal Farm power control simulations

A Matlab/Simulink tidal farm model consisting of three synchronous generators driven by variable speed constant-pitch tidal turbines, together with diode rectifiers and field excitation control, was developed (simulation model shown in Appendix A, *Fig 8.4*) to illustrate the operation principle of the averaged model tidal control strategy when applied to a tidal farm. The tidal velocity applied to each machine was assumed constant at steady state given that electrical transients are typically much faster than mechanical transients. Tidal velocity for each device was increased after 15 seconds to demonstrate how well the controller responds to tidal velocity changes which may occur in practice due to local sea conditions. Rotor shaft power regulation was achieved via field current control as illustrated in *Fig 4.27*. The rectifiers' output terminals were connected to a

DC-bus voltage source whose value was determined by the voltage controller defined in **(4.1).**

Maximum power extraction and power limitation of the simulated tidal farm was demonstrated as follows.
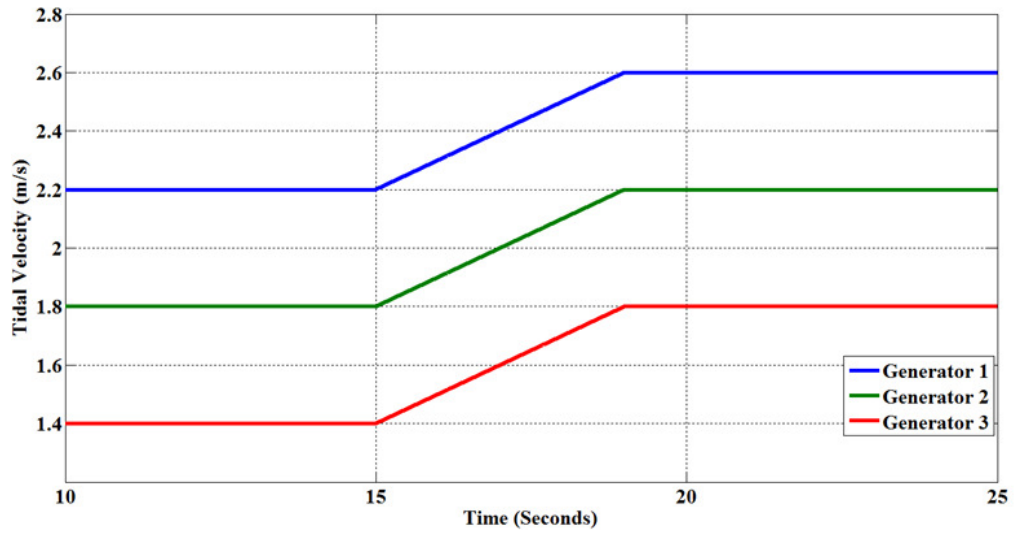
Fig 4.28: Simulated tidal Velocity
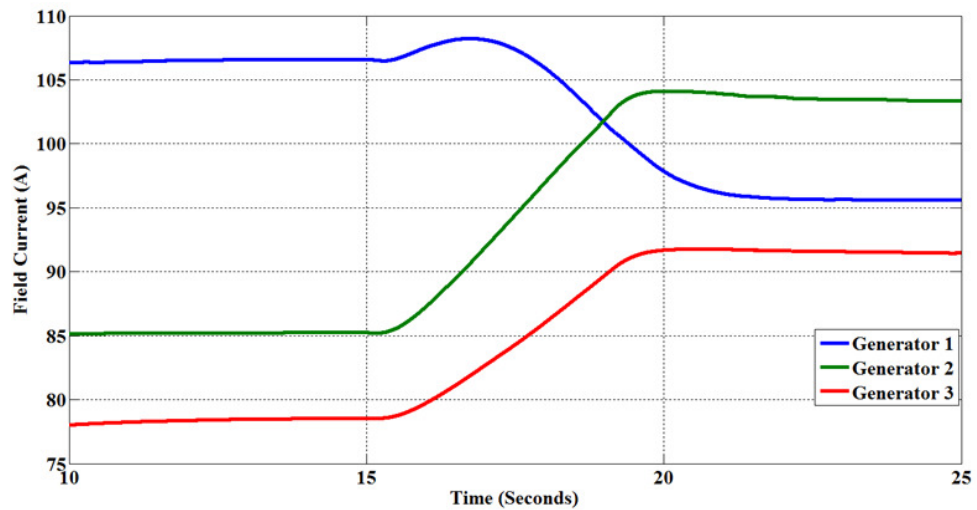
Fig 4.29: Regulated Field Current
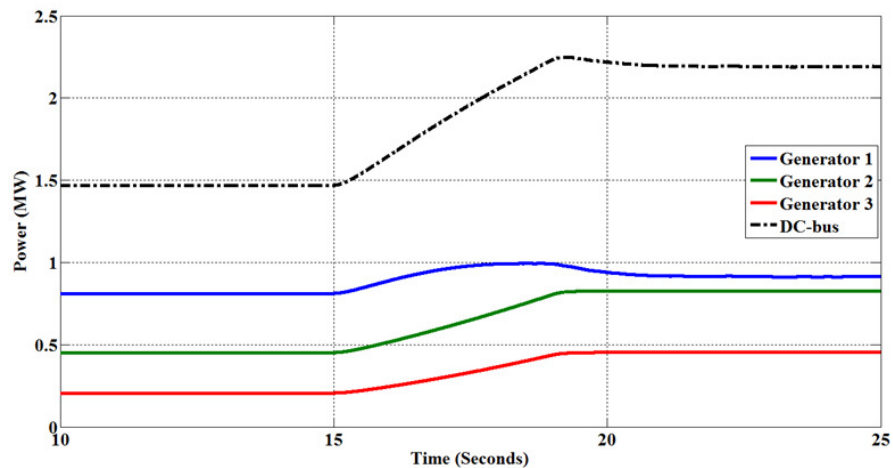
Fig 4.30: Simulated shaft power

It is demonstrated that as the tidal velocity changes as shown in *Fig 4.28* field current is regulated in-turn as shown in *Fig 4.29* to achieve the desired shaft power, for example when the available tidal power was below the generator's rated value of 0.91MW. At tidal velocities below 2.25m/s, maximum power extraction was achieved. However for the tidal velocity whose peak power is higher than rated value i.e. at 2.6m/s, shaft power was limited to the rated value as shown by Generator 1 between 20 and 25 seconds, thus demonstrating both maximum power extraction and power limitation.

Fig 4.30 represents the regulated generator shaft power under both steady state and transient conditions.
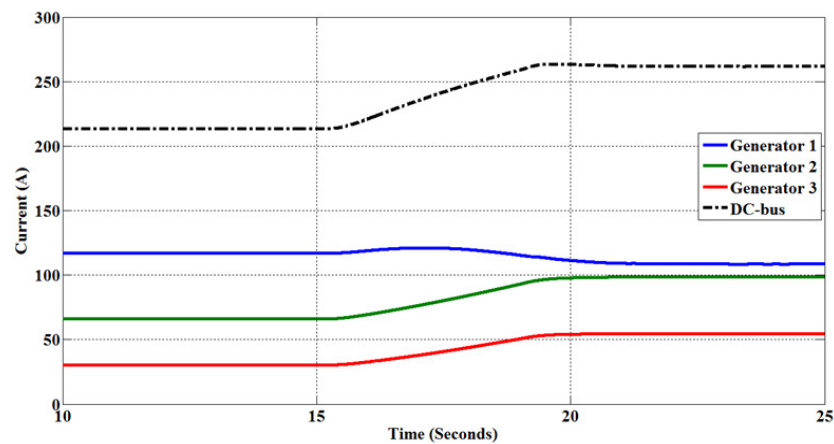
Fig 4.31: Generator and DC-bus Current

Fig 4.31 shows the simulated diode rectifier DC output currents from each generator and the DC-bus current which demonstrates that the current measured at the DC-bus is equivalent to the sum of the currents generated by the three machines. Furthermore, the output DC current from each generator is effectively proportional to its input power. For example, the input power of Generator 3 between the time period of 10 and 15 seconds is 0.21MW and its output DC current is approximately **27A**. Conversely, the input power of Generator 1 is four times that of Generator 3 in the same time period, and its averaged output current is four times of that of Generator 3 at approximately **110A**, which demonstrates that the proposed tidal power control topology is capable of controlling the electrical output power of each generator proportional to its input power, onto a fixed DC bus voltage.

It should be noted that the overshoot/undershoots noticed in the simulation results are due to the assumed tidal velocity transient rate of change which was selected for the purpose of achieving faster simulation times. However, overshoots/undershoots could be eliminated by reducing the transient rate of change. Moreover, the system's primary operation dynamics remain unchanged.
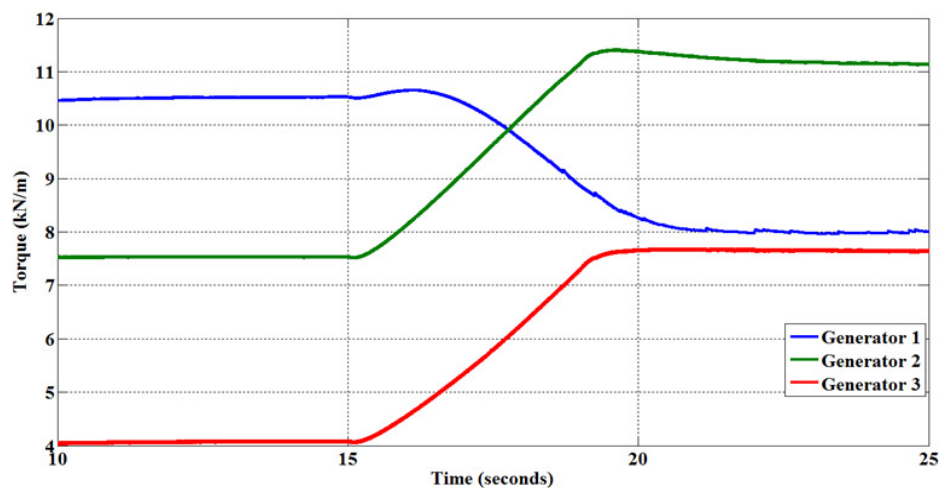
Fig 4.32: Generators' Torque

Fig 4.32 demonstrates that as the field current varies, generator torque changes as a consequence. This effect can be noticed more in Generator 1 for example, as although Generator 1 produces more power in the time period between 20 and 25 seconds its torque is much lower than that of Generator 2 in the same period, this is because field

current was lowered by the controller in order to limit shaft power to the rated value achieving power limitation control.
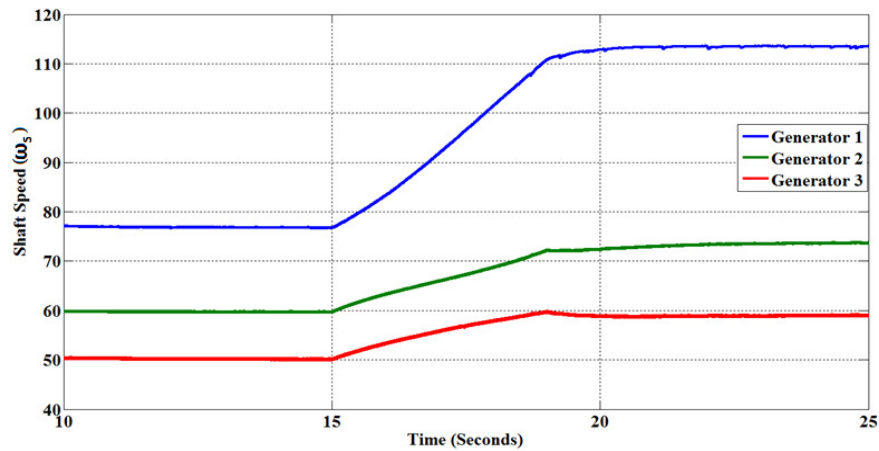
Fig 4.33: Generators' Speed

It is demonstrated in *Fig 4.32* and *Fig 4.33* that the generators' shaft power is proportional to the cube of the shaft speed, for example Generator 2 shaft is rotating at 76 rads/s between 20 and 25 seconds, producing 0.83 MW, and Generator 3 shaft is rotating at 48 rads/s between 10 and 15 seconds, generating 0.21MW. However for Generator 1 this would exceed the machine's capabilities and therefore in order to operate within the system's power envelope, its torque was reduced via field current regulation, consequently reducing shaft power.
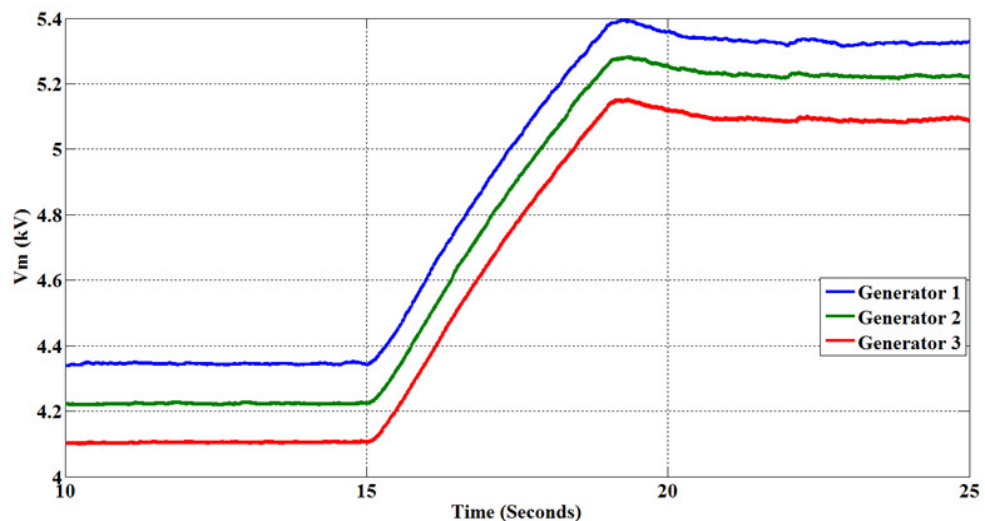
Fig 4.34: Terminal Voltage (V_m)

107
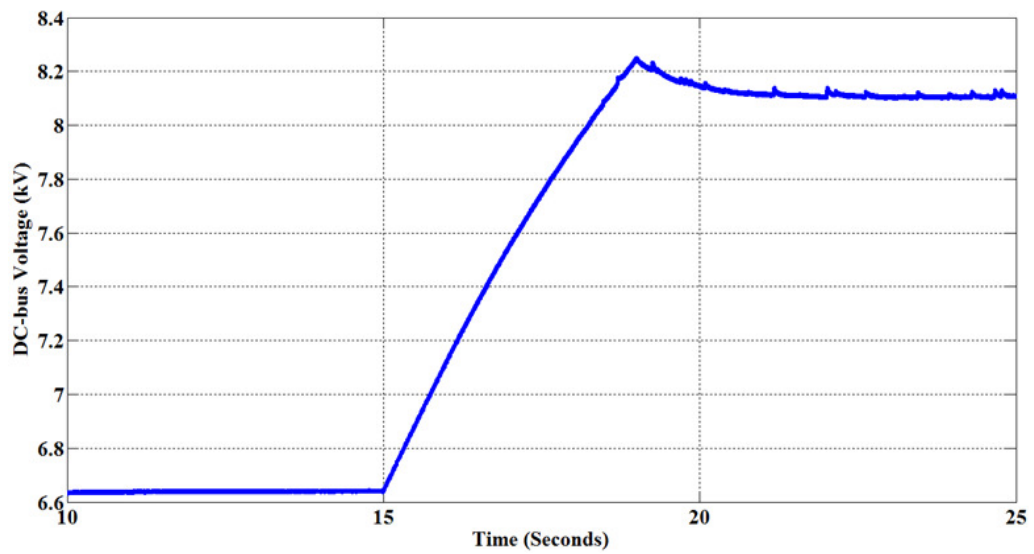
Fig 4.35: *Regulated DC-bus Voltage*

Fig 4.35 is obtained by applying (**4.1**) as the generator shaft powers increased after 15 seconds, thus it can be observed that DC bus voltage is increased by the DC-bus voltage controller as the tidal velocities/shaft power increased, for the purpose of identifying the best operation conditions for all the generators coupled onto the same DC link circuit. The effects of the change in DC-bus voltage on the generator terminal voltage (V_m) is also illustrated in ***Fig 4.34***
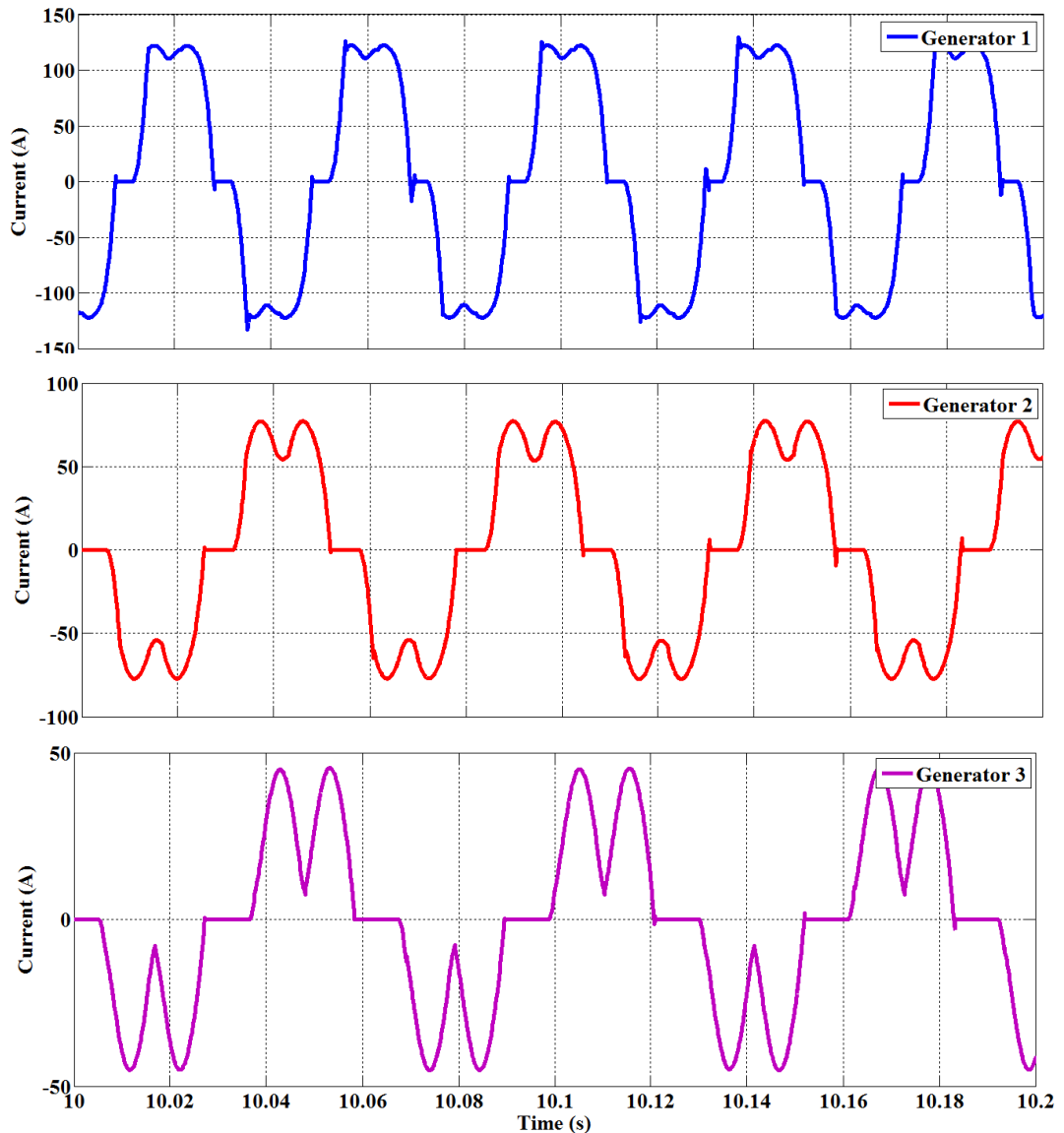
Fig 4.36: *Simulated AC current waveforms*

Fig 4.36 present the AC current waveforms of the three generators. It can be seen that the frequency of each generator is different due to a different tidal velocities applied to each generator. When a higher tidal velocity is applied to the turbine with a low generator terminal voltage, it rotates at a much higher speed producing higher current which results in higher electromagnetic torque in order to balance out the turbine driving torque reaching an equilibrium speed. As a result both the frequency and magnitude of the AC current are higher, and so is the output power.
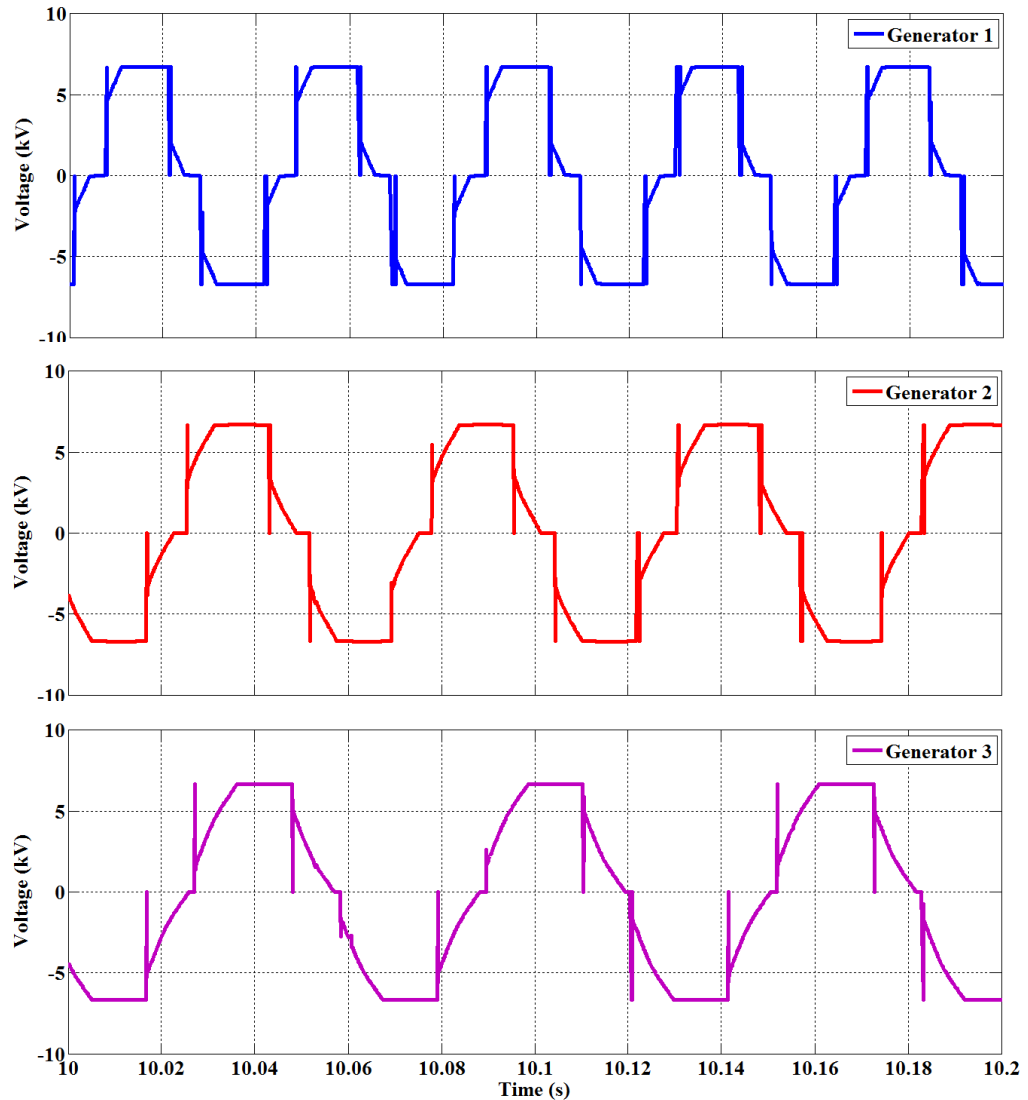
Fig 4.37: *Simulated AC voltage waveforms*

Fig 4.37 represents Generator 1, 2 and 3 line-to-line voltages at variable shaft speeds, it can be noticed that the waveforms have a 'flat' top, this is due to the connection of the bridge rectifier to a fixed DC-bus voltage source which fixes the generator terminal voltage, and therefore it does not change over an AC period.

4.9 Summary

In this chapter tidal system's components performance is discussed as well as their operation principle and characteristics illustrating their suitability for use with the proposed tidal topology under different modes of operation.

Based the system's component characteristics an automatic shaft power controller was realised and analysed via computer simulation, demonstrating maximum power extraction, power limitation and stall control. Furthermore the effects of the tidal system's input variables such as tidal velocity, field current & DC-bus voltage on the systems power transfer and controller were analysed. A DC-bus voltage controller was also realised in order to avoid over excitation at very low tidal velocities and for generator thermal protection. Stall control via field current alone was also demonstrated for when the tidal velocity is greater that the rated value, showing how shaft speed and power can be well regulated.

An analytical estimation of optimum field current is derived from the system average model presented in **Chapter 3**, which is then employed to modify the proposed field current controller, realising a simplified control topology via look-up tables. The operational characteristics of the simplified controller are presented and analysed via computer simulations.

A tidal farm consisting of three synchronous generators driven by variable speed constant-pitch tidal turbines was modelled using Matlab to illustrate how multiple tidal systems connected in parallel to a common DC-bus circuit can successfully be controlled using the average model control methodology during both steady state and transient operation.

The studies in this chapter show that field control alone is sufficient to achieve the following:

- To produce electrical output current proportional to the tidal input power, hence maximum power extraction and power limiting can be achieved.

- To allow the use of fixed pitch turbine blades instead of costly and more complicated variable pitch blades, or variable ratio gearboxes.

CHAPTER 5

5 SYSTEM VALIDATION

5.1 Introduction

In previous chapters a novel tidal stream power generation system topology was presented and discussed along with its performance and control. Its operation principle was also analysed via computer simulations. Further to this analysis a tidal power generation system test rig was developed as part of this research for the purpose of validating the system's computer simulation results presented in the previous chapters.

This chapter focuses on the hardware based tidal turbine experimental rig design and development, along with its preparation and practical analysis. Testing was done in a laboratory environment, therefore a scaled down tidal power generation system was considered. The tidal experimental rig hardware was configured as shown in **Fig 5.1**, only its steady state operation characteristics were analysed.
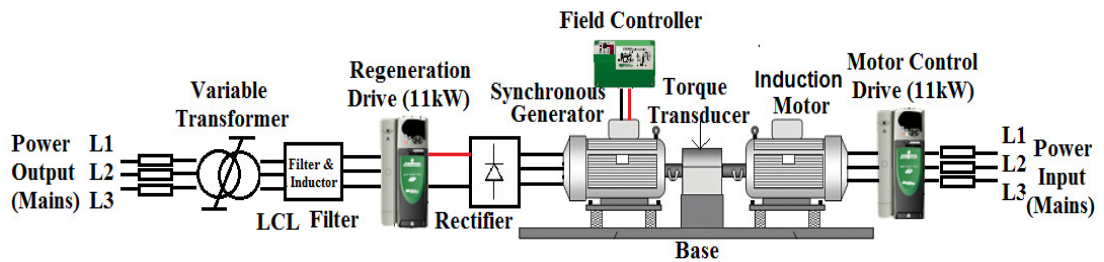
Fig 5.1: Tidal simulator configuration schematic

From the hardware set-up view point the tidal experimental rig comprised of the following main components, and operated as described in sub-section **5.1.1**:

- An Induction Motor
- Motor control drive
- A synchronous Generator loaded with a 3-phase diode rectifier
- Field current controller
- Regeneration drive (converter) and associated filter
- Variable transformer

5.1.1 Experimental rig operation overview

The above components were coupled together to form a hardware experimental rig that faithfully represented as far as possible, the dynamic behaviour of the proposed tidal power system. The induction motor was used to emulate the tidal turbine, and its torque (power)-speed characteristic were controlled via the motor control drive (inverter) to emulate that of a scaled turbine.

The induction motor shaft was then coupled to the synchronous generator, which in turn converted the shaft mechanical power into electrical power. Generator input/shaft power regulation was achieved via field excitation control.

The generator output power terminals were connected to a diode bridge rectifier which converted AC power into DC, whose voltage was regulated by the regeneration control drive (converter).

The regeneration drive was coupled to the utility mains via a 3-phase filter and a variable transformer. The filter minimised the electrical harmonics caused by the operation of the regeneration drive, and the variable transformer stepped down the main supply voltage seen by the regeneration drive at very low DC bus voltage set points. This allowed for power generation even at very low generator output voltages, given that power could only be recovered from the generator when its output voltage is higher than the DC-bus/mains voltage.

The electrical power generated by the experimental rig was fed back into the mains to replicate what would be expected on a practical tidal generation system as it connects to the utility grid.

Real-time control of the tidal simulator was undertaken using a data acquisition unit acting as an interface between the hardware and computer/software (LABVIEW) as described in Appendix A, section 7.1.

5.1.1 Objective

The reason for undertaking this experiment was to validate the proposed tidal system's operations characteristics predicted via computer simulations presented in **Chapter 4**.

Achieving this objective involved the following investigations:

- Synchronous generator power capability hardware experiments
- Steady state operation point realisation
- System performance under different modes of operation as well as the analysis of the:
  - Effects presented by DC-bus voltage variation on energy capture and system controllability
- Maximum Power Extraction and Power Limitation control.
- Energy capture at low tidal velocities.
- Speed regulation (Stall control).

However the core objective of the hardware based tidal turbine experimental rig was the ability to emulate actual tidal turbine rotor characteristics accurately and to faithfully represent the proposed tidal turbine topology.

5.2 Components selection and configuration

5.2.1 Induction motor (IM)

A 7.5kW induction motor was employed as the prime mover to represent the tidal turbine rotor blades and gearbox expected on the practical tidal power extraction system, in addition to emulating actual tidal rotor characteristics. Given that the speed of the induction motor is determined by the amplitude and frequency of the voltage supply. An IGBT inverter bridge/motor control drive was employed to regulate the induction motor's input voltage frequency and amplitude in turn determining its shaft speed at a given torque, subsequently emulating tidal rotor characteristics as will be discussed later in this chapter.

5.2.1.1 Tidal flow

The hourly stream velocities used during simulations were determined from published charts that presented both spring and neap tidal conditions as shown in *Fig 5.2* [102].
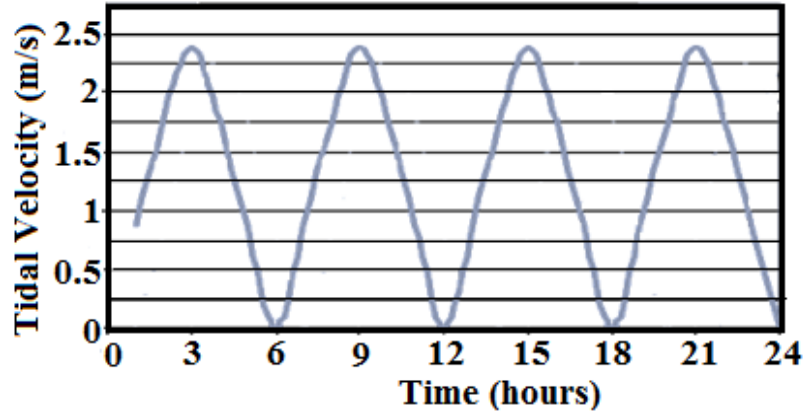
Fig 5.2: *Tidal Stream Velocity vs time*

It can be observed in ***Fig 5.2*** that the tidal period is 6 hours which implies that the variations in tidal stream velocity with time are very small during any electrical period of interest. Therefore constant tidal velocity at any electrical transient was assumed during experiments, given that electrical transients are much faster than mechanical transients.

5.2.2   Tidal Rotor Characteristics

To realise the induction motor operation profile, a tidal turbine model was developed in Matlab/Simulink, the developed model had the same power rating as the proposed experimental rig as described below.

The experimental tidal rig rotor characteristics model was realised as follows:

$$P_{ts} = (K_1 . Cp_{(\gamma)} V_t^3) . K_2 \qquad\qquad 5.1$$

$$K_1 = \rho . A * 0.5 = 314 \qquad\qquad 5.2$$

Where ρ and A are as defined in **Chapter 3**, P_{ts} is the available tidal power (scaled to induction motor rated output mechanical power of 7.5kW), K_2 is the scale down factor as defined in (5.3):

$$K_2 = \frac{P_{rig}}{P_{tide}} = 3.57e^{-3} \qquad\qquad 5.3$$

P_{rig} and P_{tide} are the induction motor rated output power (7.5kW) and the actual tidal rotor rated power (2.1MW as presented in **Chapter 4**) respectively.

From equations (5.1-5.3) tidal rotor characteristics were realised via Matlab/Simulink as shown in *Fig 5.3*. The experimental rig generator was rated at 5.2kW
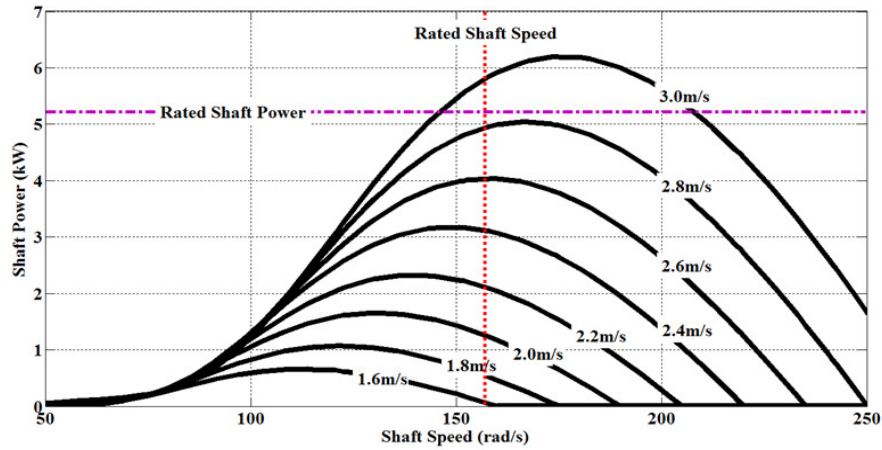
Fig 5.3: induction motor desired operation characteristic

From *Fig 5.3* available turbine power $\left(P_{t_s}\right)$ at a given shaft speed can be identified and therefore shaft torque (T_{mT}) at a given shaft speed (ω_s) was calculated as defined in equation **(5.4)** realising *Fig 5.4*:

$$T_{mT} = \frac{P_{t_s}}{\omega_s}$$

5.4

Fig 5.4 illustrates the calculated rotor torque characteristics

Fig 5.4: Simulation rig desired torque characteristic curves

116
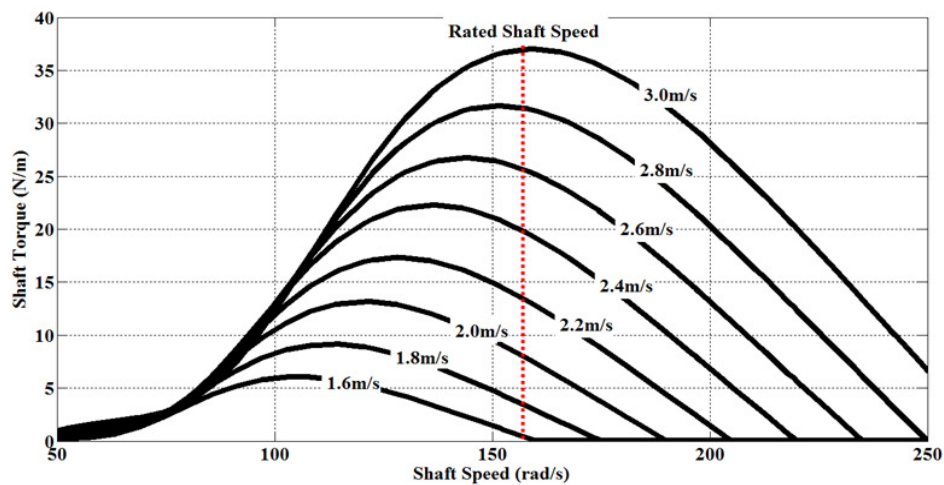
From *Fig 5.4* a 2D Look-up presented as *Table 5.1* illustrating resultant torque for a given tidal velocity and shaft speed was realised.

Shaft Speed ω_s (rad/s)	Tidal velocity (V_t)							
	1.6	1.8	2	2.2	2.4	2.6	2.8	3
52	0.2	0.4	0.5	0.6	0.8	0.9	1.1	1.2
58	0.4	0.5	0.7	0.8	1.0	1.2	1.4	1.6
63	0.6	0.7	0.9	1.1	1.3	1.5	1.7	1.9
69	1.3	1.4	1.5	1.5	1.7	1.8	2.0	2.3
75	2.3	2.5	2.6	2.5	2.5	2.5	2.6	2.8
80	3.4	3.9	4.1	4.1	4.0	3.8	3.7	3.7
86	4.4	5.4	6.0	6.2	6.2	5.8	5.5	5.2
91	5.2	6.7	8.0	8.5	8.7	8.4	8.0	7.5
97	5.8	7.8	9.7	10.8	11.5	11.3	10.9	10.5
103	6.0	8.6	11.2	12.9	14.2	14.4	14.3	13.9
108	6.0	9.0	12.2	14.6	16.6	17.4	17.6	17.5
114	5.8	9.1	12.9	15.9	18.7	20.0	20.9	21.2
115	5.7	9.1	13.0	16.2	19.1	20.6	21.6	22.0
121	5.3	8.9	13.2	16.9	20.6	22.8	24.4	25.5
123	5.1	8.7	13.1	17.1	21.0	23.4	25.3	26.6
128	4.4	8.2	12.9	17.3	21.8	25.0	27.6	29.5
130	4.2	8.0	12.7	17.3	22.0	25.4	28.2	30.4
136	3.5	7.2	12.1	17.0	22.3	26.3	29.8	32.8
138	3.2	6.9	11.8	16.9	22.3	26.5	30.2	33.4
143	2.4	6.0	10.9	16.2	22.0	26.7	31.2	35.1
145	2.2	5.7	10.5	15.9	21.8	26.7	31.4	35.5
151	1.4	4.7	9.4	14.9	21.0	26.5	31.7	36.5
152	1.2	4.4	9.1	14.6	20.8	26.3	31.7	36.6
153	1.1	4.3	9.0	14.5	20.7	26.3	31.6	36.7
158	0.3	3.2	7.8	13.2	19.6	25.5	31.4	37.0
160	0.0	2.9	7.3	12.8	19.2	25.2	31.2	37.0

Table 5.1: 2D Shaft Torque Look-up Table

For the induction motor to emulate the tidal rotor characteristics presented in *Table 5.1*, a controlled drive (**Motor Control Drive**)was employed**.**

5.2.3   Motor Control Drive (MCD)

Given that the speed of induction motor is dependent on the supply voltage & frequency, An 11kW Emerson Unidrive SP Drive was used as the motor control drive (MCD) to regulate the induction motor input voltage and frequency, consequently controlling shaft speed and torque as per the rotor profile presented in *Table 5.1.*

The employed MCD is composed of a diode rectifier which converts input AC power into DC. An inverter which controls a network of switches to alternate the positive and negative voltage buses of the DC power to produce AC voltage across the induction motor power input terminals, as well as generating controlled sinusoidal input current to a desired operating frequency and as a result emulate tidal rotor behaviour.

A representation of the employed MCD is depicted in *Fig 5.5*.
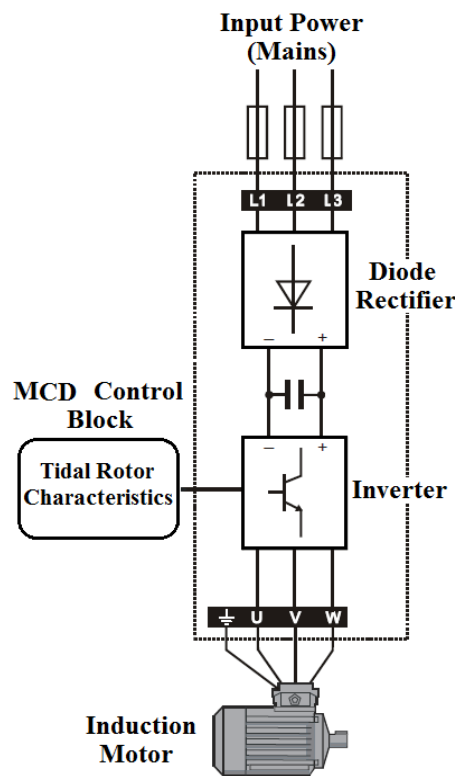
Fig 5.5: Motor Control Drive (MCD) electrical configuration

The employed MCD is configured as described Appendix A, section **7.2.**

5.2.4   Emulating tidal turbine rotor behaviour

To accurately validate the proposed tidal turbine topology the tidal turbine experimental rig had to reproduce as faithfully as possible the speed-torque and power characteristics of a practical tidal turbine as presented in *Fig 5.3: induction motor desired operation characteristic* and *Fig 5.4: Simulation rig desired torque characteristic curves*.

The tidal rotor emulator control algorithm was configured as illustrated in *Fig 5.6* below.
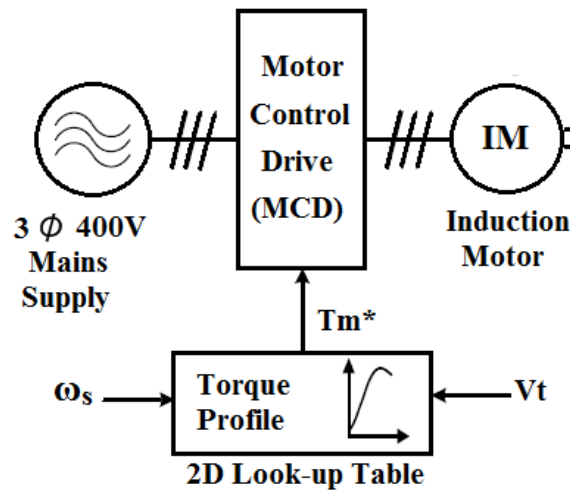
Fig 5.6: Turbine emulator control algorithm

Where (ω_s) is the motor shaft speed and V_t is the assumed tidal velocity.

Fig 5.7 and *Fig 5.8* below illustrate the induction motor shaft characteristics for both the power and torque respectively when the tidal velocity was set between the values of 1.8m/s and 2.6m/s. these results were realised when the control algorithm presented in *Fig 5.6* was applied**,** and compared to the actual (computer simulated) rotor characteristics presented in *Fig 5.3: induction motor desired operation characteristic* and *Fig 5.4: Simulation rig desired torque characteristic curves*, respectively
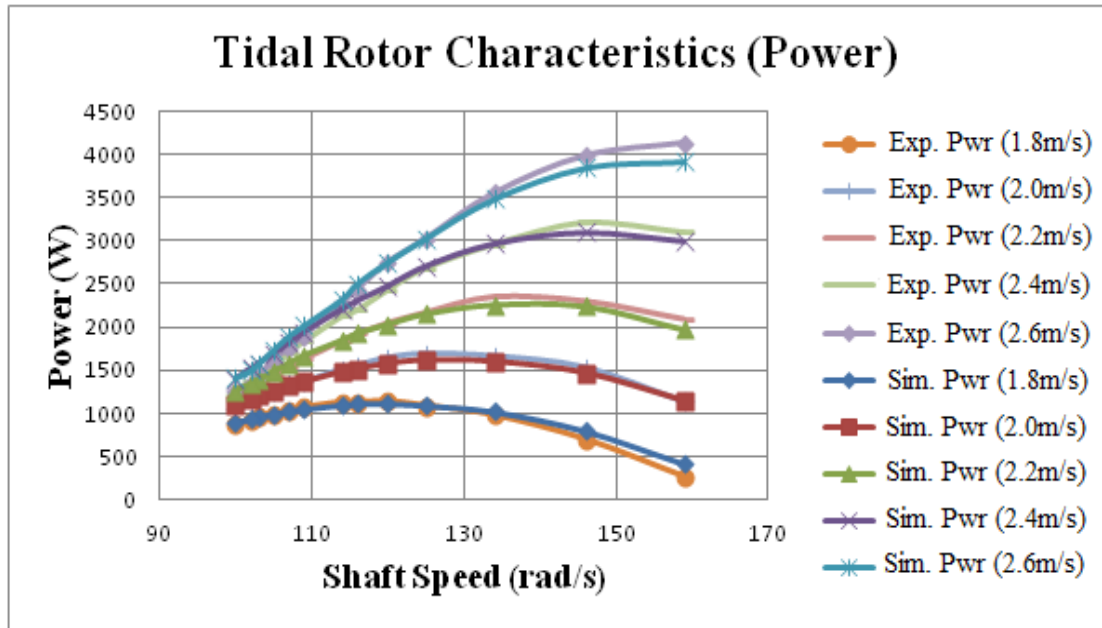
Fig 5.7: Shaft power characteristics
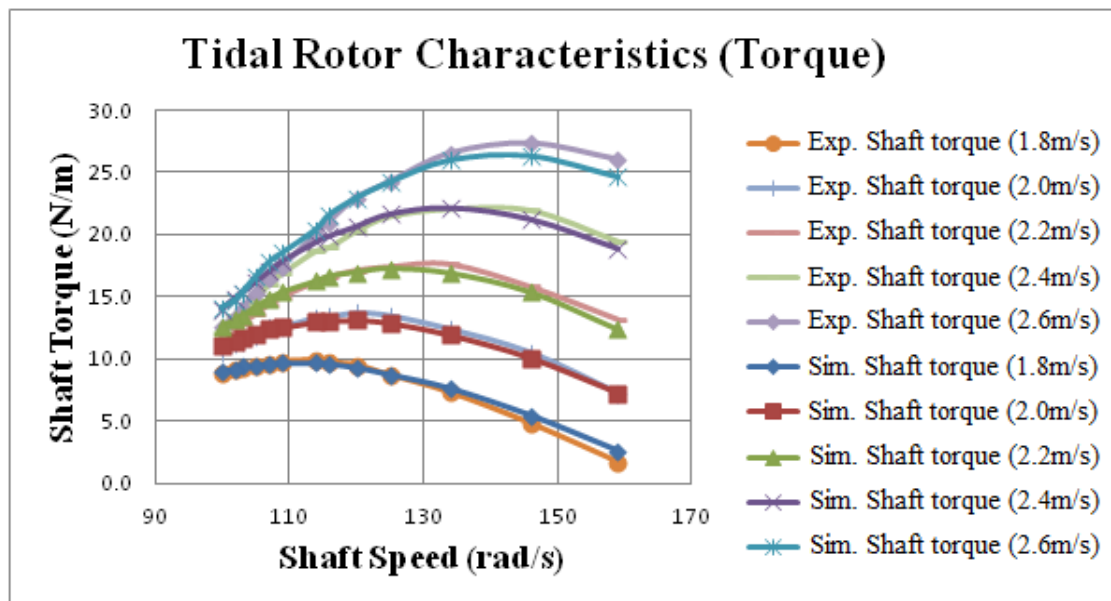
Fig 5.8: Shaft torque characteristics

It can be observed that the experimental rotor characteristics closely match the simulated tidal rotor dynamic behaviour predicted in *Fig 5.3: induction motor desired operation characteristic* and *Fig 5.4: Simulation rig desired torque characteristic*

120

curves, rendering the employed experimental rig appropriate for the proposed system validation.

To obtain the experimental results presented in *Fig 5.7* and *Fig 5.8*, the MCD was set in torque control mode as described in Appendix A, section **7.2** and then *Table 5.1: 2D Shaft Torque Look-up Table*, was modelled within LABVIEW simulation platform at various IM shaft speeds (ω_s). The tidal velocities (V_t) and the resultant 2D look-up table torque output was then sent to the MCD via the c-RIO (hardware and software interface module) as shown schematically in *Fig 5.6: Turbine emulator control algorithm*, in turn obtaining the IM shaft characteristics presented in *Fig 5.7: Shaft power characteristics*, and *Fig 5.8: Shaft torque characteristics.*

IM shaft torque was measured via a torque transducer coupled onto the shaft, and by using the measured shaft speed, shaft power could be realised.

The shaft speed at which the experimental rig started to generate power "*cut-in*" speed was approximately 100rad/s as illustrated in *Fig 5.7: Shaft power characteristics*

After validating the IM's ability to emulate tidal rotor characteristics it was then coupled onto the synchronous generator shaft via torque transducer as illustrated in *Fig 5.9.*
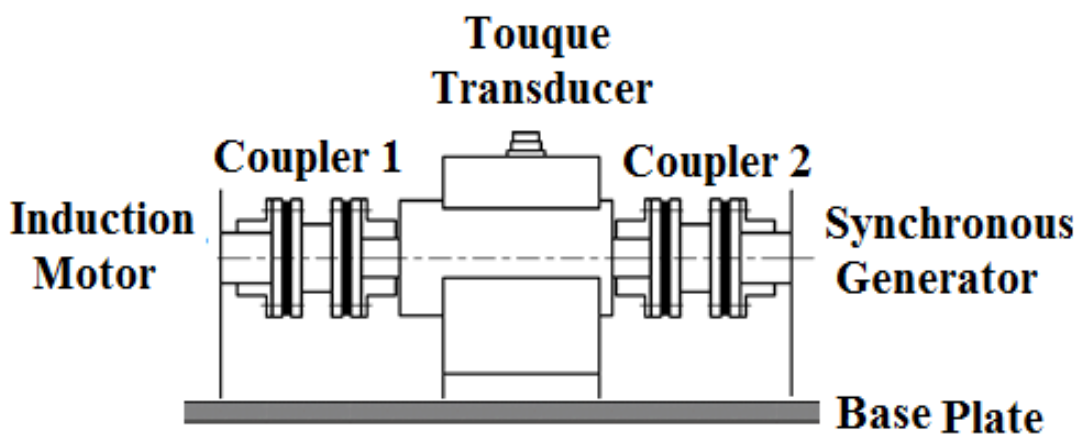
Fig 5.9: Generator and Motor coupling arrangement (Drive Train)

Fig 5.10 shows the hardware set-up for the Induction Motor - Synchronous Generator tidal experimentation dynamometer used.
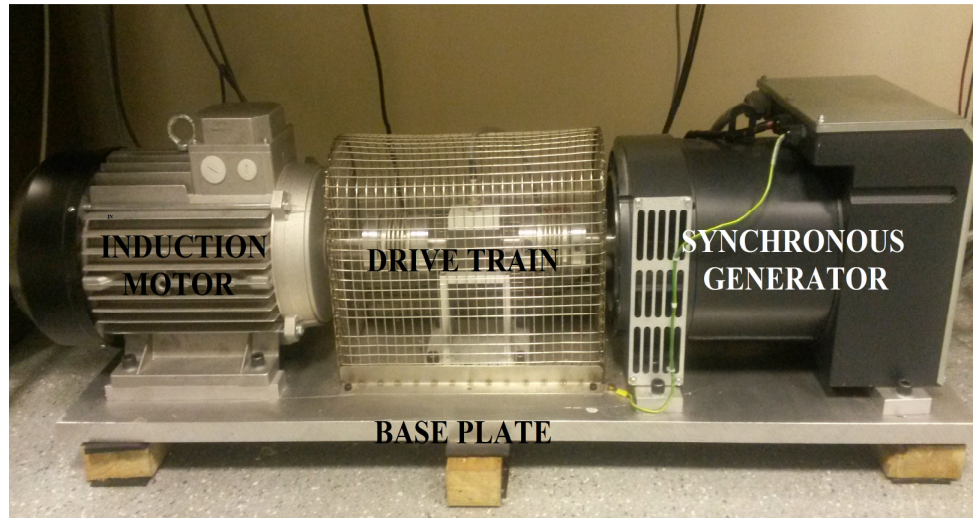
Fig 5.10: Dynamometer configuration

5.2.5   Synchronous Generator

A 3phase, 5.2 kW, 400V synchronous generator was employed. The generator's primary objective was to convert torque from the tidal turbine emulated by the IM drive into electrical power which could then be fed into the mains.

It should be noted that in practice the power generated by the tidal turbine is fed onto the utility grid.

The excitation current of the employed generator was by default supplied by an electronic regulator (AVR) which would also be responsible for regulating its DC excitation depending on the load changes maintaining a constant AC output voltage from the machine. This AVR was not used in the experiment, thus the generator's original field current regulation circuit was re-configured as shown in *Fig 5.11* which illustrates the sensing and auxiliary winding wires that were not used and the DC voltage source connection point introduced for separate field excitation of the generator.
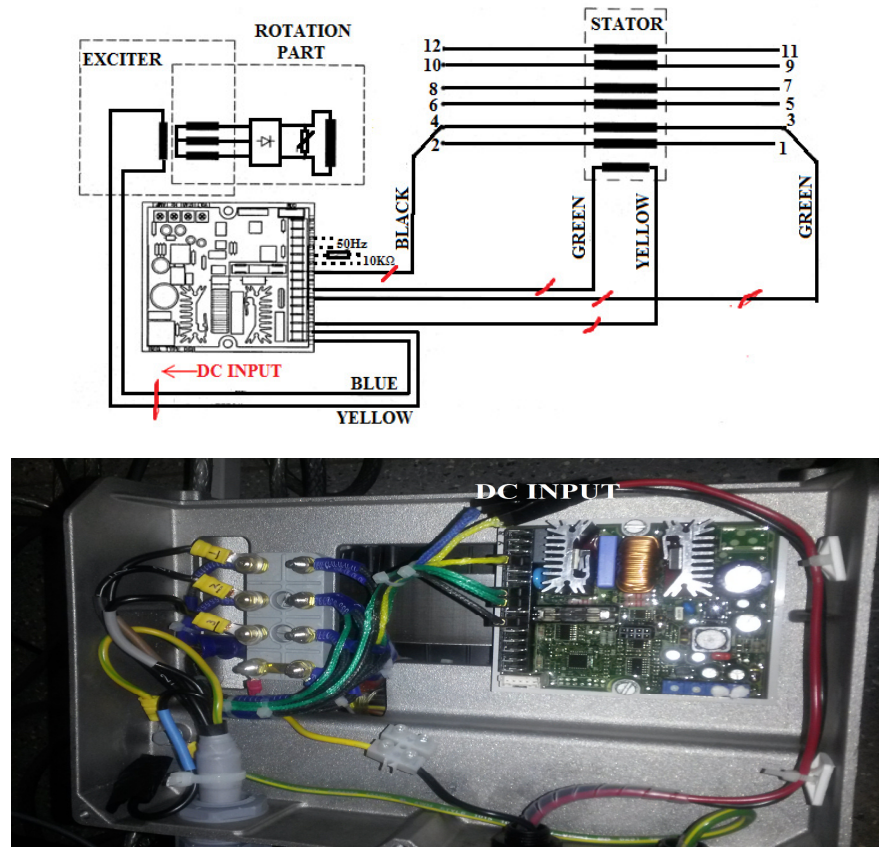
Fig 5.11: *Generator field excitation circuit*

Field current control was achieved by a controllable DC Power Supply coupled to the generator exciter input terminals. The employed controllable power supply consisted of non-isolated inputs and outputs terminals which were used to regulate generator field current. The control input signals to the controllable DC power supply were referenced to the positive output in the range of 0-10V. The control signals to the controllable DC power supply were determined in LABVIEW and sent to the DC power supply via the c-RIO.

The employed generator exciter was the TTi QPX1200 DC power source shown in Appendix B, ***Fig 9.1*** and ***Table 9.1***

5.2.5.1 Generator power characteristics

The employed 5.2kW generator capability characteristics were realised using the hardware experimental set-up by varying the field current applied to the rotor between

0.4A and 0.7A to analyse the generator's shaft power characteristics as the field current varied to confirm the computer simulations illustrated in *Fig 5.12* (a) below.
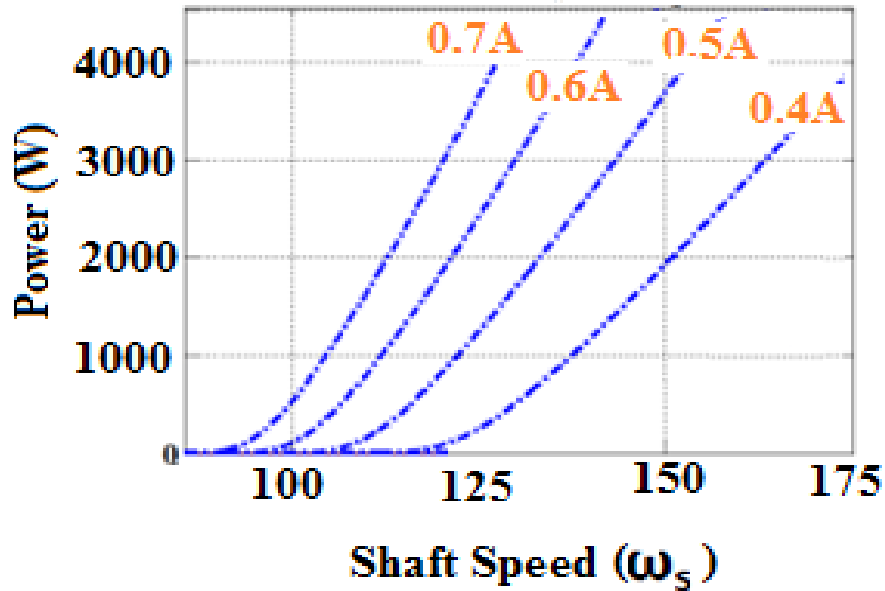
(a) Computer simulation results
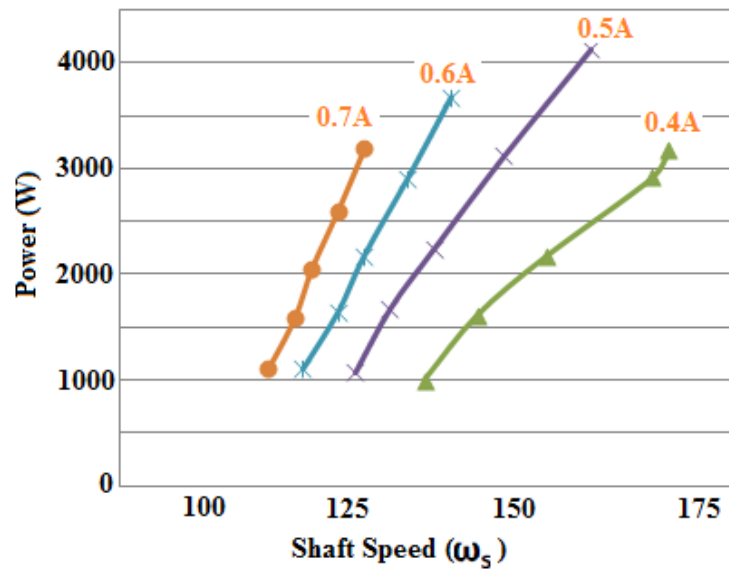
(b) Experimental Results

Fig 5.12: Generator capability curve at 420VDC voltage set point, at various field currents

Fig 5.12 **(b)** shows the experimental generator input power as a function of its rotational speed when the field current was varied. These results were obtained when the MCD was configured in torque control mode as described in Appendix A, section 7.2. This test was performed by varying the field current applied to the SG rotor via the controllable DC power supply, the DC link voltage was set to 420VDC and maintained by the regeneration drive. The regeneration drive operation principle will be discussed later in the chapter.

Fig 5.12 **(b)** illustrates that when the field current was increased generator shaft power increased as a consequence and the cut-in speed reduced in turn.
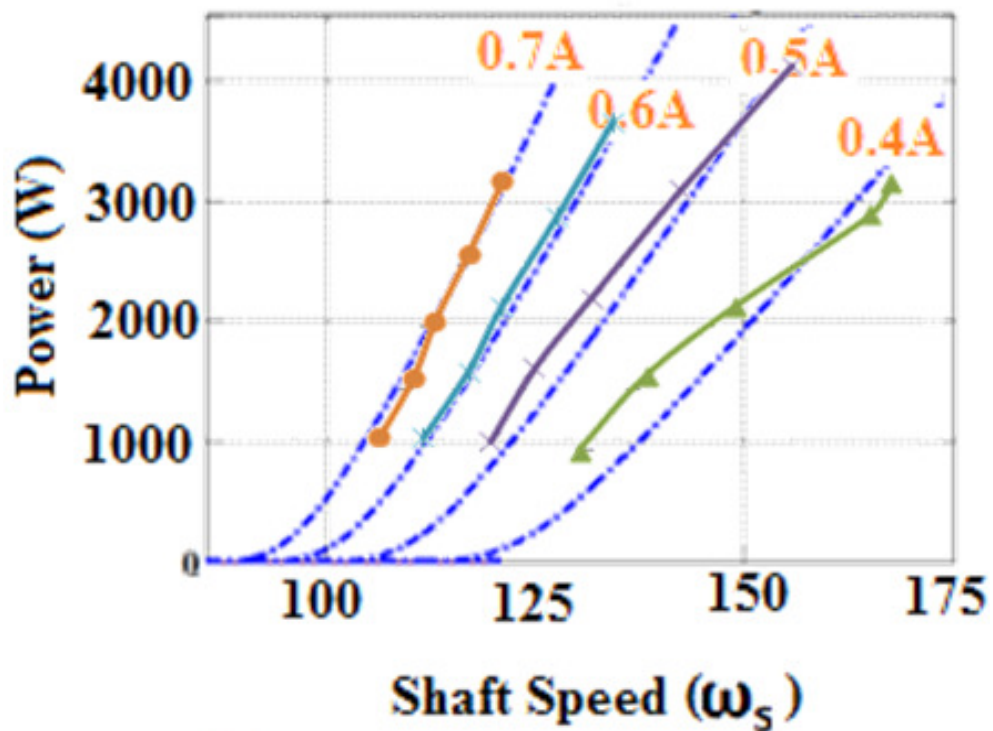
Fig 5.13: Generator capability curve experimental and computer results comparison

Fig 5.13 shows the comparison between the simulated results and the experimental results presented in *Fig 5.12* **(a)** and **(b).** It can be seen in *Fig 5.13* that the reduced in turn.

5.2.5.2 Steady state operation points prediction

To verify the ability of the proposed power shaft control topology achieving shaft power regulation via field excitation for a given tidal velocity, *Fig 5.7: Shaft power characteristics*, was superimposed onto *Fig 5.12: Generator capability curve at 420VDC voltage set point, at various field currents*, to realise the system's steady state operation power points at various tidal velocities which can be identified by the intersection points as shown in *Fig 5.14*.
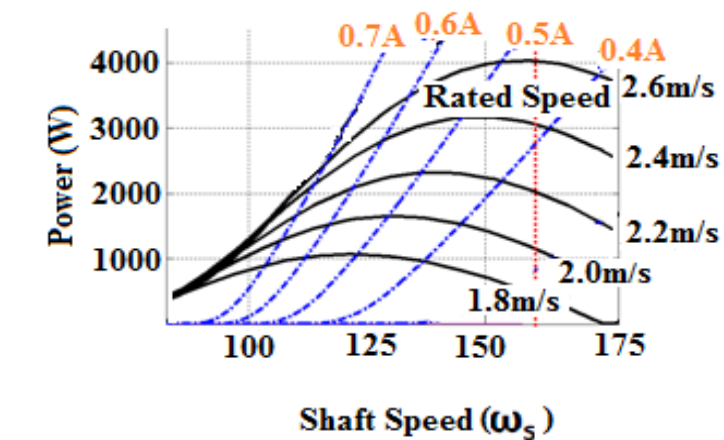
(a) Computer simulation results
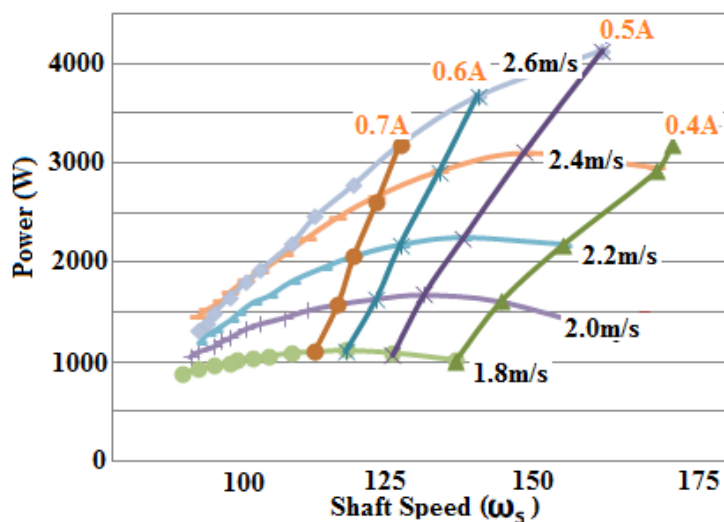
(b) Experimental Results

Fig 5.14: steady state operation points

Fig 5.14 shows the steady state operation points of the tidal simulation rig at 420VDC identified by the intersection points of these graphs. This indicates that for a given tidal velocity, desired shaft power can be achieved by selecting the appropriate excitation current the gives the desired intersection point.

For example; it can be observed that at tidal velocities between 2.4m/s and 2.0m/s the maximum power (peak) extraction points almost coincide with the intersection points when field current was set to **0.5A,** therefore by setting the field current to this value, maximum power extraction can be achieved for these tidal velocities.

5.2.6   DC-Bus Voltage set point

The voltage of the DC bus must be maintained at a level that is appropriate for the AC mains voltage supply that the regenerative drive is connected to i.e. For a given mains voltage supply there is a voltage range at which the DC voltage can be set.

Table 5.2 defines the ranges that applied to the developed experimental rig.

Assuming a 10% tolerance on the voltage supply, the peak input voltage plus some headroom of 2.5% as defined within the regenerative drive manufacturer's user manual [104] as the minimum value. The headroom is allowed for in order to achieve correct control of the mains injected current.

Furthermore the DC bus voltage should be set to a value lower than the maximum acceptable value giving allowance for overshoots caused by voltage transients.

Supply voltage (Vrms)	Minimum VDC	Maximum VDC
400	585	800
380	560	800
340	500	800
320	470	800
300	445	800
280	420	800

Table 5.2: DC bus voltage set point

It should be understood that the supply voltage to which the experimental rig was connected to was the standard UK mains 3phase, 50 Hz, 400Vrms. Therefore to be able to operate at lower DC bus voltages the experimental rig was connected to the mains via a variable transformer (Variac) as seen in *Fig 5.1: Tidal simulator configuration schematic*, to step down the voltage presented to the experimental rig as shown in *Table 5.2*, as a consequence this allowed for lower DC-bus voltage set-points during the experimental analysis given that the DC-bus voltage cannot be set to a value lower than the mains supply voltage.

Furthermore, the averaged model simulations presented in *Fig 3.17: DC-bus current and power waveforms*, show that at low DC bus voltage, DC bus current is high at constant power. Therefore if the desired power is very high at very low DC bus voltage, the DC bus current required to maintain power balance could be higher than the systems rated current. Thus for the tidal experimental rig to operate within its rated power envelope DC-bus voltage regulation was paramount.

It should be noted that, due to the limitation of the hardware used in these experiments the DC-bus voltage set point could only be set between the values of 420VDC and 800VDC.

5.2.6.1 DC-Bus Voltage regulation effects

To analyse the effects of DC-bus voltage the experimental rig was run at various DC-Bus voltage set-points at the same time regulating the generator's field current (shown in **Blue**) to achieve the maximum/desired shaft power as shown in *Table 5.3: Field current demand at various modes of operation*, and *Fig 5.15: Field Current Regulation*.

The results in *Table 5.3* were obtained as follows:

The MCD configuration described in Appendix A, section 7.2 was maintained during this test and the generator's field current was set to an appropriate value via the controllable DC supply to achieve the desired intersection point that corresponds to desired shaft power at a given tidal velocity as illustrated in *Fig 5.14: steady state operation points*. i.e. the magnetic flux was varied by controlling field excitation current which in turn regulated electromagnetic torque as a consequence. This varied

shaft/mechanical torque as both the electrical and mechanical torque reached equilibrium or at steady state, consequently regulating generator shaft /mechanical input power.

The employed synchronous generator field current was rated at **1.08A**.

Tidal Velocity	DC-Bus Voltage Set Point					Desired shaft power (kW) as shown in *Fig 5.3*
	420V	**480V**	**520V**	**560V**	**600V**	
1.6	**0.77**	**1.23**	**1.3**	**1.31**	**1.32**	**0.657**
1.8	**0.58**	**0.9**	**1.27**	**1.69**	**1.69**	**1.1**
2	**0.53**	**0.76**	**1.04**	**1.51**	**2**	**1.6**
2.2	**0.48**	**0.64**	**0.83**	**1.08**	**1.47**	**2.3**
2.4	**0.51**	**0.63**	**0.73**	**0.9**	**1.36**	**3.2**
2.6	**0.56**	**0.66**	**0.75**	**0.98**	**1.19**	**4.0**

Table 5.3: Field current demand at various modes of operation

However given that field current is a function of the generator induced voltage as well as DC-bus voltage, at high DC bus voltages and very low tidal velocities higher field current would be required to achieve maximum power extraction as discussed in **Chapter 4**. However, over-excitation for the purpose of achieving high terminal voltage at very low shaft speeds could damage either or both the exciter and main rotor.

It can be observed in *Table 5.3* that as DC-bus voltage increased the field current required to achieve desired power also increased. For example; when the DC-bus voltage set point was fixed to 420VDC the field current required to achieve the desired shaft power of 1.6kW at 2m/s tidal velocity was **0.53A**, compared to that when the DC bus voltage was set to 600VDC at the same tidal velocity which was **2A**. However since the generator's rated field current was **1.08A**, maximum power extraction at 2m/s tidal velocity when VDC was set to 600V could not be maintained for a long time as the generator field would be saturated, and as a consequence this also triggered the drives

protective trip out mechanism when this high field current was maintained for over 10 seconds to avoid rotor damage.

Resultant shaft power was realised by multiplying the torque transducer measured shaft torque by the shaft speed realised from the MCD as described in appendix A, section **7.2.1.**

Fig 5.15 is adopted from *Table 5.3* representing field current variation at various DC bus voltage set points.
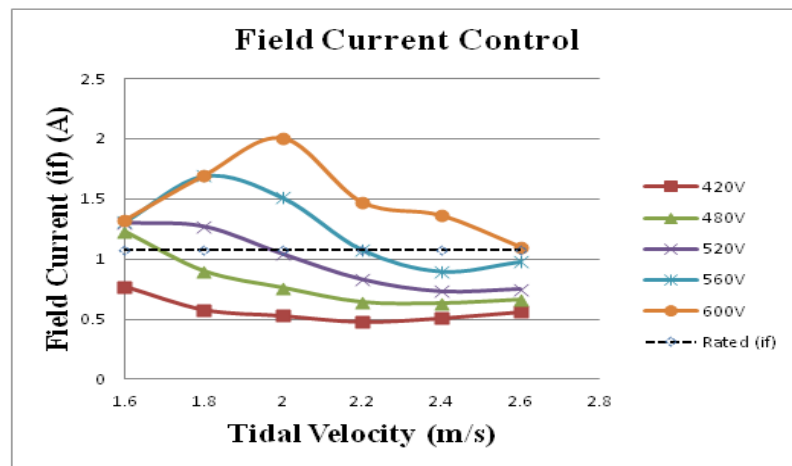
Fig 5.15: Field Current Regulation

Based on the **1.08A** generator field current rating, *Table 5.4* below is adopted from *Table 5.3* showing the generator's safe operation points in **Green** and the over-excitation operation points in **Red**

Tidal Velocity	DC-Bus Voltage Set Point					Desired shaft power as shown in *Fig 5.3*
	420V	**480V**	**520V**	**560V**	**600V**	
1.6	0.77	1.23	1.3	1.31	1.32	0.657
1.8	0.58	0.9	1.27	1.69	1.69	1.1
2	0.53	0.76	1.04	1.51	2	1.6
2.2	0.48	0.64	0.83	1.08	1.47	2.3
2.4	0.51	0.63	0.73	0.9	1.36	3.2
2.6	0.56	0.66	0.75	0.98	1.19	4.0

Table 5.4: Field current safe operation mode

130

For example, if the generator was to be operated within its rated power envelope when the DC bus voltage was set to 420VDC, desired power could be achieved when the tidal velocity was between 1.6m/s and 2.6m/s, however if the DC bus voltage set point was raised to say 560VDC desired power extraction could only be achieved when the tidal velocity is between 2.2m/s and 2.6m/s. This is because at lower tidal velocities (1.6m/s – 2m/s) the field current required to achieve desired power would be greater than the generator's rated field current value of **1.08A**. These test results confirmed the predicted effects of DC-Bus voltage variation realised and presented in *Fig 4.6*, *Fig 4.7* and *Fig 4.8* in **Chapter 4** to the systems power extraction capability as well as the need for DC-bus voltage regulation if maximum power extraction is to be achieved at any tidal velocity and at the same time operate within the generator's rated power.

All the tests described in the above sections were carried out by manually selecting appropriate values to verify the dynamic operation principle of the proposed tidal turbine topology realised in **Chapter 4** computer simulations.

Table 5.4 also shows that when multiple tidal turbines are connected in parallel onto a common DC-link circuit while being influenced by different tidal velocities, an appropriate/average DC-bus voltage that would enable all devices to extract desired power can be selected as described in section **4.4.1.1.**

5.2.6.2 DC-bus Voltage regulation

The DC bus voltage controller for the simulation rig was configured as shown in *Fig 5.16*. The primary objective of the voltage controller is to determine the optimum DC-bus voltage set-point that would allow for desired power extraction at any tidal velocity within the systems rated power envelope (within the Green zone of *Table 5.4*).
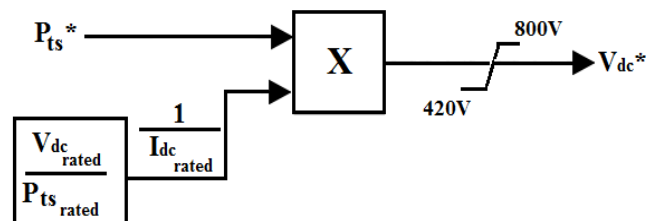
Fig 5.16: DC-bus voltage control schematic

DC-bus voltage set point can also be analytically realised as per (5.5).

$$V_{dc}{}^* = P_{ts}{}^* \, \mathbf{K4}$$

<div align="right">5.5</div>

$$\mathbf{K4} = \frac{1}{I_{dc_{rated}}}$$

Where $V_{dc}{}^*$, $P_{ts}{}^*$, and $I_{dc_{rated}}$ are the DC-bus voltage set point, desired generator shaft power, and rated DC-bus current (9.2A) respectively. Voltage regulation also provided thermal protection for the generator as well as maintaining the field current within its rated limit thus, avoiding field saturation and rotor damage.

5.3   Shaft power regulation

In previous sub-sections it has been stated that Power transfer from the generator was via a diode rectifier connected to a fixed DC bus voltage set by the voltage controller. The voltage controller also determined the generator's output terminal voltage and as a result only the output current could be regulated if shaft power is to be controlled. For that reason current control was achieved by generator field current regulation i.e. by varying generator field current as illustrated in *Fig 5.12*, shaft torque could be varied as a consequence, and due to the fact that field current is directly proportional to torque, shaft power control was also possible.

The following section will focus on the validation of the proposed tidal turbine shaft power control strategy presented in **Chapter 4** i.e. showing how the maximum power extraction, power limitation and stall control can be achieved within the systems power envelope.

Fig 5.17 shows the tidal simulation rig field controller operation principle. i.e.

When power was applied to the induction motor, its shaft started to rotate at a speed dictated by the MCD. Shaft speed (ω_s^*) and shaft torque (T_m) required by the field controller power calculation block were realised from the MCD and torque transducer (**TT**) respectively to calculate desired shaft power (P_m^*) . P_m^* was then divided by the

DC-bus voltage measured across the DC-bus terminals realising desired generator DC-bus output current (I_{dc}^*). I_{dc}^*. was then compared to the actual output DC-bus current (I_{dc}) measured at the DC-bus terminals. The error obtained was fed into the Field control block (PI controller) which provided an analogue signal to the Exc. Block (controllable DC power source) that regulated generator field current (i_f) to achieve desired generator output DC bus current and consequently shaft power. The hardware control schematic is illustrated in *Fig 5.17*.
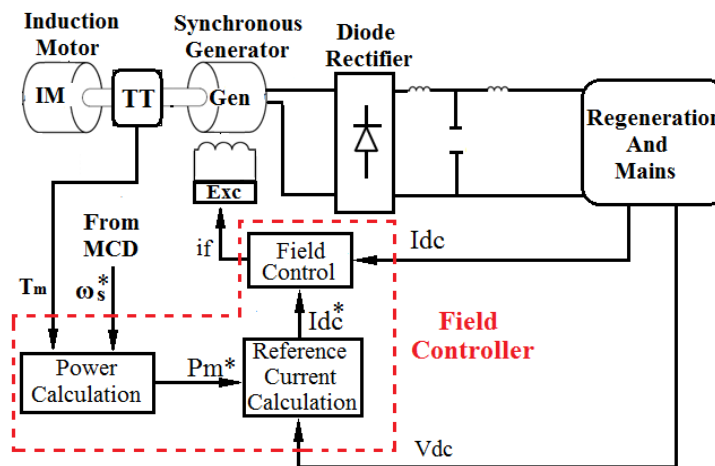
Fig 5.17: Field controller configuration

Motor shaft speed (ω_s^*) in *Fig 5.17* was realised from the motor input frequency via output terminal 9 of the MCD as illustrated by in Appendix A, section **7.2.1**, *Fig 7.5: Motor control drive speed measurement circuit.*

The power generated by the experimental rig was fed into the mains supply, however in order to successfully inject electrical power into the mains supply the rectified generator output DC power was converted back into AC power at the frequency and amplitude demanded by the mains. This was achieved by employing an electric power converter (Regeneration Drive) which also allowed for decoupled control of the active and reactive power as well as stabilising the DC-bus voltage. Reactive power was set to zero in order to achieve unity power factor.

5.3.1   Regeneration Drive (Regen)

The developed simulation rig utilised an 11kW Emerson Unidrive SP regeneration drive as the grid-side controller. The Regen drive converted DC-bus power from the rectifier

loaded generator into a regulated AC voltage as well as providing sinusoidal output currents into the mains.

Power transfer to the mains was achieved as shown schematically in *Fig 5.18*
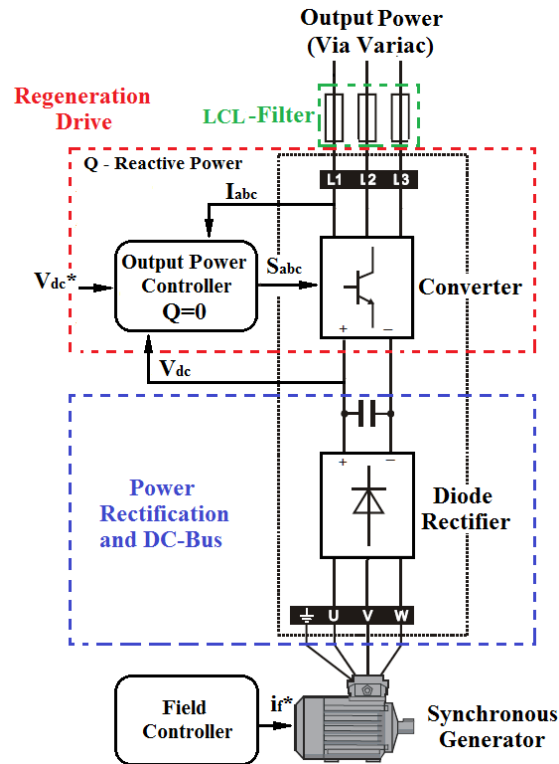
Fig 5.18: Mains-Side control configuration

The regen drive utilised a DC bus voltage controller with inner current controllers as illustrated in *Fig 7.6* to regulate active and reactive power injected into the mains as described in Appendix A, section **7.2.1.**

The input regen drive's AC terminals produces an output voltage via PWM with a sinusoidal component at line frequency containing substantial harmonics at the switching frequency and its multiples. For that reason the regen was connected to the mains power terminals via a switching frequency filter (LCL-filter). The filter prevented switching frequency harmonic currents from being fed into the mains supply as well as decoupling power between mains voltage and the generator voltage.
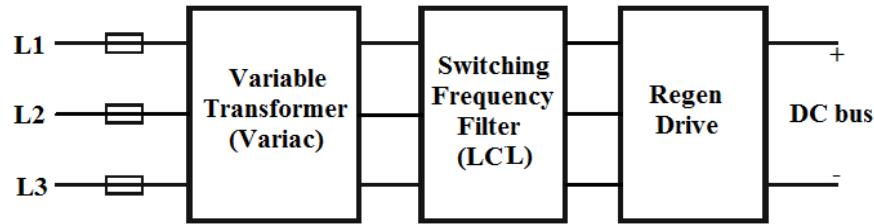
Fig 5.19: Regen drive mains connection schematic

Fig 5.19 illustrates the regen connection to the mains supply. The employed filter inductors were standard 3-phase inductors rated at drive rated current of 25A.

The tidal experimental hardware control cubical was configured as shown in Appendix B, section **9.4.**

5.3.2 Experimental results and discussions

This section focuses on the practical analysis of the proposed tidal system topology in particular, the system's automatic control strategy in addition to its ability to achieve desired shaft power i.e. maximum power extraction, power limitation and stall control when the proposed control methodology is applied.

5.3.2.1 LABVIEW model set-up

Tidal simulator power control was undertaken in the LABVIEW computer simulation platform. The LabVIEW realtime scan block diagram was configured as presented schematically in *Fig 5.20.*
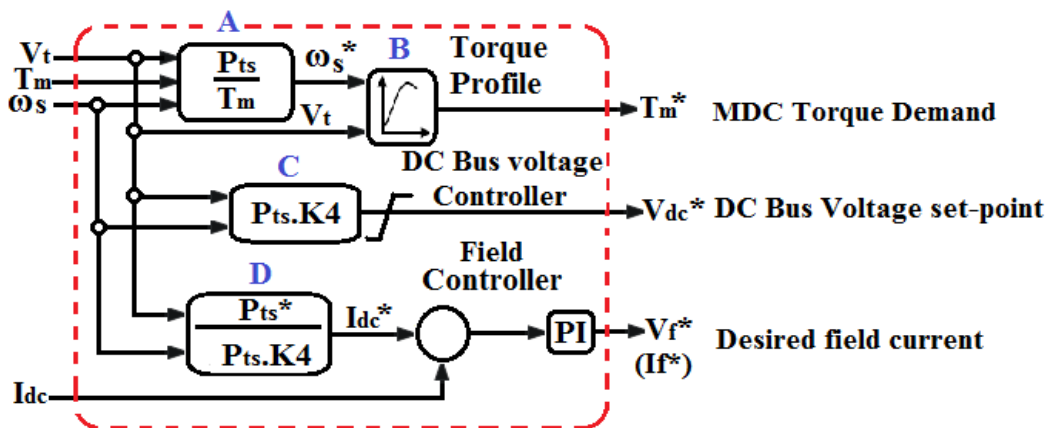
Fig 5.20: LABVIEW Tidal Simulator control algorithm

The induction motor shaft was set to rotate at a steady speed to account for practical turbine starting torque applied to the blades by the tide. Once the rotor shaft started to rotate a constant tidal velocity (V_t) was assumed and used to calculate the available tidal power (P_{ts}) using equations **(3.5)** and **(3.2)** defined in chapter 3. The calculated tidal power (P_{ts}) was then divided by the measured shaft torque (T_m) to realise desired shaft speed ($\omega_s{}^*$) required by the torque profile block B as shown in *Fig 5.20*.

(T_m) was measured by a torque transducer coupled to the IM shaft as shown in *Fig 5.9: Generator and Motor coupling arrangement (Drive Train).*

Motor shaft speed (ω_s) in *Fig 5.20* required for TSR calculation was realised from the motor input frequency via output terminal 9 of the MCD as defined in Appendix A, *Fig 7.5: Motor control drive speed measurement circuit.* The torque reference ($T_m{}^*$) obtained from the torque profile block B (*Table1.1*) together with desired shaft speed ($\omega_s{}^*$) form block A enabled the induction motor shaft to emulate tidal rotor characteristics as tidal velocity varied.

Desired DC-bus voltage set point $(V_{dc}{}^*)$ was also calculated as defined in equation **(5.5),** a voltage limiter was also included to make sure the DC bus voltage set point was within the experimental hardware operation range of 420VDC – 800VDC.

The field current controller was then modelled as presented in *Fig 5.17.* The principal input of the field controller was the generator's rectifier output DC current (I_{dc}), which was realised from the regen drive as described in Appendix A, *Fig 7.8*, and then compared to $(I_{dc}{}^*)$ and the error signal obtained was fed into a PI controller. The output signal from the PI controller was received by the controllable DC power supply via the c-RIO (software and hardware interface module) and used to determine the desired field current applied to the generator field winding yielding the shaft torque and speed that corresponded to the desired shaft power at a given tidal velocity. The **PI** Controller values were realised as described in equations **(4.10)** and **(4.11)** as follows to obtain the results presented in the following sections.

$$K_P = 0.033 \qquad\qquad\qquad T_i = 0.005$$

It should be noted that the following experimental results were obtained when the MCD was configured as described in Appendix A, section **7.2.1.**

5.3.2.2 Maximum Power extraction

In *Table 5.5: System power Regulation* the tidal experimental rig power regulation results showing both the calculated DC-bus voltage set point using equation 5.5 (shown in **Red**) and the actual experimental rig voltage set point value with respect to hardware limitation (Shown in **Green**) are presented. Field current (shown in **Blue**) was regulated as illustrated in *Fig 5.17: Field controller configuration*, to achieve desired shaft power (shown in **Brown**) at various tidal velocities.

Tidal Velocity (m/s)	Desired Maximum Shaft power (W) illustrated by *Fig 5.3*	Calculated DC-Bus Voltage(V) defined by equation (5.5)	DC-Bus Voltage (V) Set Point (within the experimental set-point envelope)	Regulated Field Current (A) illustrated in *Table 5.3*	Measured Shaft (W)
1.6	657	71	420	0.77	653
1.8	1100	120	420	0.58	1050
2	1600	174	420	0.53	1584
2.2	2300	250	420	0.48	2287
2.4	3200	348	420	0.51	3189
2.6	4000	435	435	0.58	3853

Table 5.5: System power Regulation

It can be seen in *Table 5.5* that by applying the proposed field current regulation combined with DC bus voltage control the measured shaft power is within 95% of the desired power (due to other system loses and measurement inaccuracies) thus maximum power extraction was possible for all tidal velocities. Experimental rig shaft power was realised by multiplying the shaft torque measured by the torque transducer with the shaft speed realised from the MCD..

5.3.2.3 Power limitation

Fig 5.21: *Power limitation Control illustration (420V)* shows the tidal simulated shaft power as field current was varied. It can be observed that by controlling field current, shaft power could be regulated to any desired value even to values lower than peak power. For example by applying a power limiter onto the calculated power available for extraction as shown in *Fig 4.12: Tidal turbine control methodology*, field current can be regulated to achieve the desired shaft power as demonstrated in *Fig 4.18: Rated Power Envelope,* by the yellow dots.
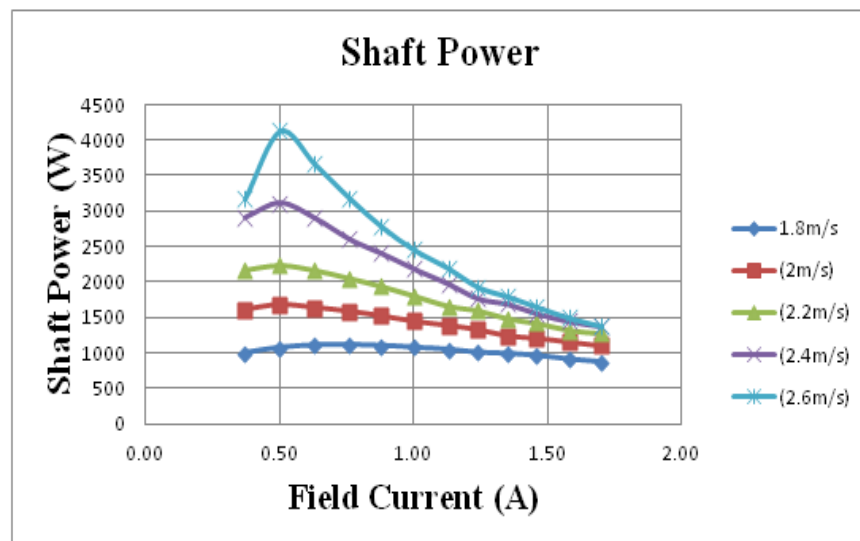
Fig 5.21: Power limitation Control illustration (420V)

The results in *Fig 5.21*, were obtained with same MCD configuration described in Appendix A, section **7.2.1**.The tests were   performed by varying the field current applied to the SG rotor via the controllable DC power supply while the DC link voltage was set to 420VDC, and maintained by the regeneration drive. Resultant shaft power was realised by multiplying the shaft torque measured by the torque transducer with the shaft speed realised from the MCD.

5.3.2.4 Shaft torque control

Fig 5.22 illustrates the measured tidal/ motor shaft torque as the field current was varied at a DC bus set voltage point of 420V. It can be noticed that as the field current increased from 0 to 0.5A shaft torque increased in turn, nonetheless when field current

138

increased beyond 0.5A shaft torque started to drop. This is because as field current increases electromagnetic torque also increases. However, when the electromagnetic torque and mechanical torque reached equilibrium as would be expected, an increase in mechanical torque would cause the tidal blades to slow down thus extract less power form the tidal current. Therefore as the power extracted from the tidal current decreases, and given that the rotor speed has also decreased, shaft torque as well as electromagnetic torque also decreases in order to maintain power balance.

Which suggests that by regulating field current a desired shaft torque can be achieved.
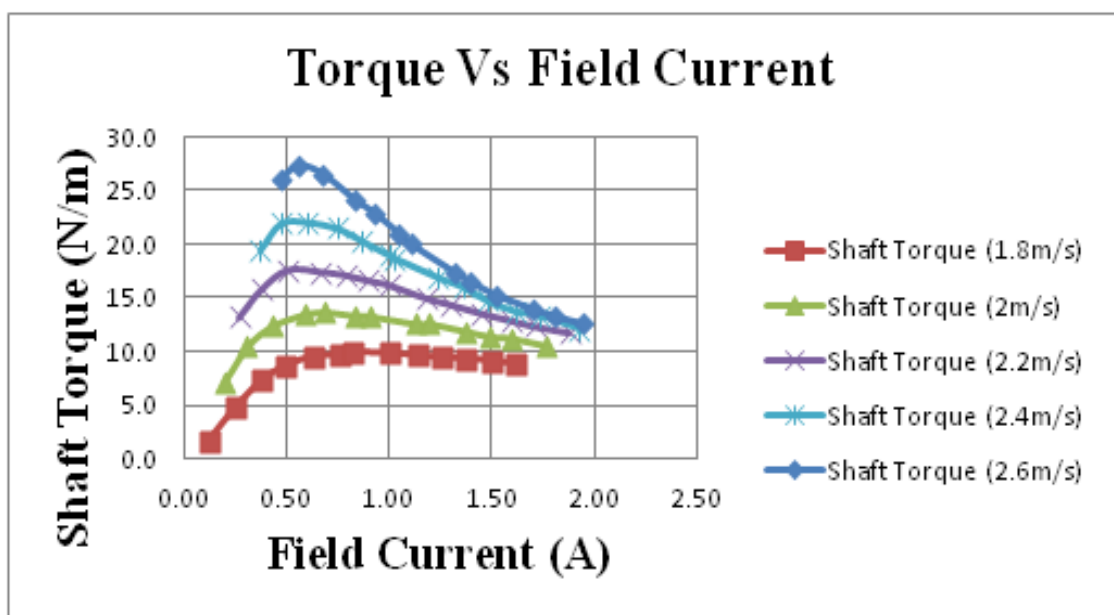

Fig 5.22: Shaft Torque Vs Field Current and 420VDC

The results in *Fig 5.22*, were obtained with same MCD configuration described in section 7.2.1. The tests were performed by varying the field current applied to the SG rotor via the controllable DC power supply while the DC link voltage was set to 420VDC, and maintained by the regeneration drive Then the resultant shaft torque was realised from the torque transducer mounted on the drive shaft.

5.3.2.5 Stall control

Fig 5.23 shows the tidal turbine simulation rig shaft speed as field current was varied. It is observed that by regulating field current, shaft speed could be regulated. This

139

suggests that if field current was to be increased to a much higher value shaft speed could decrease to nearly zero, consequently stalling the rotor shaft thus achieving stall control during very high tidal velocities to protect the turbine form overload and over-speed.
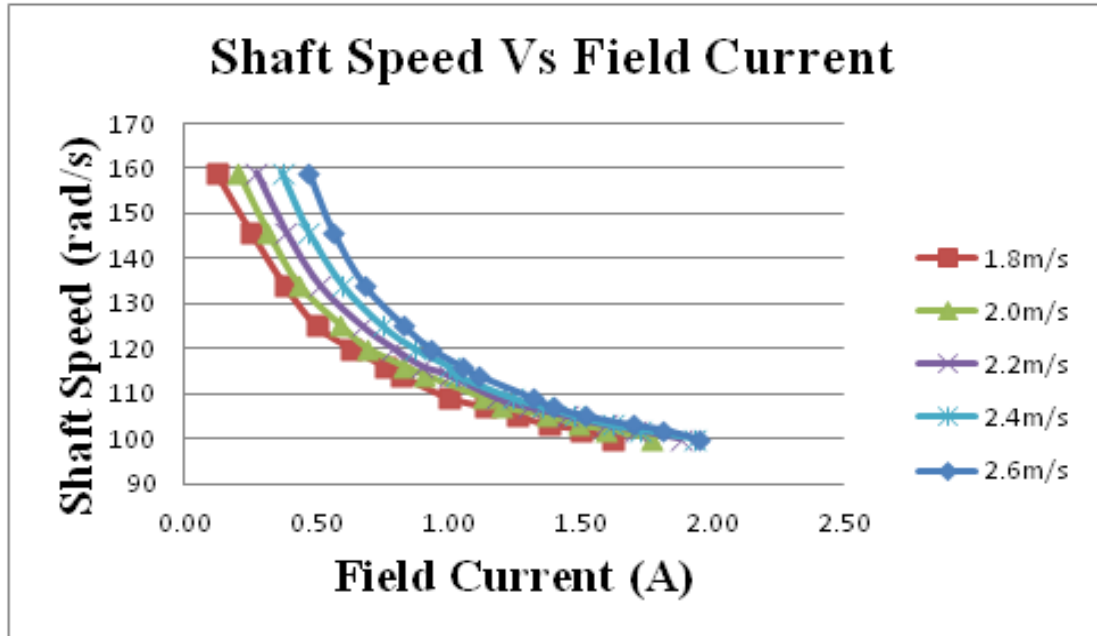
Fig 5.23: Stall control validation (420V)

The results in *Fig 5.23*, were obtained with same MCD configuration described in Appendix A, section **7.2.1.**

5.3.2.6 Mains power transfer

Table 5.6   shows the measured shaft power (Mechanical power), generator output power (Electrical power) and the power injected into the mains. It can be observed in this table that, generator efficiency was on average 76% close to its design value of 80%. However, the overall system efficiency was much lower at approximately 67%, this indicates that there are other system loses caused by the diode rectifier and the regen drive combination which have a combined measured efficiency of ≈ 85% (ignoring system measurement accuracies).

Tidal Velocity	Measured Shaft power	DC-Bus Voltage (V) Set Point	Generator Output Power (W)	Generator efficiency (%)	Power injected into the Mains (W)	System efficiency (%)
1.6	657	420	500	76	440	67
1.8	1100	420	770	70	651	60
2	1600	420	1300	81	1071	67
2.2	2300	420	1800	78	1520	67
2.4	3200	491	2500	78	2013	63
2.6	4000	560	2900	72	2735	68

Table 5.6: System power Regulation

Generator output power presented in *Table 5.6* was measured by connecting the power analyser to current and voltage AC terminals of the generator, which in turn measured and calculated the associated output power as tidal velocity varied.

Another power analyser was also connected to the voltage and current terminals between the regeneration drive and the Variable transformer to measure the power injected into the mains.

Efficiencies were calculated using equation (5.6) below.

$$Efficiency\ (\%) = \frac{Power - in}{Power - out} x100 \qquad 5.6$$

Fig 5.24 is adopted from *Table 5.6*, comparing the system's output power at different simulation rig generation stages.
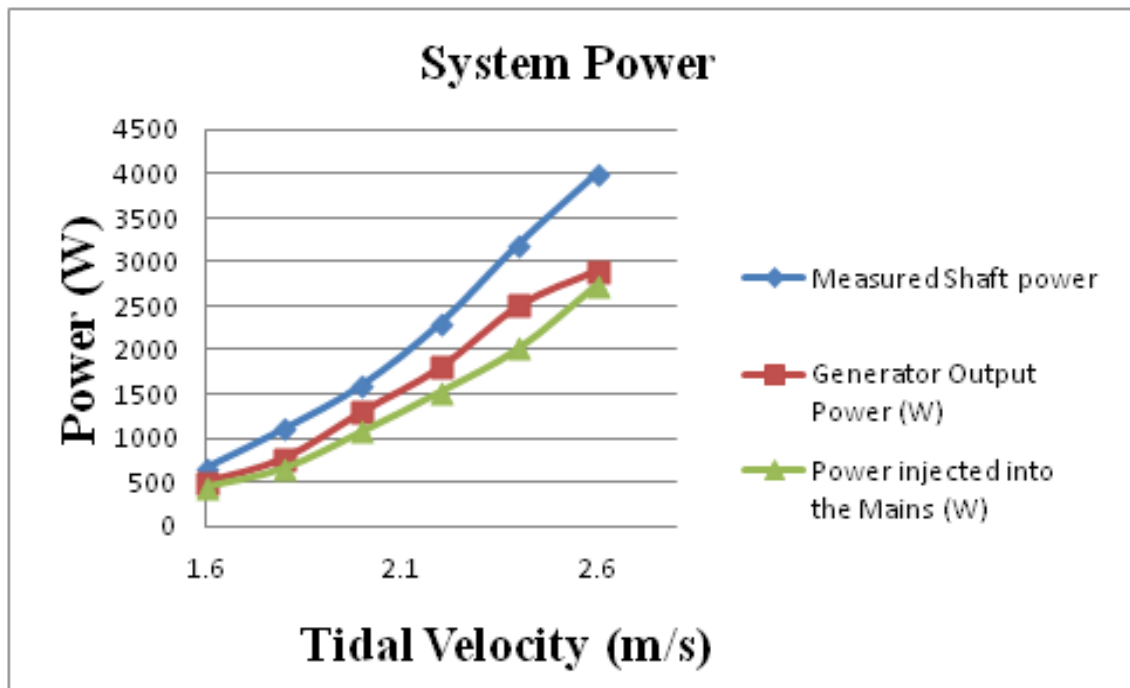
Fig 5.24: Shaft Torque Vs Field Current and 420VDC

5.4   Summary

In this chapter an experimental rig that represented the proposed tidal power generation system was developed using a motor and generator configuration, a motor control drive, a diode rectifier and a regeneration drive controlled by an NI c-RIO signal controller via LABVIEW virtual instrumentation software has been discussed.

The tidal turbine experimental rig generated speed and torque characteristic signals in accordance to the chosen tidal velocity. The generated speed and toque characteristic signals were scaled down compared to that of a practical tidal device described in **Chapter 4,** to match the input power rating of the experimental rig. The generated signals were sequentially sent to the motor control drive which enabled the induction motor to emulate actual turbine blade characteristics in turn produce the necessary torque for a 5.2kW tidal power generation system.

The feasibility of the proposed tidal system topology was first analysed via computer simulations, and then based on those simulation results a hardware experimental rig was developed and verified in the laboratory for the proposed system validation.

The built tidal experimental rig was used to confirm the computer simulation results that were presented in **Chapter 4**, analysing various electrical and mechanical characteristics of the proposed tidal power system.

The studies in this chapter showed that field control alone is sufficient to produce electrical output current proportional to the tidal input power, in turn achieving maximum power extraction, power limitation and stall control as predicted in **Chapter 4**.

It is also understood that an experimental rig consisting of three generator-rectifier sets connected in parallel onto a common DC-bus would have been preferable as it would represent the proposed tidal system behaviour much better, providing more realistic results when analysing the effects of running multiple turbines at different power levels and frequencies. However due to budget constraints only a single 'leg' system was developed for the experimental validation. Nonetheless a single leg was sufficient enough to fully analyse and validate the proposed system's core behaviour.

CHAPTER 6
6 CONCLUSION

6.1 Introduction

There is considerable amount of renewable power sources in the UK with the potential to contribute towards the countries energy future and security.

The two main renewable energy sources are wind and tidal due to the countries geographical location. Although wind power is already being generated on a commercial scale, tidal power is at the early stage of development and has not yet been developed on a commercial scale. This is mainly because tidal stream power extraction technology is still not cost effective. The high costs are primarily due to the environment in which tidal devices are installed which causes difficulty in accessing the device for maintenance and installation.

Furthermore, studies undertaken within this research suggest that current tidal turbine prototypes contain a large number of power electronic components typically installed offshore and under water to ensure that each device produces grid standard electricity. Moreover, most of the components are installed underwater thereby the capital installation and maintenance costs are relatively high compared to conventional power plants which makes tidal stream power implementation economically unviable for many investors/developers at the moment.

The main objective for tidal stream power developers today is to arrive at a cost-effective and reliable tidal power system that could be developed commercially on a large scale. Capable of accommodating multiple tidal devices operating simultaneously, taking into consideration potential gains from running the collection of tidal devices at different voltages and frequencies.

It should also be noted that, the robustness of the system is vital since tidal devices are required to operate without human intervention for long periods of time as the cost of raising an underwater turbine for maintenance could potentially be very high.

Therefore, the high costs associated with tidal stream power generation would have to be reduced if tidal power generation is to compete economically with other sources of power generation. This suggests that more technological advancements are required to make tidal stream power commercially viable.

Based on the published literature on the subject of renewable power generation and specifically in the field of tidal power generation, this thesis sought to answer the following question:

How can we reduce the high costs associated with tidal power generation to a level where it can compete successfully with other renewable energy sources?. ie. Costs associated with power generation, transmission, distribution, installation and maintenance.

The approach taken in this study was to replace major cost components with relatively low cost ones, in addition to locating as many components as possible onshore where costs are less.

The core findings are chapter specific and were summarised within the respective chapters. Therefore, this Chapter will focus on the core findings to answer the study's research question stated above.

A novel tidal power extraction topology aimed at optimising existing/prototype tidal systems referred to as "Rectification to a common DC-bus" has been presented in this thesis. The presented tidal system power generation topology utilises fixed-pitch blades feeding a multi-pole multi-phase synchronous generator, which has a tight field (excitation) control. The tidal generator's output terminals voltage is transformed to 6.6kV AC and then passively rectified to ~9kV DC before finally converting it back to AC onshore as the power is fed onto the utility grid.

In order to maximise resource utilisation a tidal farm where a number of proposed tidal devices are coupled onto a common DC-bus.

6.2 Cost reduction

The presented tidal power generation topology recommends the used of fixed pitch blades. Although the energy harnessed by fixed pitch blades is less than that harnessed by variable-pitch blades, revenue and maintenance cost would be less for fixed pitch blades due to lower downtime given that no maintenance would be required. Moreover,

capital and installation cost would also be lower since less components would be used/ required/installed offshore.

Furthermore, the use of bridge rectifiers is recommended rather than active converters, given that the failure rates of wind-farm converters appear to be relatively high. Although based on the literature search it couldn't be known whether these failures were hardware or software related. Therefore, it could be argued that maybe if the control software was to be improved these failure rates could be minimised without any significant changes to the hardware. Nevertheless, given that tidal devices are installed between 30-80m under the sea, installing such equipment within the turbine nacelle/underwater should be avoided because even a single failure could result in significant loss of revenue in addition to increased system maintenance costs. Moreover, system complexity would also be reduced. Power regulation via generator field excitation control is recommended for the proposed system because it allows the use of bridge rectifiers.

The presented tidal system topology also recommends the use of DC power transmission rather than conventional AC transmission. Although, for tidal farms within 90km of grid-connection points it could be argued that there would be no economic justification for using a subsea DC power transmission. The basis for this argument would be that for reasonably-sized tidal farms, the DC cable voltage must be relatively high, which then requires high-voltage offshore DC-AC converters, which could be relatively expensive. Nevertheless, within the analyses in this thesis, it was found that employing a common DC-link circuit for multiple tidal devices can reduce system component count in addition to the amount of equipment installed underwater/offshore.

Moreover, connection of all the devices on a common DC bus reduces the number of cable runs to shore, which can reduce system capital and installation cost. Furthermore the converter that links the tidal farm to the utility grid is installed on shore which means that although electrical and control failure rate for these devices has proven to be common for wind turbines, its installation onshore would give easy access for maintenance in turn reduce down time, maintenance and installation cost. The proposed

tidal power harnessing topology also facilitates system expandability given that additional devices could be added onto the DC-bus long after installation.

It should be noted that no other primary energy supply device found within the course of this study uses passive rectification onto a common DC-bus. Therefore, the feasibility of the proposed tidal topology was carefully examined with detailed electro-mechanical computer/theoretical and experimental simulations to ensure that field excitation control alone can adequately regulate the power harnessed by the tidal system to achieve maximum power extraction, power limitation and stall control.

6.2.1.1 Theoretical Feasibility Study

In **Chapter 3** the proposed tidal system components were analytically modelled to illustrate each component's dynamic characteristics. From the realised system models it was observed that the systems input variables such as the generator's desired input field current that generates desired generator shaft power can be calculated if the desired output variables such as DC bus voltage and tidal velocity are known. This observation suggests that, if the input variable can be identified based on the desired output variables, system components can be selected without extensive simulations/modelling. The developed analytical models were verified through extensive computer simulations which showed that the realised models represented the main dynamic features of the proposed tidal system.

In **Chapter 4** the proposed tidal system's components performance was analysed together with some aspects of their design consideration and selection as well as their operation principle and characteristics, illustrating their suitability for use with the proposed topology under different modes of operation.

Based on the system's component characteristics an automatic shaft power controller was realised and analysed via computer simulation to demonstrate maximum power extraction, power limitation and stall control. Furthermore the effects of the tidal system's input variables such as tidal velocity, field current & DC-bus voltage on the systems power transfer and controller were analysed.

The computer simulation studies showed that field control alone is sufficient to achieve the following:

- Produce electrical output current proportional to the tidal input power, hence maximum power extraction and power limiting can be achieved.

- Allow the use of fixed pitch turbine blades instead of costly and more complicated variable pitch blades, or variable ratio gearboxes.

- DC bus voltage can be successfully regulated to allow each tidal device connected on the same DC-link circuit to extract the maximum available power even at very low tidal velocities.

- Using the analytical models the field current required to achieve desired power extraction can be estimated, which would save a lot of computational time during component selection in addition to improving system control response time.

Although the proposed tidal power generation system presented a number of advantages, it should be noted that it also presents a number of challenges. For example, given that multiple machines are connected in parallel onto a common DC-bus, the peak to peak values of the line to line voltages at the terminals of all devices on the same DC-bus must be exactly the same this is because multiple tidal turbines are connected in parallel on a common DC link circuit. However, local sea conditions will inevitably cause differences in the tidal stream velocities and therefore adjacent tidal stream turbines/generators may run at different speeds thereby produce diverse output power and voltages.

Nonetheless, this would not affect the system's proposed operation principle because all devices connecting onto the DC-bus do so via a diode rectifier. This means that if any of the devices cannot generate a voltage equal or higher than the DC-bus set voltage the diodes within the diode rectifier associated with that device will remain reverse biased. Therefore, there will be no power contribution from that particular device onto the DC-bus.

All computer simulations in this thesis were based on the ABB Ltd synchronous generator type AMG 0400ES04 in order to give an indication of the proposed tidal system performance when an actual off-the-shelf generator is employed.

6.2.1.2 Laboratory Feasibility Study

Based on the theoretical feasibility study undertaken in **Chapter 4** a laboratory experimental rig was developed for practical validation of proposed system.

The developed tidal power simulator was utilised to validate the computer simulation results presented in **Chapter 4**, analysing various mechanical and electrical characteristics of the proposed tidal power system.

The laboratory experimental results showed that field control alone was sufficient to produce electrical output current proportional to the tidal shaft power, in turn achieving maximum power extraction, power limitation and stall control as predicted in **Chapter 4**.

Furthermore power transfer to the grid was also demonstrated by feeding the power generated by the experimental rig into the mains illustrating grid synchronisation as would be expected in the practice.

6.3 Study Limitations

This study provided perspective on how tidal power generation could contribute towards the UK's energy security by employing the proposed tidal system topology. The feasibility of the proposed system was conducted via computer simulations and in the laboratory using an experimental rig purposely built to emulate tidal turbine behaviour. As a direct consequence of this methodology the following limitations were identified.

It has been discussed in the thesis that field current control alone is sufficient to achieve optimum power extraction form all the devices connected onto a common stiff DC-bus. However, if the difference in the tidal velocity acting on different devices is very large i.e. more than 1m/s, maximum power extraction at the lowest tidal velocity cannot be achieved within the system's power envelope. On the other hand, it should be noted that this kind of difference in tidal velocity in unlikely to occur in practice between tidal devices at the same site.

Stall control has been proposed within this study, although it should be noted that without an extensive study of tidal blade strength stall control via field excitation alone could damage tidal blades. This is because although tidal blade stall can be achieved in theory, in practice the pressure exerted on to the blades could destroy the blades if pitch control is not employed. On the other hand, it should be noted that high gusts of tidal current are unlikely to occur in practice moreover, the site resource is identified in advance so that a suitably sized device can be installed.

149

6.4 Future work

To fully validate the proposed tidal system extraction topology as the optimum cost effective solution for a practical tidal farm configuration, there is need for further analysis on its practical viability and exploring the following as future research strategies can facilitate the attainment of this goal.

In this thesis field excitation control was carefully regulated when analysing the feasibility of the proposed tidal topology. Therefore, further investigation on the effects of error or lag in the excitation control on the systems controllability and the generator field windings will be necessary.

Electronic stall/speed control has been proposed for this system, however this passive stall methodology has to be able to cope with the torque at the rotor shaft when applied to a large scale tidal machine which may be very large. Therefore further analysis is deemed necessary to establish the viability of stall control via field excitation alone on a practical 1MW tidal device. Moreover, as described in Chapter 4 a brief surge of current was observed and this over-current could cause the generator windings to fail and/or trip-out the system protective device.

The effect of turbulence on the machine cannot be ignored because without it gearbox wear would be minimal and would not have the reputation of causing significant turbine down-time given that the torque ripples created by turbulence cause wear through variable stresses. Therefore the effects of turbulence on the proposed fixed pitch blade tidal turbine with its power regulation carried out by field excitation alone must be extensively investigated.

This thesis did not analyse yaw control, and further analysis would be required if yaw control was to be employed on the proposed tidal system due to the absence of any AC supply to the nacelle from shore. Since main power conversion is passive rectification, employing a yaw scheme would require a separate auxiliary supply in the nacelle i.e. a low-power converter rated to 9kVDC which might be expensive due to the high voltage in the nacelle.

6.5 Conclusion

Due to the time allocated for this research, it was very difficult to account for all the factors that would affect the proposed tidal system topology. Therefore, further analysis in the immediate future will have to be to concentrate on the aforementioned technical aspects in isolation with the aim of bringing together all the information in future as appropriate.

In addition to the above, detailed further analysis will be extended to further system studies i.e.

- subsea cables
- hub, converter, and offshore network design
- grid connection faults
- electrical power market, pricing, and cost/benefit

References

[1]   T. J. Hammons, "Tidal Power (Invited Paper)," *Proceedings IEEE (Special Issue on Advanced Power Generation Technologies),* vol. 81, pp. 419-433, 1993.

[2]   E. Ares, "Climate Change Bill," Bill 97 of 2007-08, Science and Enviromental section, House of Commons Library, London 2008.

[3]   L. Turner., "Building a low-carbon economy – the UK's contribution to tackling climate change," Committee on Climate Change 2008.

[4]   Y. Da and A. Khaligh., "Hybrid Offshore Wind and Tidal Turbine Energy Harvesting Systems With Independently Controlled Rectifiers," *Illinois Institute of Technology, Electric Power and Power Electronics Centre*, 2009.

[5]   W. Fengxiang, H. Qingming and P. Jian "Study on Control Systems of Low Speed PM Generator Direct Driven By Wind Turbine,"*School of Electric Engineering, Sherryang University of Technology*. 2000.

[6]   F. Wang*, et al.*, "Study on Control Systems of Low Speed PM Generator Direct Driven by Wind Turbine, "*School of Electric Engineering, Sherryang University of Technology*. 2000

[7]   "UK Renewable Energy Roadmap Update 2013 " Department of Energy & Climate change 2013.

[8]   T. J. Hammons, "Tidal Energy Techinologies: Currents, Wave and Offshore Wind Power in United Kingdom, Europe and North America," *UK Sustainable and Renewable Energy Group,University of Glasgow*, 2009.

[9]   D. Krohn, "Wave and Tidal Energy in the UK - Conquering Challenges, Generating Growth" *Renewable UK, The Voice of Wind And Marine Energy,* 2013.

[10]   "The Energy Challenge - Energy Review Report " *Department of Trade and Industry*, 2006.

[11]   J. King and T. Tryfonas, "Tidal Sream Power Techinology - State of the Art," *Faculty of Engineering, University of Bristol,* 2009.

[12]   R. H. Charlier, "A ''sleeper'' awakes: tidal current power," *Elsevier*, *Renewable and Sustainable Energy Reviews,* 2003.

[13] "Feasibility of Developing Wave Power as a Renewable Energy Resource for Hawaii" *Department of Business, Economic Development, and Tourism* 2002.

[14] wikipedia.org. (2011, *Tidal Power* Available: http://en.wikipedia.org/wiki/Tidal_energy

[15] A. M. Gorlov, "TIDAL ENERGY," *Northeastern University, Boston Massachusetts, USA*, 2001.

[16] J. Khan and G. Bhuyan"Ocean Energy: Global Technology Developement Status," *Powertech Labs Inc*, *British Columbia, Canada, IEA-OES Document No.: T0104,* 2009.

[17] "Environmental Impact of Tidal Energy Barrages" *Paliamentary office of Science and Technology Postnote No.:435,* 2013.

[18] M. Maser, "Tidal Energy - a primer," *Blue Energy Canada Inc,* 2006.

[19] 10-03-2014). *Verdant Power*. Available: http://www.verdantpower.com/

[20] T. J. Hammons, "Tidal Energy Techinologies: Currents, Wave and Offshore Wind Power in United Kingdom, Europe and North America," *UK Sustainable and Renewable Energy Group,University of Glasgow*, 2009.

[21] J. R. Moore, C.E. Brown and W.S. Cooper, "Qualification of Exploitable Tidal Energy Resource in UK Waters," *n-power Juice* 2007.

[22] J. King and T. Tryfonas, "Tidal Sream Power Techinology - State of the Art," *Faculty of Engineering, University of Bristol,* 2009.

[23] P. Fraenkel, "Energy from the oceans ready to go on-stream.," *Renew Energy World,* vol. 8, pp. 223–227, 2002.

[24] T. Burton, N. Jenkins and D. Sharpe, *Wind Energy Handbook, 2nd Edition*: ISBM: 978-0-470-69975-1, John Wiley & Sons Ltd, 2011.

[25] *Open Hydro*. Available: http://www.openhydro.com/technology.html

[26] "Research and Development of A 150kW Tidal Sream Generator," *Engineering Business Limited*, 2002.

[27] R. Williams, (2010, *Hydraulic Wind Turbines*. Available: http://machinedesign.com/energy/hydraulic-wind-turbines

[28] 02-09-2011). *Lunar Energy.* Available: http://www.lunarenergy.co.uk

[29] "Innovate.on technologies: Marine energy ", *Eon Press Release*, 2008.

[30]   "Tidal & Current Energy Resources in Ireland," *Sustainable Energy Ireland*, 2002.

[31]   02-09-2011). *Hammerfest Strom*. Available: http://www.hammerfeststrom.com.

[32]   02-09-2011). *Swanturbines.* . Available: http://www.swanturbines.co.uk.

[33]   *Nippon*. Available: http://www.nippon.com/ja/files/a01203_ph071.jpg

[34]   "A Guide to an Offshore Wind Farm," *The Crown Estate*, 2006.

[35]   H. Polinder, D. Bang, H. Li*, et al.*, "Concept Report on Generator Topologies, Mechanical & Electromagnetic Optimisation," *Delft University of Technology, Aalborg University*, 2006.

[36]   Z. Chen, J. M. Guerrero and F. Blaabjerg, "A Review of the State of the Art of Power Electronics for Wind Turbines," *IEEE Transactions on Power Electronics,* vol. 24, 2009.

[37]   R. K. Thakur, "Analysis and Control of a Variable Speed Wind Turbine drive system dynamics," *Collage of Military Engineering, Pune India,* 2009.

[38]   "Requirements for Offshore Grid Connections in the E.ON Netz Network," *Eon* 2008.

[39]   "The Grid Code," *National Grid Electricity Transmission* 2013.

[40]   Z. Chen and E. Spooner, "Voltage source inverters for high-power variable-voltage dc power sources " *IEE Proceedinds, Generation, Transmission and Distribution,* vol. 148, 2001.

[41]   N. Patin, L. Vido, E. Monmasson*, et al.*, "Control of a Hybrid Excitation Synchronous Generator for Aircraft Applications," *IEEE Transactions on Industrial Electronics,* vol. 55, 2008.

[42]   Y. Nishida, "A Harmonic Reducing Scheme for 3-Phase Bridge 6-Pulse Diode Rectifier," *IEEE, Industrial Electronics Society, IECON '99 Proceedings,* 1999.

[43]   Y. Nishida, "A 12-pulse Diode Rectifier Using 3-Phase Bridge 6-Pulse Diode Rectifier with 2 Additional Diodes and An Auto-Transformer," *IEEE, Power Electronics and Drive Systems ,* 1999.

[44]   R. A. Flo, "Configuration of large offshore wind farms," *Norwegian University of Science and Technology*, 2009.

[45]   P. Meisen and A. Loiseau, "Ocean Energy Technologies for Renewable Energy Generation," *Global Energy Network Institute*, 2009.

[46]   A. Ragheb and M. Ragheb, "Wind turbine gearbox technologies," *1st International Nuclear and Renewable Energy Conference (INREC10),* pp. 21-24, 2010.

[47]   Enercon. direct-drive 2MW wind turbine [Online]. Available: www.enercon.de

[48]   Enercon, "Enercon wind energy Converters," [Online]. Available: www.enercon.de.

[49]   F. Blaabjerg, Z. Chen, R. Teodorescu*, et al.*, "Power Electronics in Wind Turbine Systems," *Power Electronics and Motion Control Conference,* 2006.

[50]   A. Roscoe, "Collection of offshore tidal and wind energy," *University of Strathclyde*, 2010.

[51]   P. J. Tavner, V. Bussel and F. Spinato, "Machine and Converter Reliabilities in Wind Turbines," *Power Electronics, Machines and Drives Conference,* 2006.

[52]   B. Hahn, M. Durstewitz and K. Rohrig, "'Reliability of wind turbines - Experiences of 15 years with 1,500 WTs'," *Institute of Wind Energy*, 2007.

[53]   H. T. Guo, "Reliability analysis for wind turbines with incomplete failure data collected from after the date of initial installation," *Reliability Engineering & System Safety,* pp. 1057-1063, 2009.

[54]   E. Echavarria, B. Hahn and W. Van Bussel, "Reliability of wind turbine technology through time" *Solar Energy Engineering,* 2008.

[55]   RenewableUK. (2013, Guidance regarding inverter changes in small wind turbine systems. *The voice of wind and marine energy*.

[56]   L. C. G. Vasquez, "Control of a variable Speed Drive with a Multilevel Inverter for subsea applications," *Master of Science, Electric Power Engineering, Norwegian University of Science and Techinology*, 2010.

[57]   "Europe's onshore and offshore wind energy potential" *European Environmental Agency,* 2009.

[58]   P. Bresesti, W. King and R. Vailati., "Transmission expansion issues for offshore wind farms integration in Europe," *IEEE/PES Transmission & Distribution Conference & Exposition,* vol. 1-3, pp. 357-363, 2008.

[59]   H. Polinder, F. van der Pijl, G. Vilder*, et al.*, "Comparison of direct-drive and geared generator concepts for wind turbines," *IEEE Transactions on Energy Conversion,* pp. 725-733, 2006.

[60]   S. D. Wright, A.L. Rogers, J.F. Manwell, *et al.*, "Transmission options for offshore wind farms in the United States," *AWEA,* 2002.

[61]   I. Erlich and U. Bachmann, "Grid code requirements concerning connection and operation of wind turbines in Germany," *IEEE Power Engineering Society General Meeting,* vol. 1-3, pp. 1253-1257, 2005.

[62]   "Economic viability of a simple tidal stream energy capture device" *Department of Business, Innovation and Skills*, 2007.

[63]   N. Mohan, M. Undeland, *et al.*, *Power electronics: converter applications and design*, 3rd ed. Newyork: Wiley, 2002.

[64]   Liqiu Han, J. Wang and D.Howe., "State-space average modelling of 6- and 12-pulse diode rectifiers," *IEEE, power Electronics and Applications Conference*, 2007.

[65]   T. Hoevenaars. (1999) A New Solution for Harmonics Generated by Variable Speed Drives. *Power Quality Assurance LTD, Toronto, Ontario*.

[66]   K. Mikkelsen, "Effect of free stream turbulance on wind turbine perfomance," *Masters, Energy and Process Engineering, Norwegian University of Science and Technology*, 2013.

[67]   Y. Li and S. M. Calisal, "Analysis of Turbine Hydrodynamic Interactions - A Preliminary Investigation," *OCEANS*, 2007.

[68]   L. S. Blunden and A. S. Bahaj, "Tidal energy resource assessment for tidal stream generators," *IMechE Power and Energy,* vol. 221, 2007.

[69]   D.M. Grogan, S.B. Leen, C.R. Kennedy, *et al.*, "Design of composite tidal turbine blades," *Elsevier Renewable Energy,* vol 57 , 2013.

[70]   R. F. Nicholls-Lee, S.R. Turnock and S.W. Boyd., "Application of bend-twist coupled blades for horizontal axis tidal turbines," *Elsevier Renewable Energy,* 2013.

[71]   D. V. Val and L. Chernin, "Reliability-Based Design of Rotor Blades in Tidal Stream Turbines," *School of the Built Environment, Heriot-Watt University,* 2013.

[72]   I. Paraschivoiu, *wind turbine design with emphasis on darrieus concept*: Presses internationales Polytechnique, 2009.

[73]   *Aerodynamics and Loads*. WE Handbook 2.

[74]   L. N. McEwen, R. Evans and M. Meunier., "Cost-Effective Tidal Turbine Blades," presented at the 4th International Conference on Ocean Energy, 2012.

[75]   J. Aho, A. Buckspan, J. Laks*, et al.*, "A Tutorial of Wind Turbine Control for Supporting Grid Frequency through Active Power Control," presented at the American Control Conference, Montréal, Canada, 2012.

[76]   H. Polinder*,* D. Bang, H. Li*, et al.*, "Concept Report on Generator Topologies, Mechanical & Electromagnetic Optimisation," *Delft University of Technology, Aalborg University*, 2006.

[77]   M. Mansour, M.N. Mansouri and M.F. Mimouni., "Comparative Study at Fixed Speed and Variable Speed Wind Generator with Pitch Angle Control," *IEEE, Communications, Computing and Control Applications,* 2011.

[78]   F. D. Bianchi, H. de Battista and R.J. Mantz., *Wind Turbine Control Systems. Principles Modelling and Gain Scheduling Design (1st ed.).* London UK: Springer, 2006.

[79]   J. F. Manwell and J.G. McGowan*.*, *Wind energy explained: theory, design and application*. Sussex UK: Willey, 2002.

[80]   S. Heier and R Waddington, *Grid Integration of Wind Energy Conversion Systems*: John Wiley & Sons Ltd, 1998.

[81]   R. Teodorescu and F. Blaabjerg, "Flexible Control of Small Wind Turbines With Grid Failure Detection Operating in Stand-Alone and Grid-Connected Mode," *IEEE, Transactions on Power Electronics,* 2004.

[82]   I. Moore and J. Ekanayake, "Design and Development of a Hardware based Wind Turbine Simulator," Cardiff University, 2010.

[83]   National Renewable Energy Laboratory. (2013, *Modeling of Type 1 Wind Turbine Generators*. Available: http://www.uwig.org:8080/index.php?title=Modeling_of_Type_1_Wind_Turbine_Generators#cite_note-B.Kuo-3

[84]   National Renewable Energy Laboratory, "Dynamic Models for Wind Turbines and Wind Power Plants," The University of Texas at Austin Austin, Texas, 2011.

[85] H. Lia, B. Zhao, C. Yang*, et al.*, "Analysis and estimation of transient stability for a grid-connected wind turbine with induction generator," *Elsevier Renewable Energy,* vol. 36 pp. 1469–1476, 2011.

[86] I. Jadric, "Modeling and Control of a Synchronous Generator with Electronic Load," Master of Science, Electrical Engineering, Virginia Polytechnic Institute and State University, Blacksburg, Virginia, 1998.

[87] P. M. Anderson and A. A. Fouad, *Power System Control and Stability* IEEE Press, 2003.

[88] Y.-Y. Hsu and C.-H. Cheng, "A Fuzzy Controller for Generator Excitation Control," *IEEE Transactions on Systems, Man And Cybernetics,* vol. 23, 1993.

[89] N. Mohan, Undeland, T., Robbins, W.,, "Power electronics: converters applications and design," *New York: Wiley* vol. 3rd edition, 2002.

[90] H. Zhu, R.P. Burgos, F. Lacaux*, et al.*, "Average Modeling of Three-phase and Nine-phase Diode Rectifiers with Improved AC Current and DC Voltage Dynamics," *IEEE 31st Annual Industrial Electronics Society Conference,* 2005.

[91] Y. Du, J.M. Guerrero, C. Liuchen*, et al.*, "Modeling, Analysis, and Design of a Frequency-Droop-Based Virtual Synchronous Generator for Microgrid Applications," *IEEE ECCE Asia-down under,* 2013.

[92] P. C. Krause and T. A. Lipo, "Analysis and Simplified Representation of Rectifier-Inverter Reluctance-Synchronous Motor Drives," *IEEE Transactions on power Apparatus and Systems,* vol. Pas-88, 1969.

[93] D. Aguglia, P. Viarouge, R Wamkeue*, et al.*, "Selection of Gearbox Ratio and Power Converters Ratings for Wind Turbines Equipped With Doubly-Fed Induction Generators," *IEEE Electric Machines and Drives Conference,* 2007.

[94] K. Smolders and H. Long, "Reliability Analysis and Prediction of Wind Turbine Gearboxes," presented at the Europe's Premier Wind Energy, Warsaw, 2010.

[95] J. Cotrell, "A preliminary evaluation of a multiple-generator drive train configurations for wind turbines," presented at the 21st American Society of Mechanical Engineers (ASME) Wind Energy Symposium, Reno, Nevada, 2002.

[96] S. D. Rubira and M. D. McCulloch, "Control of Doubly Fed Wind Generators connected to the Grid by Asymmetric Transmission Lines.," *IEEE Industrial Applications Conference,* 1998.

[97]   M.J.Hoeijmakers, "The (In)stability of a synchronous machine with diode rectifier," presented at the Internatinal Conference on Electrical Machines Manchester, 1992.

[98]   C. Yuan and M. Jin, "Research on PID Parameters Optimization of Synchronous Generator Excitation Control System," *IEEE Critical Infrastructure 5ᵗʰ international conference,* 2010.

[99]   Y. Guo, P. Zeng, W. Deng*, et al.*, "Modeling and simulation of Grid side Converter based Wind Power Generation System," *IEEE 2ⁿᵈ annual Information Science and Engineering Conference,* 2010.

[100]   M. Roman, "Modification of Symmetric Optimum Method," *ASR seminar instrumentation and control,* 2005.

[101]   V. Nicolau, C. Miholca, D. Aiordachioaie*, et al.*, "Aspects of Pole Placement Technique in Symmetrical Optimum Method for PID Controller Design," *Department of Electronics and Telecommunications, "Dunarea de Jos" University of* Galati, 2005.

[102]   J. A. Clarke, A.D. Grant and C.M. Johnstone*.*, "Output characteristics of tidal current power stations during spring and neap cycles," Energy Systems Research Unit, Department of Mechanical Engineering University of Strathclyde, Glasgow, 2004.

[103]   National Instrument, "LabVIEW User Manual," Austin, Texas, 2003.

[104]   National Instrument. (2013, CompactRIO cRIO-9072/3/4 Operating Instructions and Specifications.

APPENDIX A

7 Experimental rig system configuration

7.1 Signal Processing

A National Instruments (NI) c-RIO data acquisition unit was used in this experiment, c-RIO stands for Compact Reconfigurable Input/Output. It is an integrated system which combines a real-time processor and a reconfigurable field-programmable gate array (FPGA) within the same component.

The employed data acquisition unit (c-RIO) is shown in *Fig 7.1.*

Fig 7.1: Signal processing unit (c-RIO)

The c-RIO has analog input and output modules with a 266 MHz industrial realtime processor for analysis, data logging, and control. The analog input/output modules employed for this experiment were the NI 9213 (analog input module) with 16 analog inputs, ±10 V input

range (12-bit resolution single-ended) , 500 kS/s aggregate sampling rate, and the NI 9201 (analog output module) with four simultaneously updated analog outputs, 100 kS/s (16-bit resolution).

The employed analog input/output modules are shown in *Fig 7.2.*

Fig 7.2: Analog Input/output modules

Signal processing was carried out via LabVIEW real-time simulation platform; LabVIEW (Laboratory Virtual Instrumentation Engineering Workbench) programs are termed virtual instruments (VIs), due to their ability to emulate physical instruments. For example, the LABVIEW user platform consists of a broad set of tools for displaying, acquiring, storing, analysing as well as troubleshooting code. The LABVIEW user interface consists of controls which include knobs, push buttons, and dials, in addition to indicators that include LEDs, graphs and other output displays [103]

When the user interface is designed, the VIs and structures code is added to run the front panel objects. The LABVIEW graphical model containing this code is then used to interface the hardware with the software via the data acquisition unit

There are two modes of operation available in LabVIEW which are real time project, and FPGA project. The real time mode comprises of two programming modes: scan interface mode and LabVIEW FPGA mode**.** These programming modes are basically the interfacing techniques. The scan interface mode is used for retrieving data of lower frequency with simpler processing techniques. In this mode the acquisition of data and processing of the blocks takes place in the c-RIO device. When the frequency of the data acquired by the c-RIO is higher and the processing demands accurate and faster processing, then LabVIEW FPGA mode is preferred [104]. In this mode, the c-RIO analog input and output modules are interfaced with the FPGA. Basically, in this mode, the real time data is acquired by means of analog input modules and the processing is done inside the LabVIEW FPGA.

Nonetheless, due to the nature of the analysis undertaken in this experiment and the low frequency at which tidal velocity varies. LabVIEW real-time scan interfacing technique was used.

7.2 Experimental Drives configuration
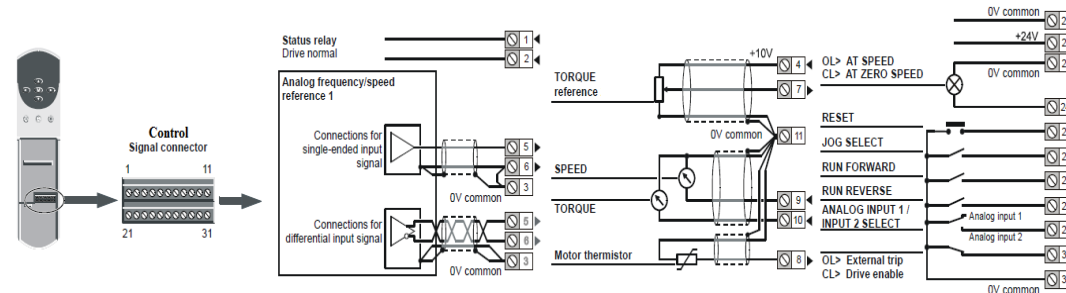
Fig 7.3: Unidrive terminal configuration

For the purpose of descriptions, the following terminologies are defined

Destination parameter - indicates the terminal controlled parameter.

Source parameter - indicates the terminal mode output parameter

Mode parameter

Analog - indicates the terminal operation mode, i.e. current 4-20mA, voltage 0-10V.

7.2.1   MCD Control Block

To realise the rotor characteristics in **Table 5.1:** *2D Shaft Torque Look-up Table*: using an induction motor, the MCD control mode parameter 4.11(Torque mode selector) was set to 1 which enabled the drive to operate in torque control mode.
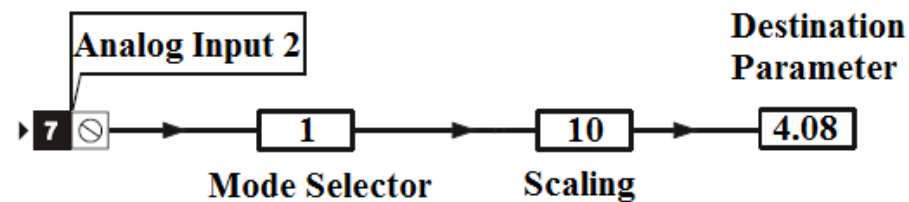
Fig 7.4: Motor control drive torque control circuit

The desired/reference torque signal was sent/received by the MCD via input terminal 7 (Analog input 2) as shown in **Fig 7.4**. The terminal destination parameter was set to 4.08 (Torque reference) which determined the amount of active current supplied to the motor. The input terminal mode selector was set to 1 which rendered the terminal active and ready to receive an input analog voltage signal ranging from 0-10V, the scaling factor of 10 was used to convert the input signal into motor torque percentage as demanded by the MCD.
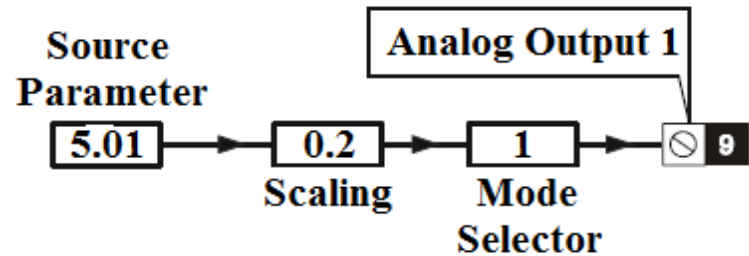
Fig 7.5: Motor control drive speed measurement circuit

Fig 7.5 shows the MCD shaft speed measurement circuit, the terminal mode selector was set to 1 rendering output terminal 1 active and ready to send out an output voltage signal ranging from 0-10V, the scaling factor of 0.2 was used i.e. multiplying the estimated drive frequency by 0.2 converted it into an output voltage signal that represented shaft speed. The source parameter was set to 5.01 which correspond to the drive's measured motor frequency in Hz.
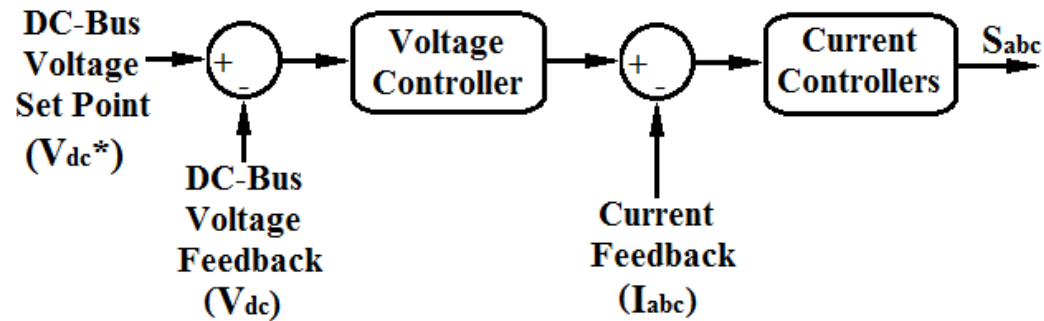
Fig 7.6: Output power controller

When the power was applied to the Regen drive it went through a line synchronisation cycle, during which test pulses were applied to the incoming line to realise the voltage and phase (PLL) of the mains. When synchronisation to the mains was complete, the DC bus voltage controller was activated raising the DC bus voltage to the desired set point determined by the voltage controller.

The regen drive control terminals configuration was identical to the MCD shown in *Fig 7.3*
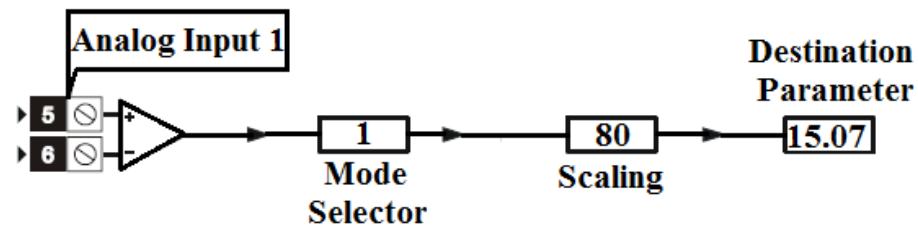
Fig 7.7: Regen drive DC bus voltage set point control circuit

The DC bus voltage reference signal was received by the Regen drive via input terminal 5 (Analog input 1) as shown in *Fig 7.7.* The terminal's destination parameter was set to 15.07 (DC bus Voltage set point) which determined the DC-bus voltage. The terminal mode selector was set to 1 which rendered the terminal active and ready to receive an input voltage signal ranging from 0-10V, and the scaling factor of 80 was used to convert the input voltage signal into an actual voltage value. Since the Regen drive was rated at 800VDC, which meant that a 10V input signal = 800VDC.

It should be noted that analog input terminal 1 was by default a bipolar differential voltage input thus for a single ended use terminal 6 was connected to terminal 3 which is a common terminal 0V as shown in *Fig 7.3.*

The actual DC-bus voltage (DC-bus voltage feedback) and current (Current feedback) required by the field controller shown in ***Fig 5.17: Field controller configuration***: were measured and realised from the Regen Drive as follows.
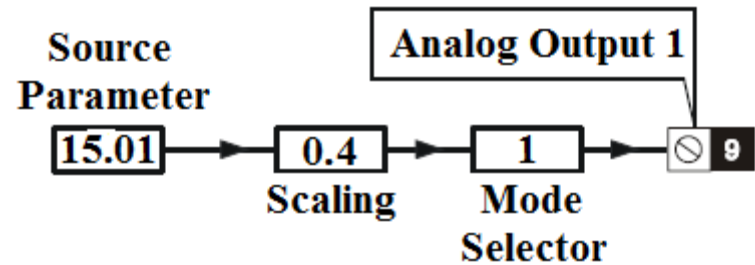
Fig 7.8: *Regen drive current feedback measurement circuit*

Fig 7.8 illustrates the Regen DC bus current measurement circuit, the terminal mode selector was set to 1 rendering output terminal 1 active and ready to send out an output voltage signal ranging from -10 to +10V, and the scaling factor of 0.4 was used i.e. multiplying the measured Regen drive DC-bus current by 0.4 converted is into the corresponding value of voltage signal (-10 to +10V) that represents the actual current value, the Regen drive was rated at 25A.

The source parameter was set to 15.01 which represents supply current. The active rectifier controlled the current to make sure that the fundamental voltage and current are in phase at the drives output terminals.
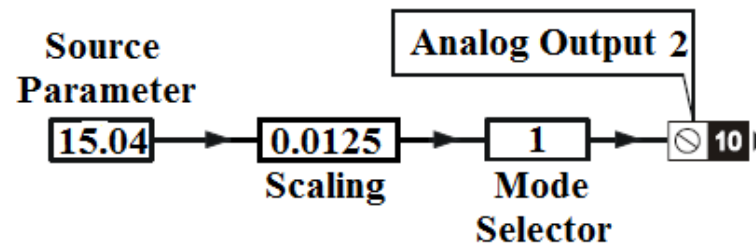
Fig 7.9: Regen drive DC bus Voltage measurement circuit

Fig 7.9 illustrates the Regen DC bus Voltage measurement circuit, the terminal mode selector was set to 1 rendering output terminal 1 active and ready to send out an output voltage signal ranging from 0 to 10V, and the scaling factor of 0.0125 was used i.e. multiplying the measured Regen drive DC-bus voltage by 0.0125 converted it into the corresponding value of voltage signal (0 to 10V) that represented the actual measured voltage.

8 Matlab Simulation Models

8.1 Tidal Turbine Model

The tidal turbine simulation presented in this thesis was modelled in Matlab Simulink as presented in *Fig 8.1*.
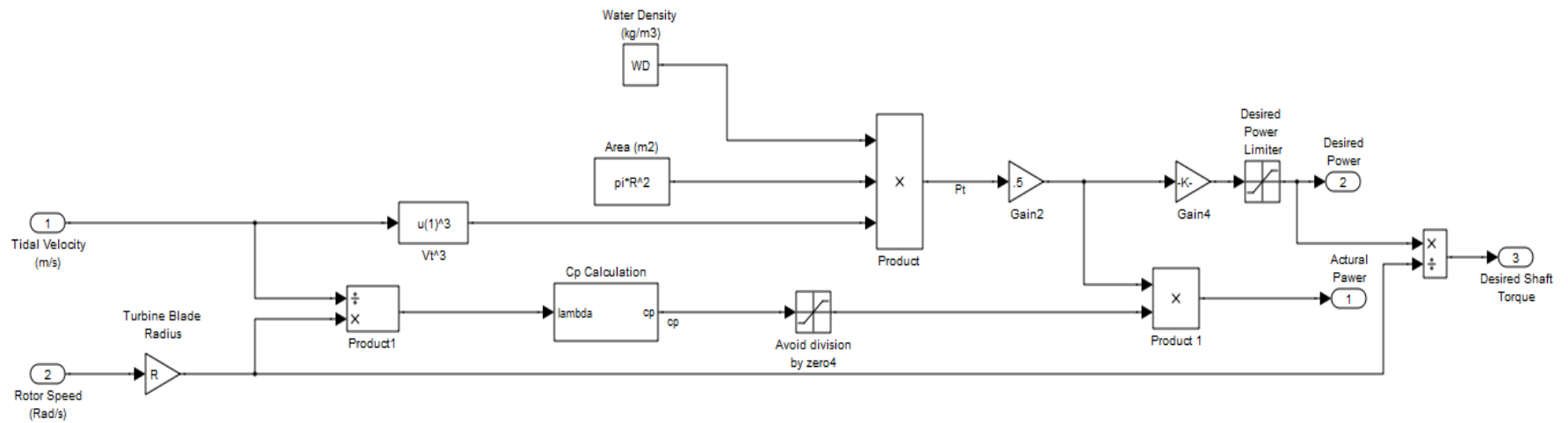
***Fig 8.1:** Simulation model of the implemented tidal turbine*

8.1.1   Turbine power coefficient C$_P$ Calculation Model

The TSR is used in this thesis to calculate the turbine power coefficient, denoted by C$_p$. was modelled as shown in ***Fig 8.2***
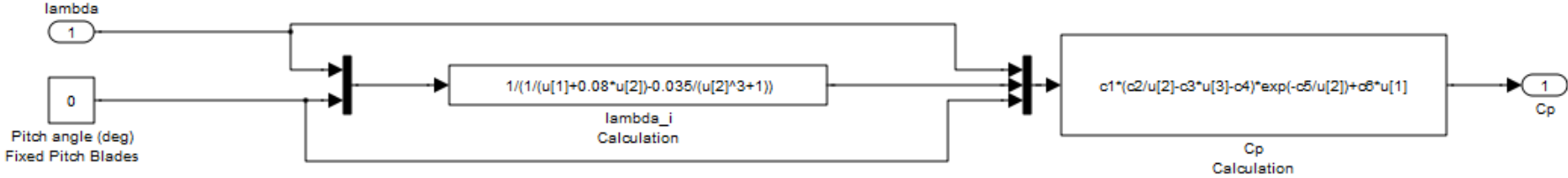
Fig 8.2: Turbine power coefficient Simulation model

8.2 Tidal turbine configuration Model
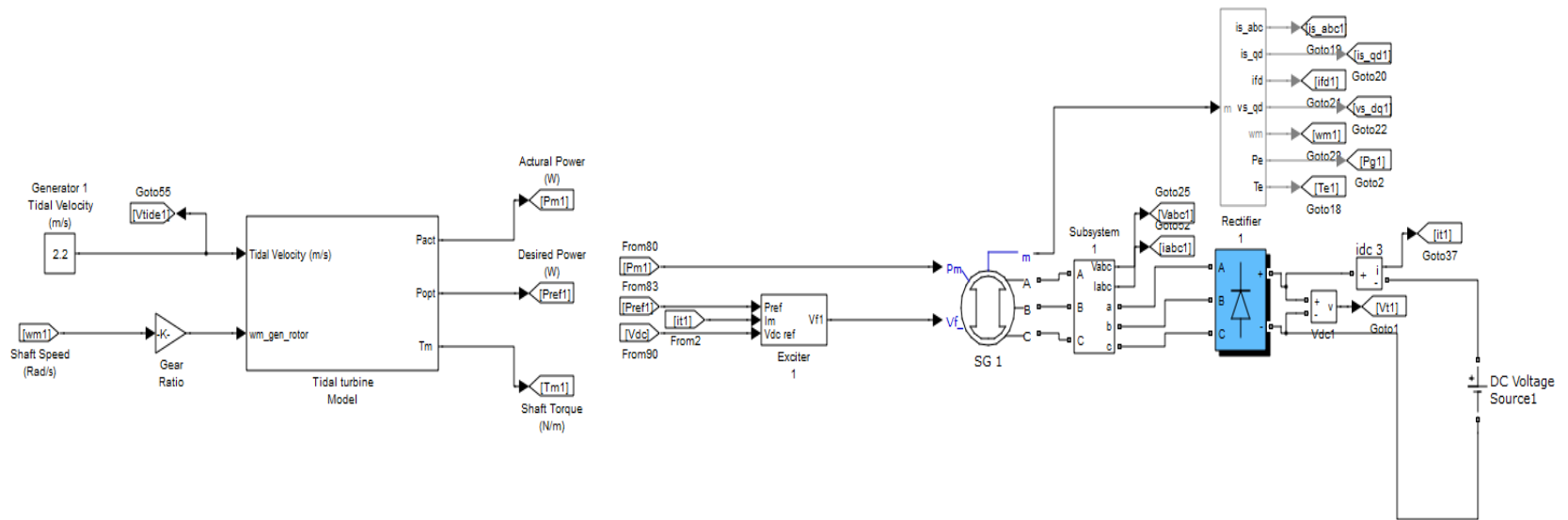
Fig 8.3: *Tidal turbine Nacelle Simulation model*

8.3 Tidal turbine farm configuration Model
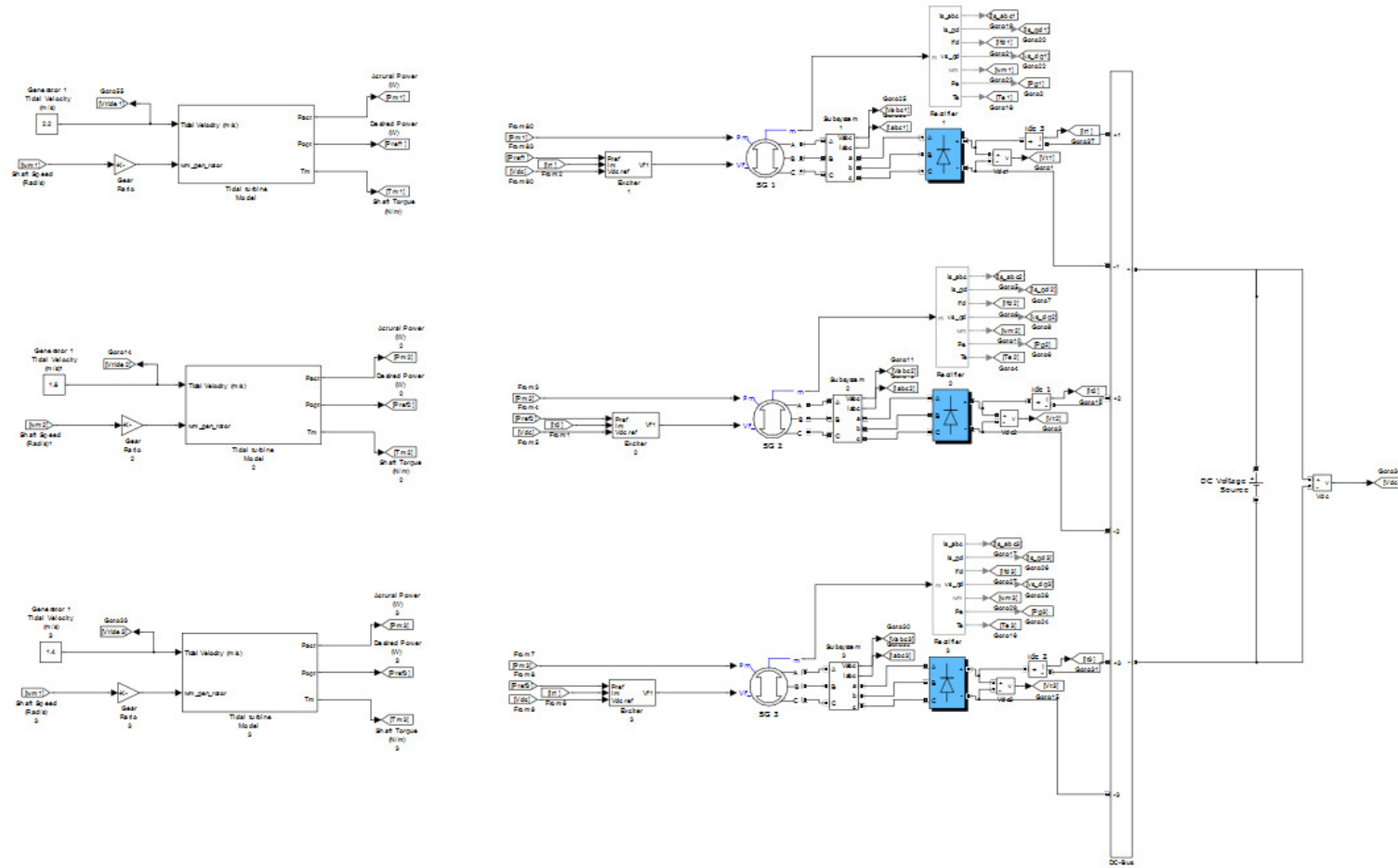
Fig 8.4: *Tidal turbines farm Simulation model*

APPENDIX B

9 Experimental validation

9.1 Controllable DC Power Supply

Field current control was achieved by a controllable DC Power Supply coupled to the generator exciter input terminals. The employed power supply consisted of non-isolated inputs and outputs terminals which were used to regulate generator field current. The control input signals to the DC power supply were referenced to the positive output in the range of 0-10V.

The employed generator exciter was the TTi QPX1200 DC power source shown in *Fig 9.1*.
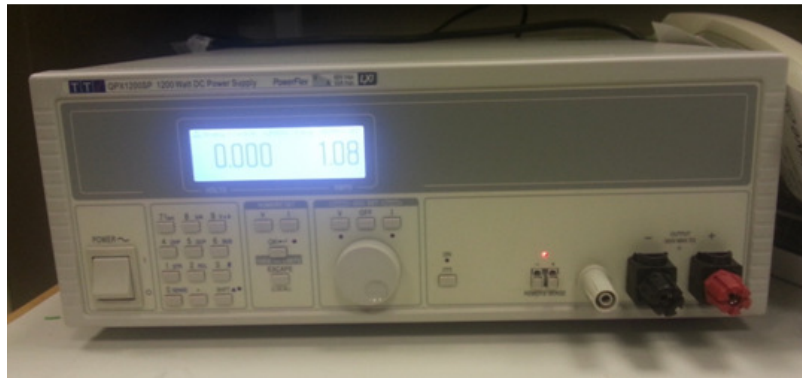
Fig 9.1: Controllable DC Power source

The employed DC-power source had the following parameters:

|	
Voltage Range:	0V to 60V
Current Range:	0.01A to 50A
Power Range:	Up to 1200W
Accuracy:	0.1% of setting ± 2mV
Current Setting:	Resolution 10mA
Accuracy:	0.3% of setting ± 20mA

Table 9.1: *Exciter power source parameters*

DC power source operating mode was constant voltage or constant current with automatic cross-over provided that the power demanded it stayed within its operation envelope.
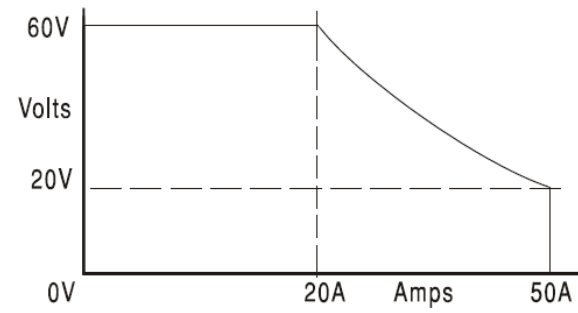
Fig 9.2: DC Power Supply power envelope

9.2 Simulation rig SG configuration
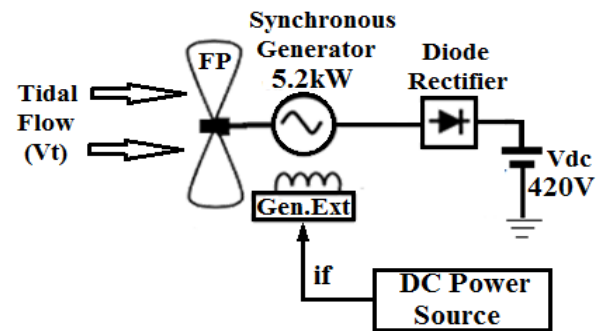
Fig 9.3: Tidal turbine equivalent electrical schematic

9.3 Generator parameters

Nominal Power	-	5.2kW	Nominal Voltage	-	400Vrms
Nominal Frequency	-	50Hz	Pole Pairs	-	2
Stator Winding Resistance	-	1.938Ω	Efficiency	-	82%
Rotor Winding Resistance	-	6.078Ω	Power Factor	-	0.8

Table 9.2: Tidal Simulator Generator Parameters

Generator excitation characteristics were as follows:

0.41A at no load

1.08A at full load

Exciter stator resistance - 15.71 Ohms, thus exciter voltage was:

6.44VDC at no load +/-30%

17VDC at full load +/-30%

If excitation was raised to maintain a high output voltage at a very low shaft speed, a higher DC excitation value would be required i.e. could get to above 17VDC which may cause overheating due to over excitation which could damage either or both the exciter and main rotor.

Fig 9.4 shows the generator efficiency curve as the load varies
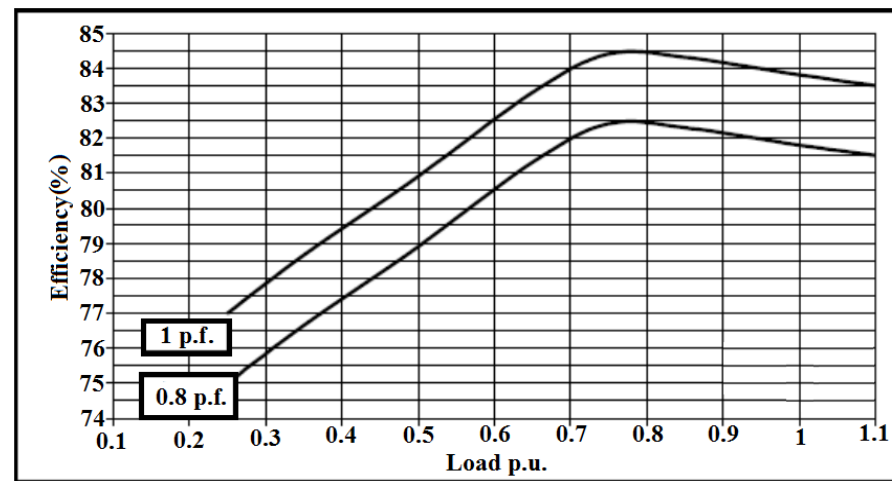
Fig 9.4: Generator efficiency Curve at both 0.8 and unity power factor (p.f.)

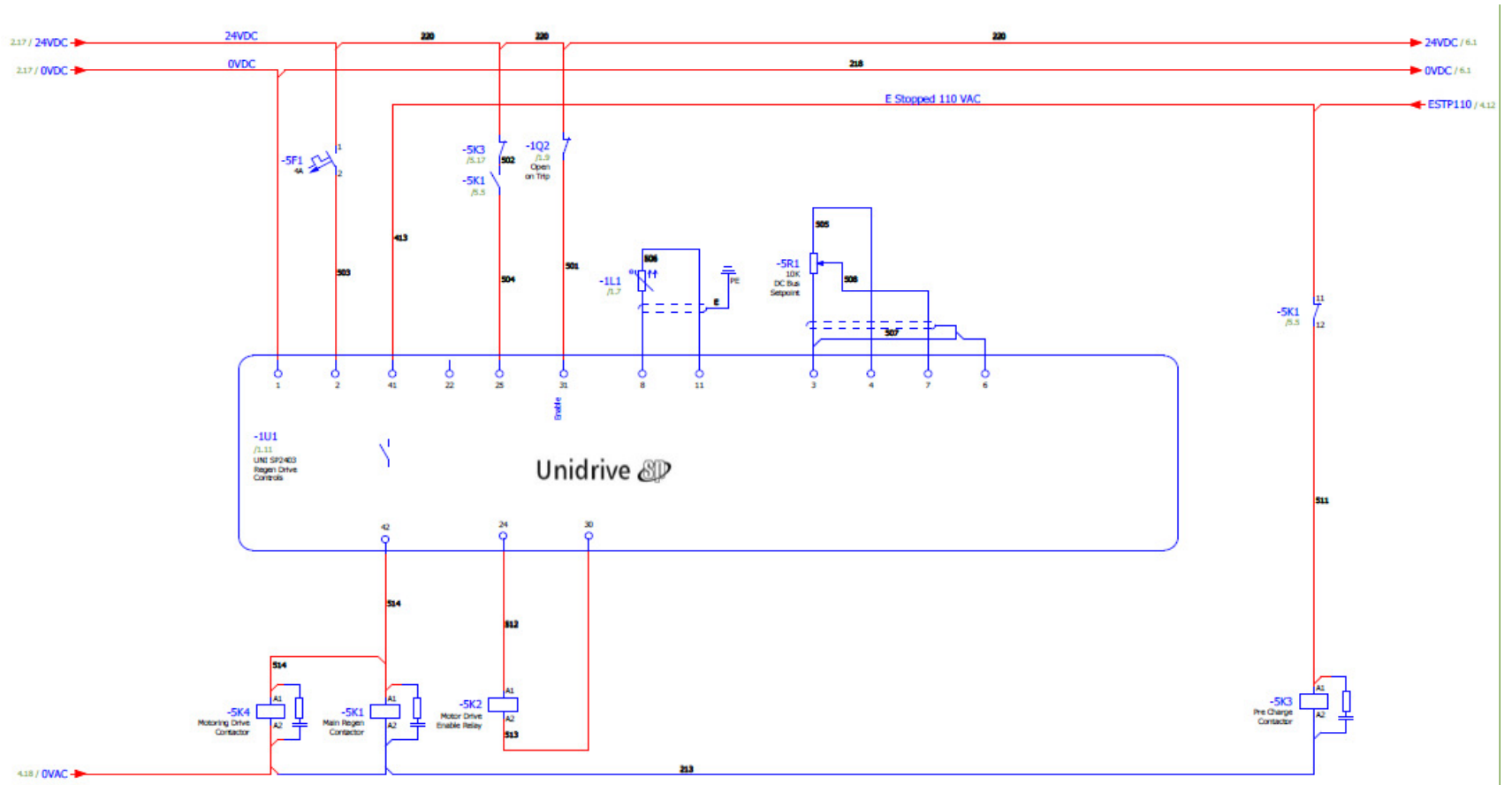## 9.4 Simulation rig control drives configuration
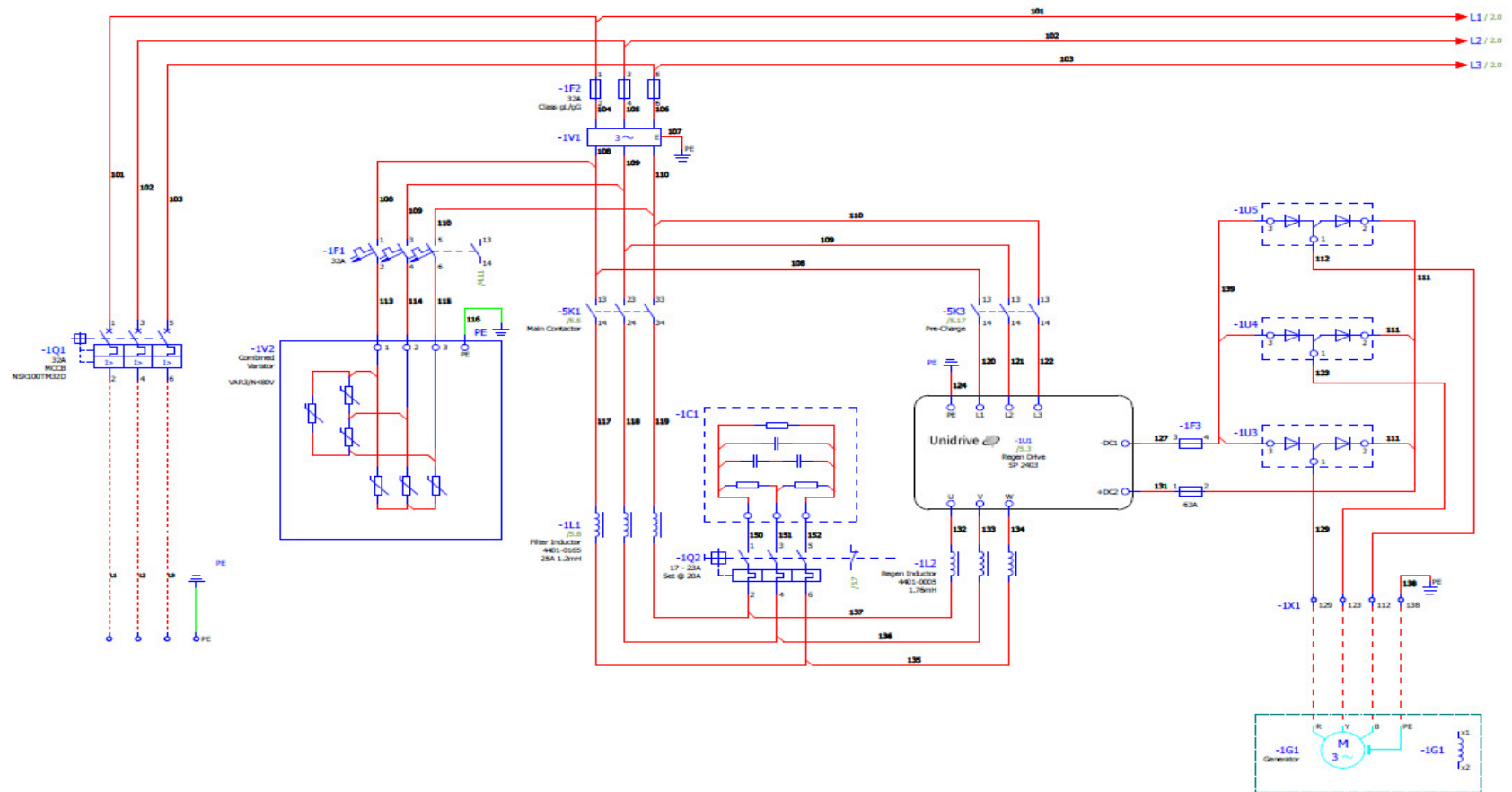
Fig 9.5: *Test Rig Control Drives Cubical Power in schematic*
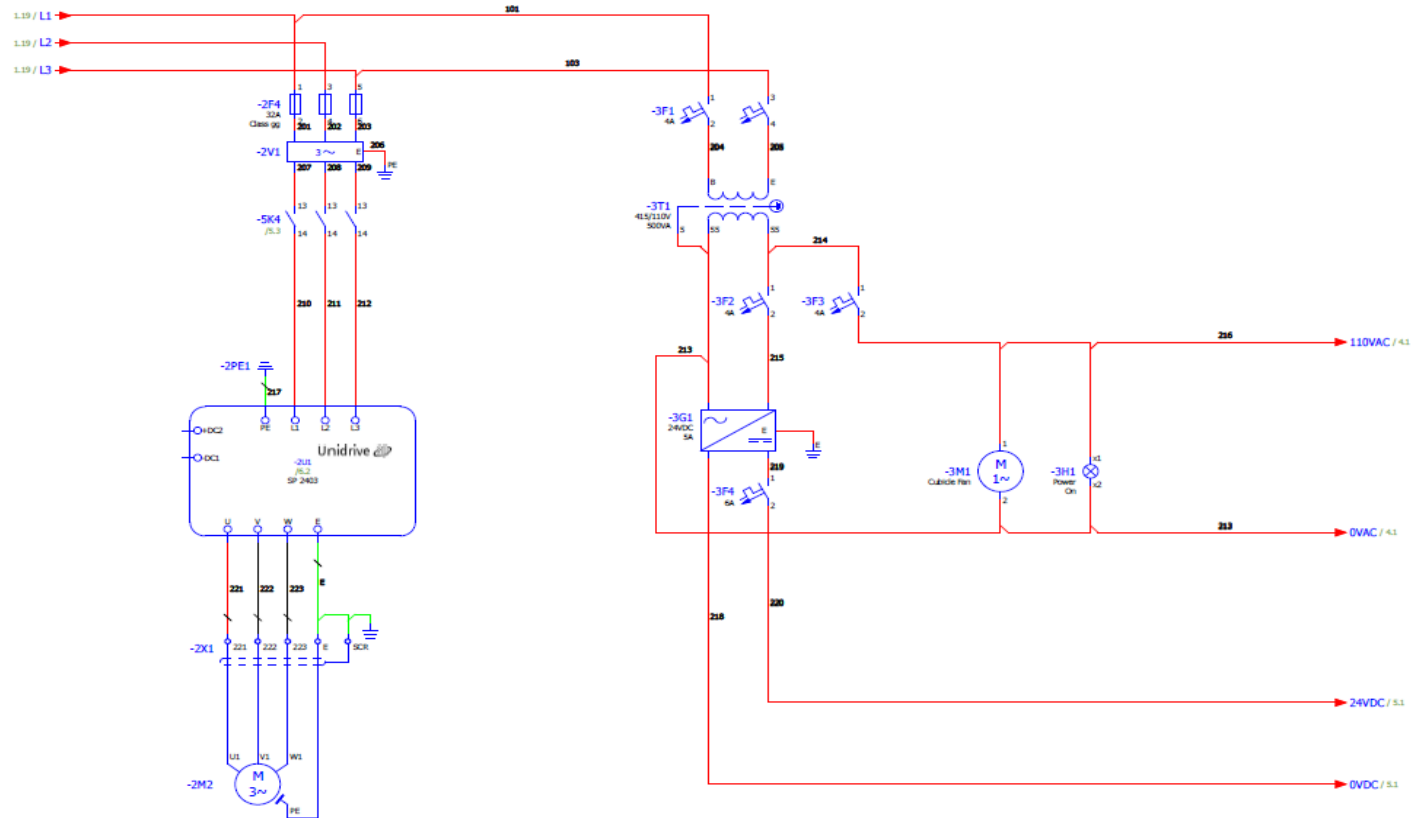
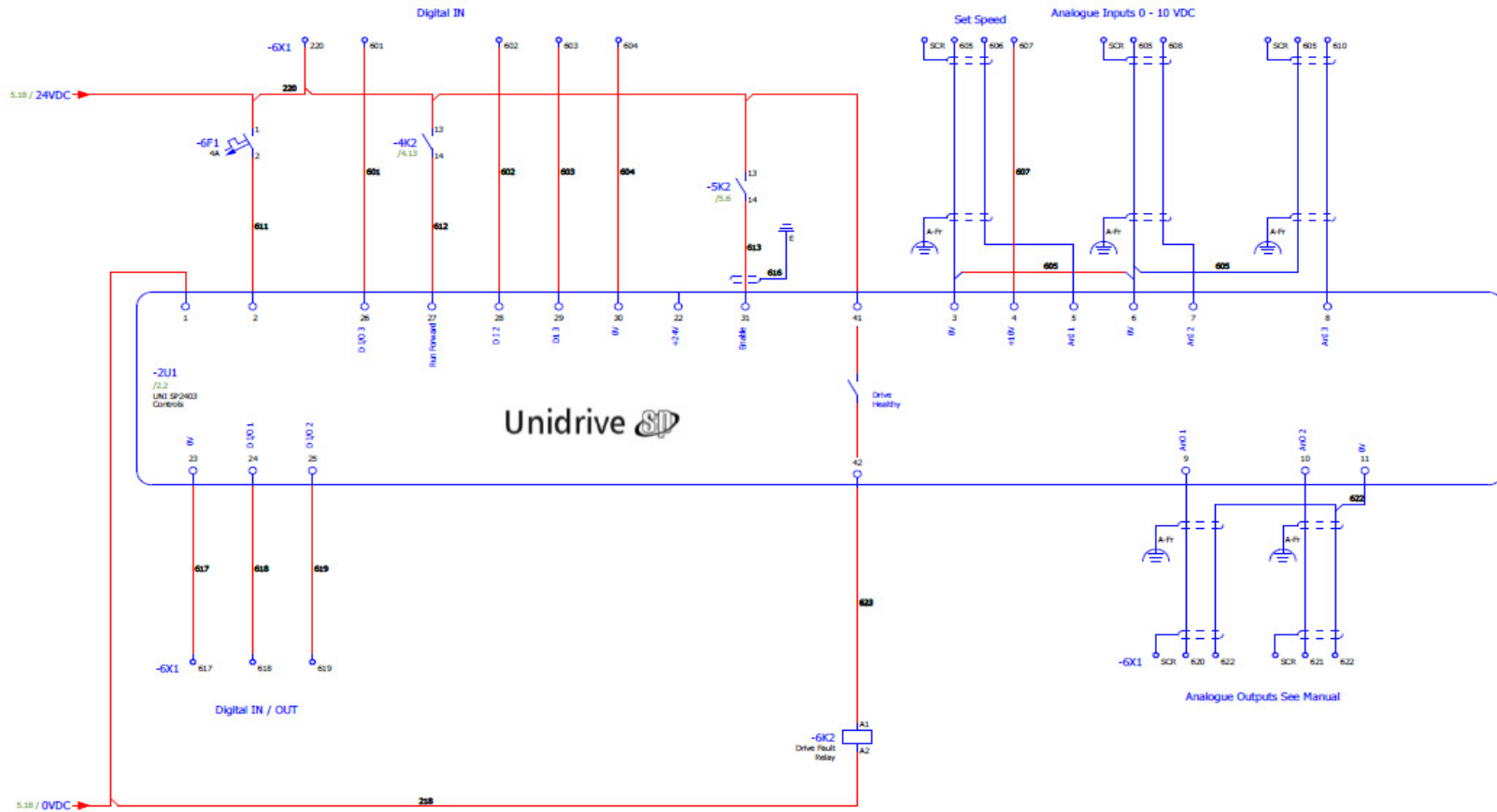**Fig 9.6:** *Test Rig Control Drives Cubical MDC and control power schematic*

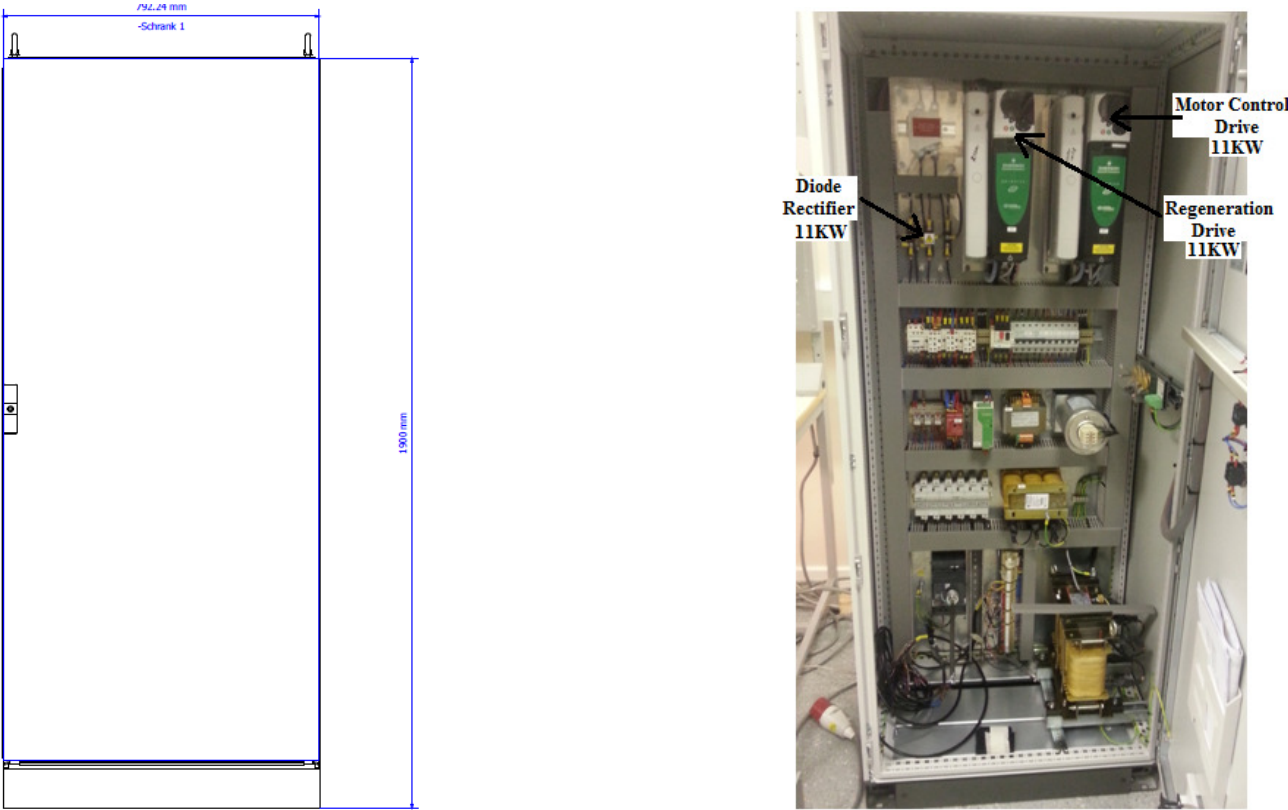***Fig 9.7:*** *Test Rig Control Drives Cubical Regen drive control schematic*

Fig 9.8: Test Rig Control Drives Cubical MDC control schematic

The tidal simulator hardware control cubical was configured as shown in *Fig 9.9.*

Fig 9.9: *Test Rig Control Drives Cubical*